NASA Technical Memorandum 88278

Comparison of Flight-Measured and Calculated Temperatures on the Space Shuttle Orbiter

Leslie Gong, William L. Ko, Robert D. Quinn, and W. Lance Richards

November 1987

National Aeronautics and
Space Administration

NASA Technical Memorandum 88278

Comparison of Flight-Measured and Calculated Temperatures on the Space Shuttle Orbiter

Leslie Gong, William L. Ko, Robert D. Quinn, and W. Lance Richards
Ames Research Center, Dryden Flight Research Facility, Edwards, California

1987

NASA
National Aeronautics and
Space Administration
Ames Research Center
Dryden Flight Research Facility
Edwards, California 93523-5000

SUMMARY

Aluminum structural temperatures and thermal protection system (TPS) surface temperatures were measured on the space shuttle orbiter during the flight of the space transportation system 5 (STS-5). The measured data are compared with values calculated at wing stations 134, 240, and 328 and at fuselage station 877. The theoretical temperatures were calculated using the structural performance and resizing (SPAR) finite-element thermal analysis program. The comparisons show that the calculated temperatures are, generally, in good agreement with the measured data.

INTRODUCTION

The space shuttle Columbia has proven that the thermal protection system (TPS) is a viable method of insulating the vehicle. Following the first five orbital missions, the orbiter was declared operational and a majority of the onboard development-flight instrumentation was removed to increase payload capacity. The space shuttle structure is constructed primarily of aluminum and, to a lesser extent, graphite fiber-reinforced composite materials. Due to the weak high-temperature strength of aluminum it is paramount that no tiles fail during the high heat loads encountered from deorbit to landing. During reentry into the earth atmosphere, the aluminum skins and substructure of the vehicle must be protected from developing excessive thermal gradients. If the thermal gradients are too severe, the resulting thermal stresses could induce skin buckling that could, in turn, cause possible bond-line failure between the skin and the TPS. To protect the aluminum structure, the TPS is bonded to the skins. Due to the nonflexible nature of the shuttle tiles, a highly flexible strain isolation pad (SIP) is bonded between the skin and the tiles to absorb strain incompatibility between the skin and the TPS. The SIP is also designed to absorb any possible skin buckling effects on the TPS.

In the design of a vehicle such as the space shuttle, extensive analyses must be performed on the structure. Calculated structural temperature distributions can be used to predict thermal stresses and to verify if the thermal stresses are excessive or if skin buckling will occur. The predicted thermal stresses can also be used to correct flight load measurements that were made on the vehicle structure with strain gages.

In order to make a realistic calculation of the thermal stresses, the structural temperature distributions must be calculated accurately. For a finite-element analysis of a large vehicle such as the space shuttle, a determination has to be made between the number and types of elements necessary for accuracy and the capability and amount of resources available. The shuttle orbiter has provided a unique opportunity to perform an analytical study for both thermal and stress predictions. The initial phase of an incremental program to calculate the structural temperature and the thermal stresses with a finite-element computer program on the shuttle are presented in references 1 to 3.

Previous comparisons between the measured and the calculated temperatures (refs. 1 to 3) were limited to a few representative temperature profiles. In this

report all the measured temperatures available at wing stations (WS) 134, 240, and 328 and fuselage station (FS) 877 are presented. These temperatures are compared with the calculated results from a three-dimensional thermal analysis for WS134, WS240 and WS328. The results are also presented from a two-dimensional analysis of FS877.

NOMENCLATURE

A_i	surface area of radiation exchange element i
DFI	development-flight instrumentation
F_{ji}	view factor or fraction of radiant heat from element j incident on element i
FRSI	felt reusable surface insulation
FS	fuselage station
HRSI	high-temperature reusable surface insulation
i,j	radiation exchange elements
JLOC	joint location
K21	two-joint conduction (element)
K41	four-joint conduction (element)
K61	six-joint solid conduction (element)
K81	eight-joint solid conduction (element)
LRSI	low-temperature reusable surface insulation
R21	two-joint radiation (element)
R31	three-joint radiation (element)
R41	four-joint radiation (element)
SIP	strain isolation pad
SPAR	structural performance and resizing (finite-element computer program)
STS	space transportation system
T	temperature, °F
THEOSKN	theoretical thin-skin (NASA computer program)

TPS thermal protection system

t reentry time, sec

WS wing station

SPACE SHUTTLE ORBITER

Analysis Locations

A planform view of the space shuttle orbiter with three wing stations and one fuselage station for which heating analyses were performed are shown in figure 1. Thermal models were made for all four stations. As shown, calculations were made for WS134, WS240, WS328 and FS877.

Flight Profiles

Measured reentry flight time histories of the STS-5 trajectory are shown in figure 2. Also shown in this figure are the nominal reentry design flight trajectories. Time t = 0 sec in the trajectory corresponds to the start of reentry and is defined to occur at an altitude of 400,000 ft. The total reentry flight time for the STS-5 mission was 1821 sec. The measured values of velocity and altitude were somewhat lower than the corresponding nominal values; this was true throughout the majority of the flight, and was also the trend for the four previous STS flights. The measured values of angle of attack showed a slightly higher reading than the nominal values during the early stage of reentry and a significant drop below the nominal curve after a reentry time t = 1000 sec. The differences between the measured and the nominal STS-5 flight profiles are considered significant; therefore, the measured values were used for the calculations presented in this report.

Description of Wing Structure

Wing station 134. - The geometry of the wing section at WS134 for which TPS and structural temperatures were calculated is shown in figure 3. This wing station was selected due to the large, complex nature of the structure and the considerable amount of surface and substructure instrumentation for measuring temperatures. The entire lower surface of the wing section is covered with high-temperature reusable surface insulation (HRSI) with a strain isolatin pad (SIP) lying between the aluminum skin and the insulating tiles. The upper surface at WS134 is covered with either felt reusable surface insulation (FRSI) or low-temperature reusable surface insulation (LRSI). The LRSI tiles also use SIP between the aluminum skin and the tile. Each material is bonded using room-temperature-vulcanized (RTV) high-temperature silicone rubber. The RTV bonding takes place between the LRSI, the SIP, and the aluminum skin surfaces and between the FRSI and the aluminum skin. FRSI does not require a SIP due to the inherent flexible nature of this material.

The TPS transitions from HRSI to LRSI on the upper surface in the forward glove area occurs at a distance of approximately 572.4 in measured from the nose of the vehicle. LRSI tiles were used from 572.4 in to 707.3 in of the vehicle at this cross section. From 707.3 in to 1129.0 in, FRSI was used.

The lower and upper skins in the forward glove area consist of hat-stringer-reinforced aluminum skins. A vertical and diagonal truss system adds to the strength of the forward glove area. Construction of the wheelwell door consists of upper and lower aluminum skins, both of which are reinforced with spanwise hat stringers. The spar webs of the door are made of aluminum I-beams and C-channels. The upper surface of the wheelwell is made of aluminum honeycomb core sandwich structure. In the three bays just aft of the wheelwell, the lower and upper skins consist of hat-stringer-reinforced aluminum skins. All the vertical spar webs and the forward and aft walls of the wheelwell are made of corrugated aluminum.

Wing station 240. — The geometry of the wing section at WS240 for which TPS surface and structural temperatures were calculated is shown in figure 4. Both the upper and the lower skin and the forward spar web of bay 1 are made of aluminum honeycomb sandwich plates. The skins of bays 2, 3, and 4 are made of spanwise hat-stringer-reinforced aluminum skins. The remaining spar webs are made of corrugated aluminum. The rib webs consist of a truss system at WS254. The lower wing skin is covered with HRSI, with the SIP lying between the skin and the HRSI. Most of the upper skin of bay 1 is protected by LRSI with an inner SIP layer. The remainder of the upper skin of bay 1 and all the upper skins of bays 2, 3, and 4 are covered with FRSI. The FRSI is bonded directly to the aluminum skin with RTV high-temperature silicone rubber.

Wing station 328. — The wing section at WS328 can be seen in figure 5. The forward spar web of bay 1 is made of aluminum honeycomb sandwich plates. The upper and the lower skins of bays 1, 2, and 3 are made of spanwise hat-stringer-reinforced aluminum skins. The remaining spar webs are made of corrugated aluminum. The rib webs consist of a vertical and diagonal truss system at WS342.5. The lower wing skin is covered with HRSI and a layer of SIP between the aluminum skin and the tile. The upper skin is covered with LRSI with an inner layer of SIP.

Description of Fuselage Structure

The geometry of the fuselage cross section at FS877 is shown in figure 6. Only half of the cross section was considered, owing to symmetry. The lower skin and the side wall of the fuselage consist of T-stiffener-reinforced aluminum skins. The lower and the upper skins of the glove area are made of hat-stringer-reinforced aluminum skins with the leading edge of the glove skin made of an aluminum honeycomb-core sandwich structure. An RTV heat sink is located on part of the inner surface of the pay-load bay door. As can be seen, the lower surface of the fuselage, the lower surface of the glove and the leading edge of the glove are covered with HRSI tiles. The upper surface of the glove is covered with LRSI. The lower and the upper regions of the fuselage sidewall are covered with FRSI and LRSI, respectively. The payload bay door is protected with a layer of FRSI. In the wing sections as well as in the fuselage cross section, RTV high-temperature silicone rubber was used in bonding the TPS to the aluminum skin.

THERMAL MODELS

The structural temperatures were computed using the structural performance and resizing (SPAR) thermal analysis program (ref 4). SPAR is a finite-element program which computes transient temperature distributions in complex thermal models of one, two, or three dimensions. It utilizes an explicit algorithm based on a Taylor expansion solution or the implicit method of Galerkin or Gear (refs. 4 and 5). In this report the explicit method was used. This program was used for the reentry heat transfer analysis of WS134, WS240, WS328, and FS877. The three wing cross sections are three-dimensional thermal models and the fuselage cross section is two-dimensional. Figures 3 to 5 show the geometry of wing cross sections 134, 240, and 328, respectively. Figure 6 shows the geometry of fuselage cross section 877. The SPAR thermal models are shown in figures 7 to 9.

The number of joint locations (JLOC) and elements used in the SPAR thermal models are listed in table 1. Equivalent thicknesses were determined for chem-milled, corrugated, honeycomb, and hat-stringer-reinforced structures. These equivalent thicknesses were used for the conduction elements. External radiation to space was modeled utilizing a single radiation element with a view factor value of one for all external radiation elements.

For both external and internal thermal radiation exchanges, all the view factors were calculated from the equation:

$$A_i F_{ij} = A_j F_{ji} \tag{1}$$

where A_i is the surface area of radiation exchange element i and F_{ji} is the view factor, defined as the fraction of radiant heat leaving element j and incident on element i (ref. 6). In the calculation of view factors for the external radiation exchanges (where element i represents the space element and element j is any radiation exchange element on the wing or fuselage surface), F_{ji} is taken to be unity. Therefore, according to equation (1), $F_{ij} = A_j/A_i$.

The thermal model (not shown) for WS134 is separated into three sections — the forward glove, the wheelwell, and the aft section. The glove section has one bay, the wheelwell cavity has one bay, and the aft section has three bays. Internal radiation view factors were computed separately for each section. The large complex mass of the landing gear system was represented by a single eight-node solid conduction (K81) element. Wing stations 240 (fig. 7) and 328 (fig. 8) have four and three bays, respectively; internal radiation view-factor calculations were determined for each bay. For FS877 the entire cross section had to be used for the internal radiation view-factor calculations.

The reradiating emissivity value used for the internal heat flux calculations was 0.667, based on an emissivity value of 0.80 used for the aluminum structure. For the external radiation heat flux calculations, the emissivities used were 0.85 for HRSI tiles, and 0.80 for the LRSI tiles and FRSI material.

The HRSI and LRSI tiles were modeled in two configurations, one using 80-percent and the other using 100-percent TPS thickness values. The 80-percent values were

used to account for gap tile heating. The FRSI is a flexible insulation without gaps and remained at 100-percent thickness in the thermal models.

AERODYNAMIC HEATING

The external-surface aerodynamic heating rates and the surface static pressures for the thermal analysis were obtained by a NASA heating program called theoretical thin-skin (THEOSKN). The THEOSKN program solves the one-dimensional thin skin heating equation and computes time histories of surface temperatures, heating rates, heat-transfer coefficients, and skin friction. The input data consist of altitude, Mach number or velocity, and angle of attack time histories (fig. 2). The thermodynamic and transport properties of air used in this analysis are given in reference 7.

The heating rates for the lower surfaces of WS134, WS240, and WS328 were computed assuming laminar flow up to t = 1160 sec of the trajectory and turbulent flow from t = 1160 sec until the end of the flight. The laminar heat transfer was computed by relating heat transfer to a skin-friction equation through a modified Reynolds analogy. In this analysis, the Blasius incompressible skin-friction equation (ref. 8) was related to heat transfer by the Prandtl number to the negative sixtenth power. Compressibility effects were accounted for by using Eckert's reference enthalpy transformation (ref. 9). Details of this method for calculating heat transfer at hypersonic speeds are given in reference 10. The turbulent heat transfer was computed by a similar procedure, except that the van Driest transformation (refs. 11 and 12) was used to account for compressibility and the Reynolds analogy factor was assumed to be a constant value of 1.1.

The boundary-layer flow on the upper surface of bay 1 at WS328 and at WS240 was assumed to be attached. The rest of the upper surface of the wing was assumed to be in a region of separated flow. The heat transfer for the attached flow areas was computed using the same heat-transfer codes used to calculate the lower surface heating. To calculate the heating rates for the separated areas on the upper surface, the heat-transfer codes were empirically modified. Empirical corrections were determined from comparisons with previous flight-measured data.

Heating rate calculations for FS877 assumed that the transition from laminar to turbulent heating occurred at t = 1100 sec. The laminar heat-transfer values for the lower fuselage and the leading edge of the glove were calculated using the infinite swept cylinder theory and the heat-transfer theories of Fay and Riddell (ref. 13) and Lees (ref. 14). The heat transfer on the lower glove was increased by 20 percent, as suggested by wind-tunnel test results. The turbulent heat-transfer coefficients were computed by the method given in reference 15.

The heating rates for the upper fuselage were calculated using empirical relationships derived from comparisons between the calculated surface temperatures and the measured data obtained from previous shuttle flights.

RESULTS AND DISCUSSION

TPS Surface Temperatures

Wing station 134. – Flight temperature measurements were made on the shuttle near WS134 at 6 locations on the lower surface and at 10 locations on the upper surface. These measurements, as shown in figure 10, were made at the outer surface of the TPS. The measured and the calculated temperatures for the lower surface are shown in figures 11(a) to 11(f). As shown, peak temperatures ranged from 1710°F, on the forward glove area to 1430°F on the aft section (bay 4) of the wheelwell. The temperature data show transition from laminar to turbulent flow occurring at t = 1100 sec. At t = 1500 sec into the profile, forced convective cooling drove the measured TPS surface temperatures below the calculated values. Forced convective cooling was not included in the calculated temperature time histories shown because it was found to unduly increase the computing time; however, this cooling had a negligible effect on the structural temperatures.

Measurements obtained from two locations on the lower glove (V09T9201 and V07T9654) showed peak temperatures of 1710°F and 1700°F, respectively. As shown in figure 11(a), temperature measurements at V09T9201 are in very good agreement with the calculated values, and values from V07T9654 shown in figure 11(b) were in fair agreement with the predicted results. As can be seen in figure 11(b), the measured temperatures were higher by approximately 150°F during the high-heating portion of the profile. Temperatures measured on the lower surface, shown in figures 11(c) to 11(e), are in good agreement with the calculated values. As shown in figure 11(f), the measured data in the aft portion of the last bay showed a peak temperature of 1430°F and are in good agreement with the calculated temperatures.

The upper surface temperature comparisons are shown in figures 12(a) to 12(h). The measured temperatures on the upper surface are quite low. Peak temperatures of 330°F and 260°F occurred in the upper glove region at V09T9163 and V07T9602, respectively. As shown in figure 12(a), the calculated values are in fair agreement with the measured data. The measured temperatures in figure 12(b) are significantly lower than the calculated values during the high-heating portion of the profile. In the wheelwell section, the measured temperatures were quite low, with varying peak temperatures of 360°F, to 60°F. These temperature comparisons are shown in figures 12(c) to 12(f). The predicted values are higher than the measured data but are in fair agreement, considering the low magnitude of these temperatures. Peak temperatures of 170°F, 80°F, and 160°F were measured at the three locations in bay 3; these peak temperatures are shown in figures 12(g) and 12(h). On joint location 614, shown in figure 12(g), two temperature measurements (V07T9606 and V09T9162) were plotted. Joint location 614 is in close proximity to both of these measurements. The measured surface temperatures show an increase at t ≈ 1200 sec. This increase in the surface temperature occurred at the same time as a rapid change in the angle of attack. In light of the low peak temperatures on the upper surface and the complex nature of the flow fields, the calculated temperatures are considered in fairly good agreement with the measured data.

Wing station 240. – The flight-measured temperature data were obtained on the shuttle orbiter at the locations shown in figure 13. Locations are shown for the TPS surfaces and for the aluminum skins, spars, and webs. The measured and the calculated

temperatures are shown in figures 14(a) to 14(g) and figures 15(a) to 15(d). As shown, transition from laminar to turbulent flow occurred at t = 1100 sec. Peak temperatures of 1780°F, 1600°F, 1600°F, and 1490°F occurred at the forward locations of the lower surface. Measured temperatures obtained from V07T9666 (fig. 14(a)) are in excellent agreement with the calculated values. Measurements from V07T9668, V09T9171, and V07T9670 (see figures 14(b), 14(c), and 14(d)), show that the measured temperatures are in very good agreement with the calculated values.

The last four lower-surface TPS measurements are located in bays 3 and 4. Measurement V07T9671 is located in bay 3. The measured temperatures at this location show a peak temperature of 1480°F (fig. 14(e)); the measured data are in very good agreement with the calculated values. Measurements V07T9181 and V07T9674 are located at bay 4. Shown in figures 14(f) and 14(g) are the data from V07T9181 and V07T9674. The peak temperatures at these two locations are 1545°F and 1350°F. The comparisons between the measured and the calculated results at these two locations are considered in fair and good agreement, respectively.

Four TPS upper surface temperature comparisons are shown in figures 15(a) to 15(d). Peak temperatures of 590°F, 470°F, 75°F, and 105°F, were measured at V07T9622, V07T9623, V07T9625, and V07T9627, respectively. Comparisons between calculated and measured data obtained from V07T9622 and V07T9623 located in bay 1 are shown in figures 15(a) and 15(b), respectively. As can be seen, the agreement between the measured and the calculated data is good in figure 15(a) and very good in figure 15(b). Figure 15(c) shows the data from V07T9625 located in bay 3. Calculated temperatures at this location overpredicted the measured temperatures, but the agreement is still considered satisfactory. Results from measurement V07T9627 in bay 4, is shown in figure 15(d). As shown in this figure, the peak temperature is 105°F and the agreement between the measured and predicted temperatures is good.

Wing station 328. - Shuttle flight temperature measurement locations for WS328, which has only three bays, are shown in figure 16. Temperatures obtained from seven lower-surface and three upper-surface locations are shown in figures 17(a) to 17(g) and figures 18(a) to 18(c), respectively. Also shown in these figures are the calculated temperatures obtained from the SPAR thermal analysis. Measured temperatures on the lower surface showed peak temperatures varying from 1910°F at bay 1 to 1400°F at bay 3. Figures 17(a) and 17(b) show the comparisons of measured and calculated temperatures for bay 1. In figure 17(a), the measured data between t = 850 to 1000 sec does not follow the same trend as the other temperature measurements on the lower surface, therefore this data is considered to be erroneous. With the exclusion of this portion of the measured data, the overall agreement with the predicted temperatures is considered good. Temperatures obtained from V07T9705 at JLOC 525 are shown in figure 17(b). As can be seen, the predicted temperature time history somewhat under-predicted the measured data. The measured peak temperature at this location is 1840°F, and the comparison between the measured and the calculated values are considered fairly good. The dip in the flight-measured temperatures from t = 1500 to 2000 sec was due to forced convective cooling which was not accounted for in the calculations.

Figures 17(c), to 17(e, show data from bays 2 and 3 of WS328. The measured data at these three locations, V07T9702, V07T9708, and V07T9710 show an upward shift after transition to turbulent flow. This shift is not reasonable and may have been caused by a malfunction in the shuttle data acquisition system. Measurements from V07T9710,

shown in figure 17(e), also show what appears to be questionable data between t = 300 to 400 sec. Discounting the transition temperatures at these three locations, the peak temperatures are 1720°F, 1720°F and 1620°F, respectively. Despite the shift in the measured data after transition from laminar to turbulent flow, the temperature comparisons at these three locations are considered good.

Data from V07T9704 is shown in figure 17(f). The measured data are in fair agreement with the calculated temperatures and attained a value of 1400°F. Data from the aft-most measurement (V07T9711) on the lower surface is shown in figure 17(g). The measured data immediately after transition to turbulent flow are higher than the calculated values (this is also true for figures 17(a) to 17(e)). This is probably fortuitous because the calculated temperatures during the turbulent peak heating were not printed out at frequent enough intervals to obtain the maximum temperature. The measured temperatures in figure 17(e) between t = 300 sec and 900 sec are questionable, but the overall agreement with the calculated values is considered good.

Three temperature measurement locations on the upper surface of WS328 are in close proximity to a spar web (fig. 16). Comparisons between measured and calculated temperatures at these three locations on the upper surface of WS328 are shown in figures 18(a) to 18(c). Locations V07T9634 and V07T9635 show peak temperatures of 600°F and 380°F, respectively (figs. 18(a) and 18(b)). However, measurement V07T9636 yielded a peak temperature of only 250°F (fig. 18(c)). The discrepancy between the measured and the calculated values between t = 1500 to 1700 sec resulted from inaccurate heating rates computed by the THEOSKN program. The THEOSKN program does not account for conduction; therefore, it computed inaccurate surface temperatures during this part of the flight profile, which resulted in incorrect heating rates. Nevertheless, comparisons between the measured and the calculated temperatures, shown in figures 18(a), to 18(c) are considered good.

Fuselage station 877. – Shuttle temperature measurement locations for the TPS surface and the internal structure at FS877 are shown in figure 19. Measured and predicted temperatures for five TPS surface locations are shown in figures 20(a) to 20(e). Figure 20(a) shows a peak temperature of 1720°F for V09T9201 located on the lower glove; the measured and the calculated results are in excellent agreement. Data from V09T9509 and V09T9521, located on the lower fuselage surface, are shown in figures 20(b) and 20(c) and have peak temperatures of 1600°F and 1500°F, respectively. The measured temperatures are in good agreement with the calculated values. Shown in figure 20(d) are measured and calculated temperatures for V09T9163 on the upper glove. A peak temperature of 330°F was measured at this location, and the agreement between the measured and the calculated values is considered good. Figure 20(e) shows the measured and the calculated temperatures for measurement V09T9518 located on the payload bay door. Although some discrepancies exist between the measured and the calculated values, the agreement is considered fair.

Aluminum Structural Temperatures

Wing station 134. – Five flight temperature measurements were made on the lower substructure in addition to six on the upper substructure of the shuttle. These locations are shown in figure 21. The measured results are compared to calculated results based on an 80- or 100-percent TPS thickness value and are shown in fig-

ures 22(a) to 22(i). The 80-percent TPS value that was used only on HRSI and LRSI tile locations was to account for gap tile heating effects. The FRSI material used primarily on the upper surface is a felt material and does not have existing gaps. The initial temperature for all calculations was assumed to be 0°F. As shown in figures 22(a) to 22(f) and 22(i), this was not always a good assumption. Although the discrepancy between the assumed initial temperatures and the measured initial temperatures would have improved the agreement between the measured and the calculated profiles, the magnitude of this improvement did not justify the cost of making additional computer runs. All the measured data show a significant deviation from the calculated values starting at t = 1800 sec. This deviation could be attributed to the internal forced convective cooling caused by external cool air entering the shuttle which was not accounted for in the calculations. Data from measurement V09T9205 is shown in figure 22(a). The measured temperatures appear to agree with the calculated values up to touchdown, assuming 100-percent TPS thickness. However, if the starting temperature for the SPAR calculations were adjusted to agree with the measured data, the calculated temperatures using an 80-percent TPS thickness would be in better agreement with the measured data. Although the correction on shifting the startup temperature is not a one-to-one shift on the temperature curve, it still has an effect on the overall comparison.

Figure 22(b) shows data from two measurements (V51T9210 and V51T9310) located on the lower skin of the wheelwell door. One measurement is located on the left side of the wing and the other measurement is located at the same coordinates on the opposite side of the wing, respectively. As can be seen the temperatures measured on the right side of the wing are as much as 43°F lower than on the left side of the wing. This difference is thought to be caused by differences in the forced internal convection cooling in the left and right sides of the wing. The data for the left side of the wing prior to t = 1100 sec were not available. It should be noted that some flight-measured temperatures were recorded from a ground tracking station; hence, data prior to t = 1100 sec were lost during the communications blackout portion of reentry. Discounting the measured temperatures aft of 1800 seconds and adjusting the starting temperatures, the measured data would agree best with the calculated values using the 100-percent TPS thickness. Shown in figure 22(c) are data from measurement V09T9145. As shown, the measured temperatures are in very good agreement with the predicted values using the results for the 80-percent TPS thickness. A peak temperature of 153°F occurred at t ≈ 1700 sec for this location. V09T9106 is located on the spar cap between bay 3 and bay 4. The measured and the calculated temperatures for this location can be seen in figure 22(d). A peak temperature of 98°F was reached, and the measured temperatures are in excellent agreement with the predicted values using the 80-percent TPS thickness.

The upper surface aluminum structural temperature comparisons are shown in figures 22(e) to 22(j). Measured temperatures on the upper surface are quite low, less than 80°F. Temperatures from measurement V09T9157 shown in figure 22(e), are in very good agreement with the calculated values for the 80-percent TPS thickness. The measured data shows a bump in the temperatures at t = 1500 sec with a gradual rise in temperature to 72°F after touchdown.

Shown in figure 22(f) are the measured and the calculated temperatures for location V09T9160. The temperatures calculated using 100-percent TPS thickness are about 20°F lower than the measured data. However, if the calculated values were adjusted to coincide with the initial measured temperature, good agreement with the

measured data would be obtained. A near-peak temperature of 77°F can be seen at 3000 sec. Measurements V09T9211 and V09T9311 are located on the left and right sides, respectively, on the wheelwell upper skin. Measured-temperature time histories for these locations are almost identical, as can be seen in figures 22(g) and 22(h). Measurement V09T9211 measured a peak temperature of 54°F, and V09T9311 measured a peak temperature of 52°F. The calculated values overpredicted the measured data from t = 1100 to 1500 sec. This is due to a higher calculated heating rate on the TPS surface, as indicated in figure 12(e).

Data from measurement V09T9155 are shown in figure 22(i). As can be seen, the measured and the calculated results for both the 80- and 100-percent TPS thickness thermal models are quite close, and the comparisons are considered good for both cases. Shown in figure 22(j) are temperatures from V09T9107 located on the upper spar cap between bays 3 and 4. The calculated results for the SPAR thermal model with 100-percent TPS thickness are in excellent agreement with the measured data. It should be mentioned that due to the difficulty in determining the local flow conditions on the TPS upper surfaces, and due to the low heating rates obtained on the upper TPS surface, the overall comparisons between measured and calculated results for the aluminum structure are considered good.

Wing station 240. -- Shown in figures 23(a) to 23(w) are comparisons of the measured and the calculated temperature results. A total of 23 temperature measurements were located on the aluminum substructure as shown in figure 13. Five measurements were on the lower skin, two were on the lower rib caps in bay 3, two were on the lower spar caps, four were on rib truss members, five were on the upper surface skin, two were on the upper surface spar caps, two were on the upper surface rib cap, and one was on a spar web. Temperature measurements from V09T9143 are shown in figure 23(a). The measured flight temperature values are between the calculated results for the 80- and 100-percent calculated results up to t = 1800 sec. It appears that the 80-percent TPS thickness values that were used are a little conservative; if the gap heating effects were properly accounted for, the agreement between the measured and the calculated results would be excellent. Figure 23(b) shows the measured temperatures from measurement V09T9175. A maximum temperature of 111°F occurred at this location, and the comparisons between the measured and the calculated results are good up to t = 1800 sec. As was noted in the previous section, when determining the agreement between the measured and the calculated temperatures, only the first 1800 sec of the flight profile was considered. Comparisons between measured and calculated lower-skin temperatures for bay 3 from measurement V09T9124 are shown in figure 23(c), and those from measurement V09T9129 are shown in figure 23(d). The data in figure 23(c) agree quite closely with values calculated using the 80-percent TPS thickness, while the data in figure 23(d) agree with the 100-percent TPS thickness values. It is not known why the data in figure 23(c) agree with the 80-percent thickness values when the other skin measurements agree more closely with the 100-percent TPS values. Data obtained on the lower skin of bay 4 (V09T9185) are shown in figure 23(e). The predicted values using the 100-percent TPS thickness values are in very good agreement with the measured data. A peak temperature of 117°F occurred at this location.

Shown in figures 23(f) and 23(g) are two temperature comparisons for the lower rib cap locations. Measured flight temperatures from V09T9119 are in very good agreement with the results for the SPAR thermal model using the 100-percent TPS thickness. Measured data from V09T9123 agrees best with the calculated values

using the 100-percent TPS thickness. Measurement V09T9128 is located on the spar cap between bays 3 and 4. The measured and the calculated temperatures are shown in figure 23(h) for this location. As can be seen the calculated results for the 80-percent TPS thickness thermal model agree slightly better than the 100-percent TPS thickness. Shown in figure 23(i) are comparisons between the measured and the calculated results from measurement V09T9113, located on the lower spar cap aft of bay 4. With a slight shift of the calculated results for the 80-percent TPS thickness model to match the measured initial temperature, the agreement between the measured and the calculated results can be considered good. Figures 23(j) to 23(m) show the measured and the calculated temperatures for the vertical and diagonal trusses of bay 3. The agreement between the measured and the calculated values at the bottom and top of the vertical truss (figs. 23(j) and 23(l)), respectively, is fairly good. However, the agreement between the measured and the calculated temperatures at the center of the vertical truss (fig. 23(k)) and the center of the diagonal trusses (fig. 23(m)) is poor. This poor agreement is probably caused by the neglect of truss radiation elements in the thermal model. Internal radiation elements were added in the SPAR model for all structural components except the trusses.

Data for five upper surface aluminum skin temperature measurements are shown in figures 23(n) to 23(q). The most forward measurement V07T9152 is located in bay 1. As shown in figure 23(n), the measured temperatures at this location are in very good agreement with the predicted values for the SPAR thermal model with the 100-percent TPS thickness. A peak temperature of 116°F occurred at this location. Shown in figure 23(o) are data from V09T9158. The reason for the bump in the measured data at t = 500 sec is unknown. Excluding this anomaly, the measured temperatures are in fairly good agreement with the predicted values for the thermal model with the 100-percent TPS thickness. Figures 23(p) and 23(q) show data from two measurements, V09T9115 and V09T9125, located on the upper skin of bay 3. Both sets of measured data are in fair agreement with the predicted temperatures using the 100-percent TPS thickness thermal model. Located in bay 4 on the upper skin is measurement V09T9153. As can be seen in figure 23(r), temperature agreement between the measured and the calculated results using the 100-percent TPS thickness SPAR thermal model is fair. Shown in figures 23(s) and 23(t) are two upper rib cap temperature comparisons. Measured flight temperatures from V09T9117 are in poor agreement with calculated values during the early part of the flight profile, but the agreement improves during the latter portion of the profile. It should be noted that the measured temperatures from t = 0 to 1200 sec are much lower than those calculated. Measured temperatures shown in figure 23(t) for measurement V09T9122 located in bay 3 on the upper rib cap agree best with the calculated data from the thermal model with the 100-percent TPS thickness.

Figure 23(u) shows results from V09T9126 located on the upper spar cap between bays 3 and 4. As shown, the measured temperatures are in fairly good agreement with the calculated results obtained for the SPAR thermal model with the 100-percent TPS thickness. Measurement V09T9112 is located on the upper spar cap aft of bay 4. The measured and the calculated temperatures can be seen in figure 23(v) for this location. It appears that the flight-measured temperatures are below the set lower limit of the instrumentation from t = 0 to 1000 sec of the flight profile. From t = 1000 to 3000 sec, the measured data are in very good agreement with the calculated results for the SPAR thermal model with the 100-percent TPS thickness.

Shown in figure 23(w) are comparisons of the measured and the calculated temperatures from V09T9127 located on the web between bays 3 and 4. As can be seen, the measured temperatures are in very good agreement with calculated values for the SPAR thermal model with 100-percent TPS thickness.

Wing station 328. - The measured and the calculated aluminum structural temperatures are shown in figures 24(a) to 24(c). There are two temperature measurement locations on the lower skin, and one on the upper skin, as shown in figure 16. Measurement V09T9142 is located in bay 1 on the lower skin. The measured data obtained from V09T9142 are shown in figure 24(a). As can be seen, the 80-percent TPS thickness is in excellent agreement with the measured data until internal convection cooling began at t ≈ 1600 to 1700 sec. A peak temperature of 116°F is shown at 3000 sec. Figure 24(b) shows the comparison of measured and calculated results at measurement V09T9358. The measured temperature shows a peak value of 122°F; for the first 1600 sec of the flight, the data are in fairly good agreement with the results for the thermal model with the 80-percent TPS thickness. As was the case for the previous measurements, after t = 1600 sec, the measured data show a sharp deviation from the calculated results due to the internal forced convection cooling that was not accounted for in the analysis. Shown in figure 24(c) is the data from measurement V09T9152 and the results from the SPAR analysis. The agreement between the measured and the calculated temperatures is considered fair.

Fuselage station 877. — The flight temperature measurement locations for this fuselage station are shown in figure 19. The measured and the predicted temperatures for 11 aluminum structural locations are shown in figures 25(a) to 25(k). In figures 25(a) to 25(c) are the measured and the predicted temperature comparisons for the lower fuselage. Until internal convective cooling began, the measured data from V09T9525 and V09T9707 were in excellent agreement with the calculated results for the thermal model with the 100-percent TPS thickness. For measurement V09T9506, the measured temperatures overpredict the thermal model with the 100-percent thickness. Peak temperatures of 164°F, 188°F, and 134°F were measured at V09T9525, V09T9506, and V09T9507, respectively. Figure 25(d) shows comparisons of the measured and the calculated temperatures for V09T9205 and V09T9210 on the lower glove. The comparisons between the measured and the calculated results for both locations are considered fair. The decrease in the calculated temperatures from t = 0 to 400 sec may have been caused by improper radiation exchange factors. Upper-glove temperature comparisons are shown in figures 25(e) and 25(f). As can be seen, the measured temperatures from V09T9160 are in poor agreement with the calculated values, and measured temperatures from V09T9157 are in fairly good agreement with calculated values using the 100-percent TPS thickness model. Measurement V09T9708 is located in the corner where the sidewall and upper glove meet. The measured and the calculated results for this location are shown in figure 25(g). The discrepancies between the measured and the calculated temperatures are probably due to lower-than-expected external aerodynamic heating or internal forced convective cooling, or both.

Shown in figures 25(h) to 25(j) are the measured and the predicted temperature comparisons for the fuselage sidewall. As can be seen, the measured temperatures from V09T9709, shown in figure 25(h) are lower than the calculated results; this difference can be attributed to internal convective cooling. Measured temperatures at V09T9377 are shown in figure 25(i). The agreement between the measured and the predicted temperatures using the thermal model with 100-percent TPS thickness is very good. The measured and the calculated temperatures for V09T9501 are shown in

figure 25(j). The agreement between the measured data and the calculated results using the thermal model with the 100-percent TPS thickness are excellent. In figure 25(k) are measured and calculated temperature comparisons for V09T9502, located on the longeron. The agreement between the measured and the calculated values is considered fairly good. It should be noted that V09T9501 (fig. 25(j)) and V09T9377 (fig. 25(i)) are in close proximity to V09T9502 and the agreement of the measured and the calculated temperatures for these two locations is very good to excellent. Therefore, the lower measured temperatures on the longeron are probably due to the effects of internal forced convective cooling.

CONCLUDING REMARKS

Measured temperature time histories at various stations of the OV102 space shuttle orbiter, Columbia, for the space transportation system number 5 (STS-5) flight reentry trajectory are presented and compared with calculated values. The calculated temperatures were obtained from a finite-element thermal analysis computer program called structural performance and resizing (SPAR). Twenty TPS lower-surface temperature locations and 16 TPS upper-surface temperature locations are presented for wing stations (WS) 134, 240 and 328. 37 structural temperature time histories at different stations of the wing are shown. Also presented are five surface temperatures and 12 substructure temperatures for the fuselage at fuselage station (FS) 877. The structural temperature distribution obtained in this investigation can be used to calculate thermal stresses using the SPAR structural models. Measured peak surface temperatures of 1710°F (V09T9201), 1780°F (V07T9666), and 1910°F (V07T9700) occurred on the lower surface of WS134, WS240, and WS328, respectively. For the benign trajectory of the STS-5, the transition from laminar to turbulent flow for the entire lower surface occurred at approximately 1100 sec into the reentry profile. Peak upper surface temperatures of 330°F (V09T9163), 590°F (V07T9622), and 600°F (V07T9634) were measured at WS134, WS240, and WS328, respectively. A peak surface temperature of 1720°F (V09T9201) occurred on the lower glove at FS877.

Measured aluminum and substructural temperatures were significantly below the design limit of 350°F. Peak measured aluminum structural temperatures of 153°F (V09T9145), 119°F (V09T9143) and 122°F (V09T9358) occurred on the lower skin of bay 3 (WS134), bay 1 (WS240), and bay 3 (WS328), respectively.

In general, the agreement between the measured and the calculated thermal protection system (TPS) surface temperatures was considered very good, and the agreement between the measured and the calculated aluminum structural temperatures were considered quite good. The agreement between the measured and the calculated temperatures may be improved by the following: (1) including internal forced convective cooling in the analyses, (2) using more accurate effective TPS thickness to account for gap tile heating, (3) including external forced convective cooling at the end of the heating cycle, and (4) fabricating a more refined mesh model to obtain a more detailed tem perature distribution. However, the increase in computer run times in addition to the required increased number of radiation view-factor calculations may make the use of a finer mesh impractical.

REFERENCES

1. Ko, William L.; Quinn, Robert D.; Gong, Leslie; Schuster, Lawrence S.; and Gonzales, David: Reentry Heat Transfer Analysis of the Space Shuttle Orbiter. NASA CP-2216, 1982, pp. 295-325.

2. Gong, Leslie; Quinn, Robert D.; and Ko, William L.: Reentry Heating Analysis of Space Shuttle With Comparison of Flight Data. NASA CP-2216, 1982, pp. 271-294.

3. Ko, William L.; Quinn, Robert D.; Gong, Leslie; Schuster, Lawrence S.; and Gonzales, David: Preflight Reentry Heat Transfer Analysis of Space Shuttle. AIAA-81-2382, Nov. 1981.

4. Marlowe, M.B.; Moore, R.A.; and Whetstone, W.D.: SPAR Thermal Analysis Processors Manual, System Level 16. NASA CR-159162, vol. 1, 1979.

5. Marlowe, M.B.; Whetstone, W.D.; and Robinson, J.C.: The SPAR Thermal Analyzer — Present and Future. Symposium on Computational Aspects of Heat Transfer in Structures, NASA CP-2216, 1982 pp. 35-50.

6. Sparrow, Ephraim M. and Cess, R.D.: Radiation Heat Transfer. Augmented ed. Hemisphere Publication Corp., Washington, DC, 1978.

7. Hansen, C. Frederick: Approximations for the Thermodynamic and Transport Properties of High Temperature Air. NASA TR R-50, 1959.

8. Schlichting, Hermann (J. Kestin, transl.): Boundary Layer Theory. Fourth ed., McGraw-Hill Book Co., Inc., New York, 1960.

9. Eckert, Ernst R.G.: Survey of Boundary Layer Heat Transfer at High Velocities and High Temperatures. WADC TR-59-624, Wright-Patterson AFB, Ohio, 1960.

10. Zoby, E.V.; Moss, J.N.; and Sutton, K.: Approximate Convective-Heating Equations for Hypersonic Flows. J. Spacecraft and Rockets, vol. 18, no. 1, Jan./Feb. 1981, pp. 64-70.

11. van Driest, E.R.: The Problem of Aerodynamic Heating. Aeronaut. Eng. Rev., vol. 15, no. 10, Oct. 1956, pp. 26-41.

12. Hopkins, Edwards J.; Keener, Earl R.; Louie, Pearl T.: Direct Measurements of Turbulent Skin Friction on a Nonadiabatic Flat Plate at Mach Number 6.5 and Comparisons With Eight Theories. NASA TN D-5675, 1970.

13. Fay, J.A.; and Riddell, F.R.; Theory of Stagnation Point Heat Transfer in Dissociated Air. J. Aeronaut. Sci., vol. 25, no. 2, Feb. 1958, pp. 73-85, 121.

14. Lees, L.: Laminar Heat Transfer Over Blunt-Nosed Bodies at Hypersonic Flight Speeds. Jet Propulsion, vol. 26, no. 4, Apr. 1956, pp. 259-269.

15. Beckwith, Ivan E.; and Gallagher, James J.: Local Heat Transfer and Recovery Temperatures on a Yawed Cylinder at a Mach Number of 4.15 and High Reynolds Numbers. NASA TR R-104, 1961.

TABLE 1. — NUMBER OF JOINT LOCATIONS AND ELEMENTS ON VARIOUS THERMAL MODELS

Thermal Model	Number of JLOCs	Number of elements							
		R21	R31	R41	K21	K31	K41	K61	K81
WS134	2075			304	397	23	457	50	890
WS240	920			137	139		287	1	341
WS328	916			103	91		236		360
FS877	605	124			250	6	516		

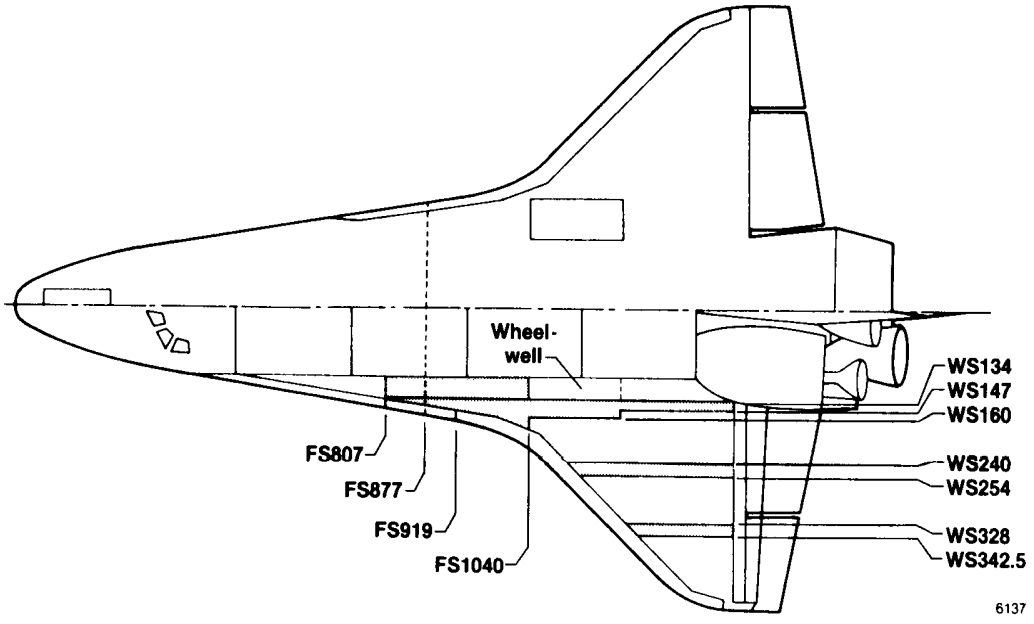

Figure 1. Locations of space shuttle wing stations and mid-fuselage cross sections that were analyzed.

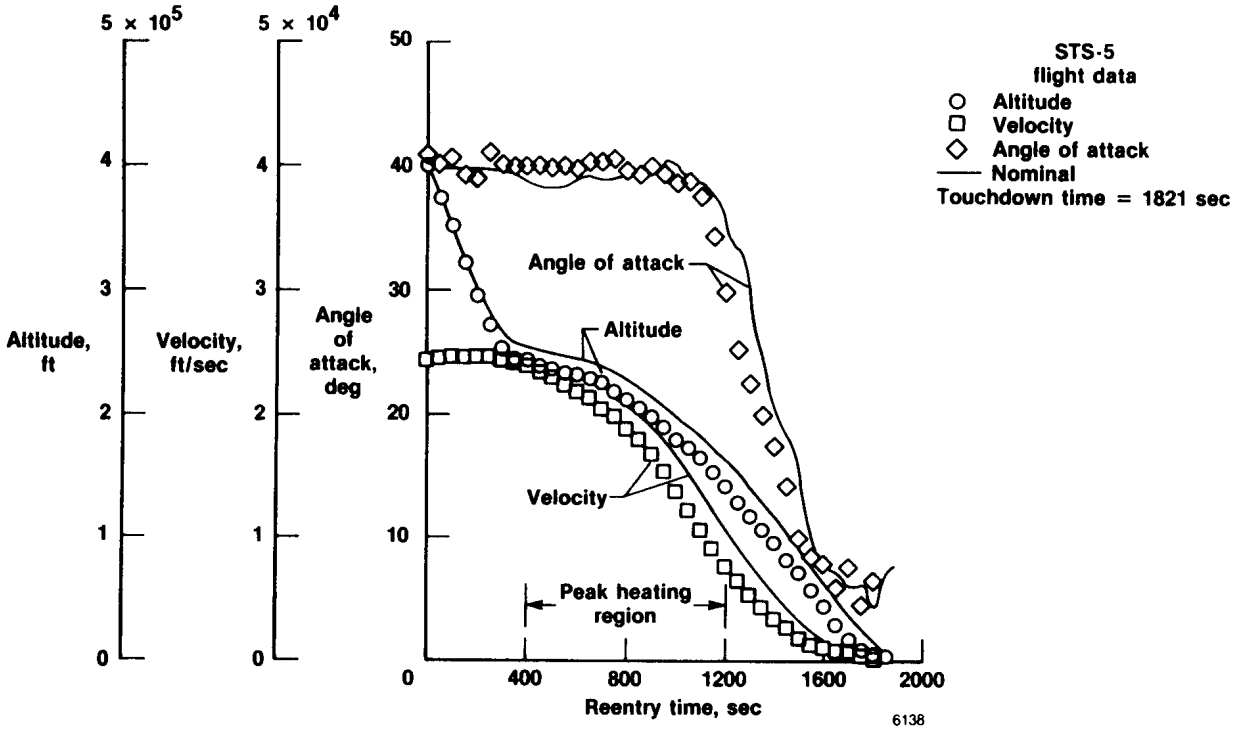

Figure 2. STS-5 reentry trajectory.

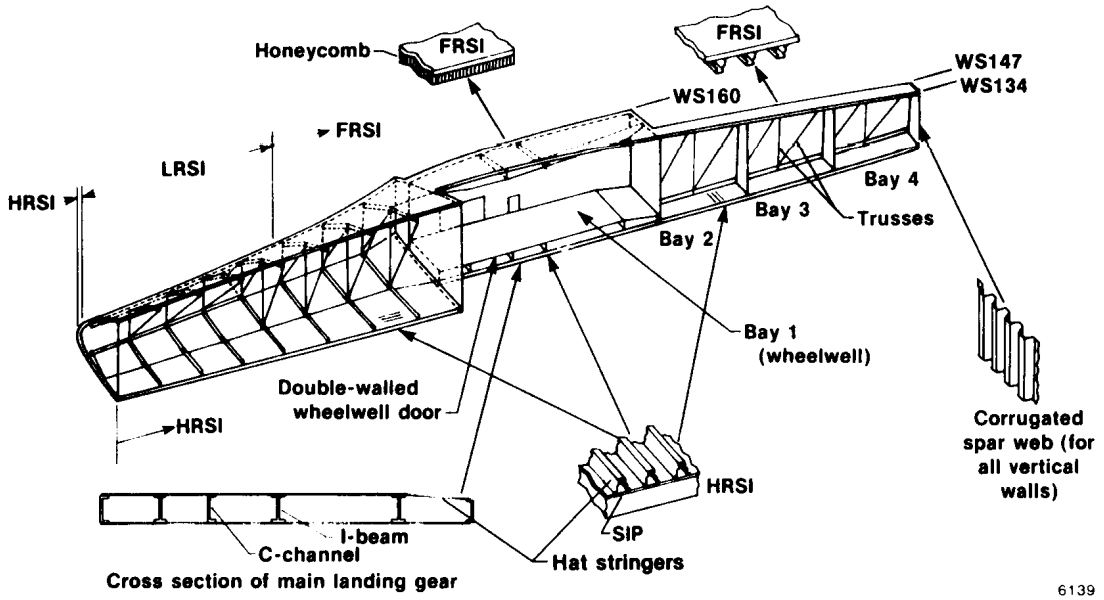

Figure 3. Geometry of the three-dimensional cross section at WS134.

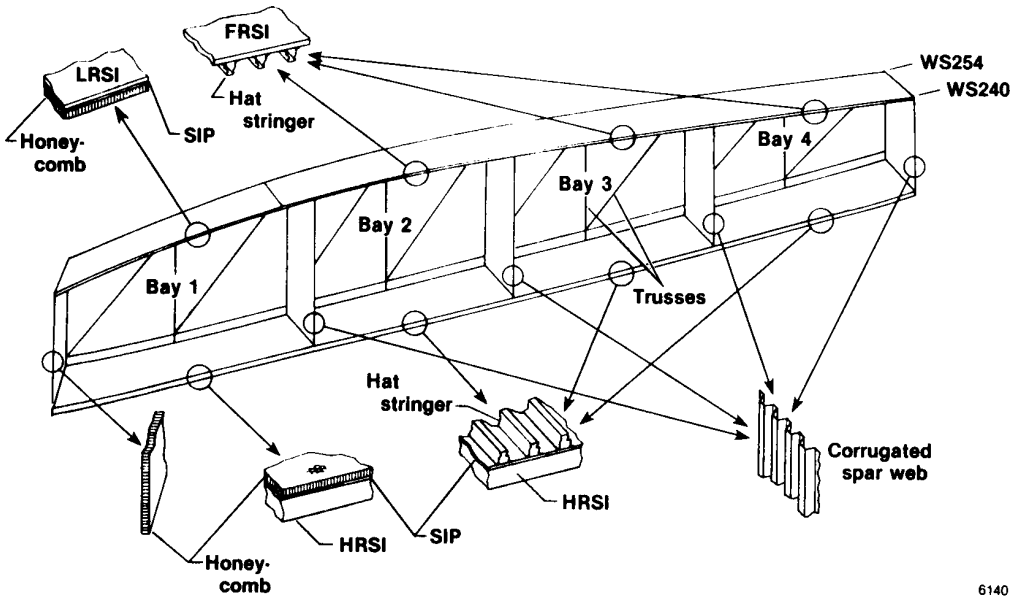

Figure 4. Geometry of the three-dimensional cross section between WS240 and WS254.

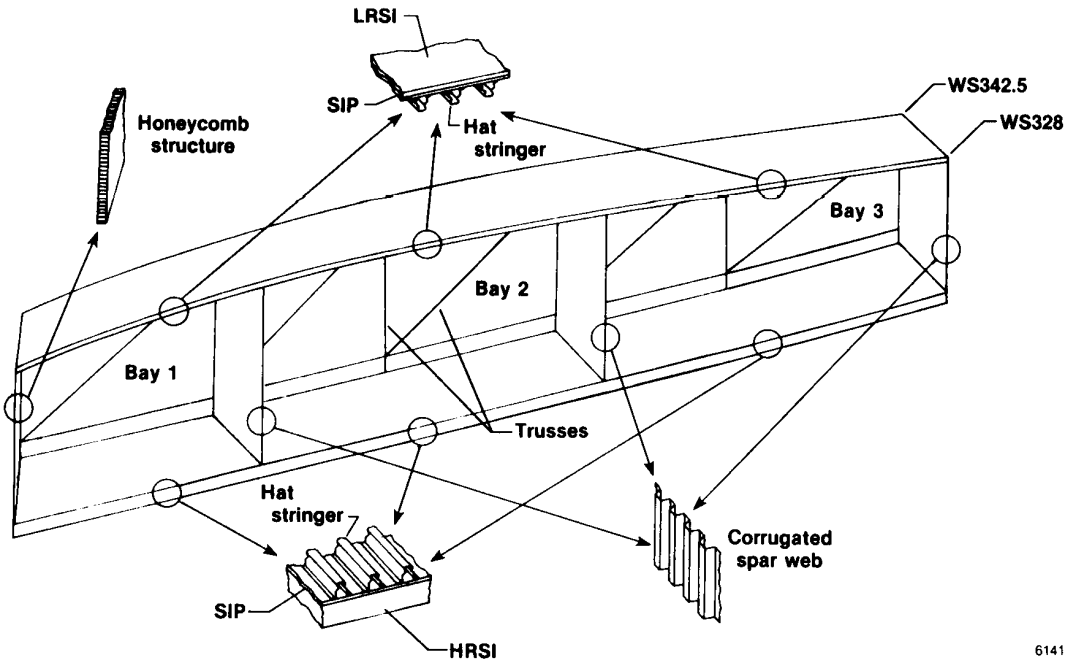

Figure 5. Geometry of the three-dimensional cross section between WS328 and WS342.5.

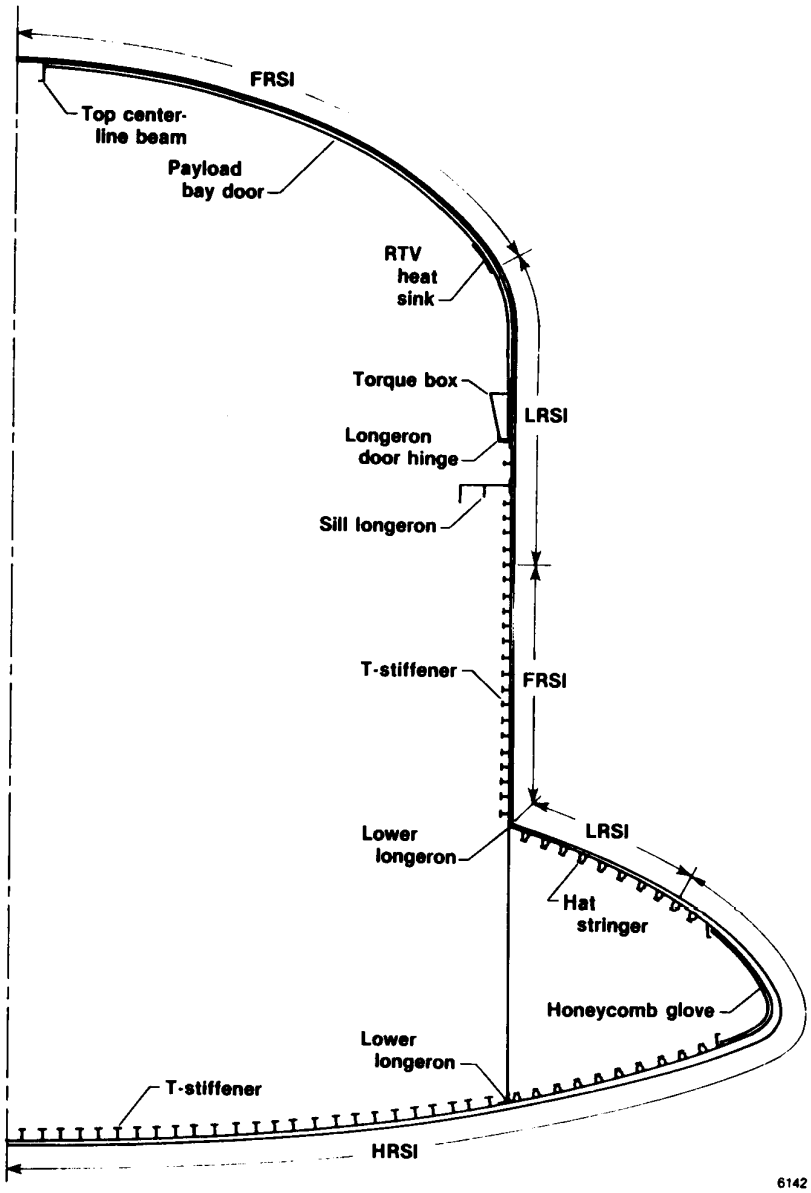

Figure 6. Geometry of two-dimensional cross section at FS877.

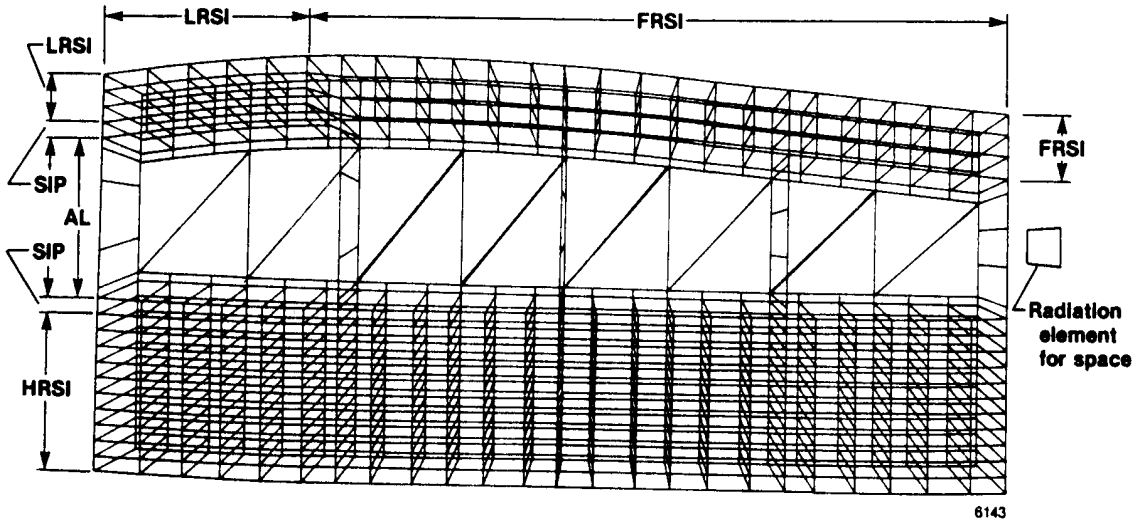

Figure 7. Three-dimensional SPAR finite-element thermal model for WS240.

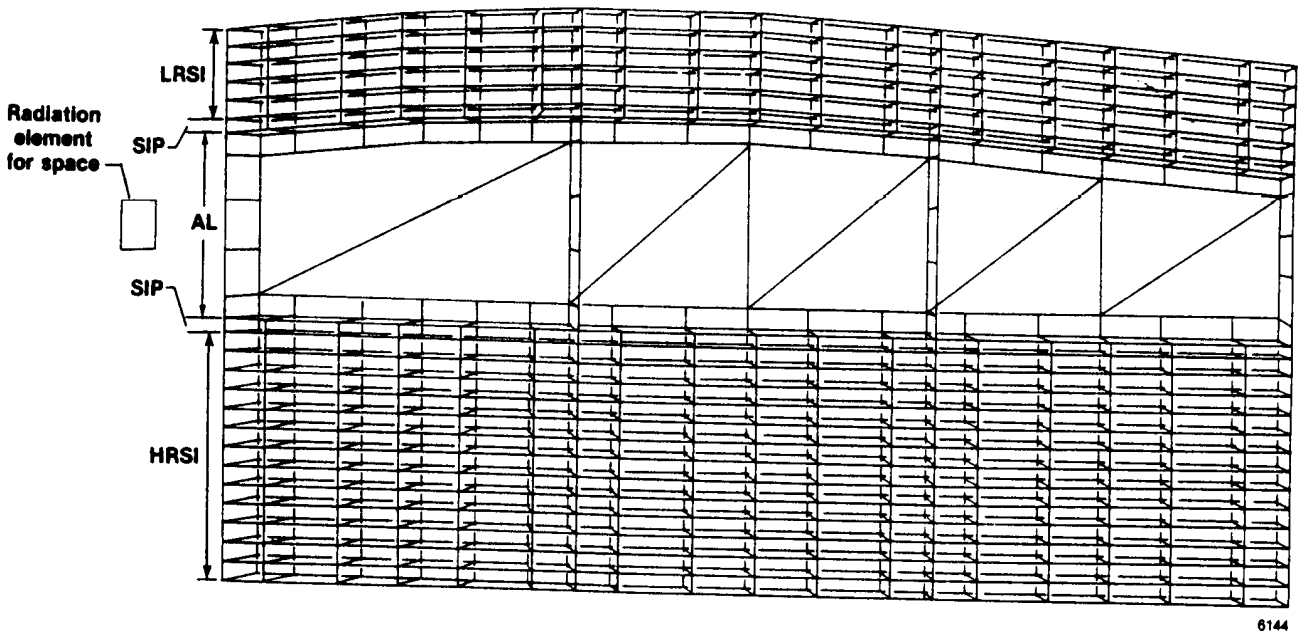

Figure 8. Three-dimensional SPAR finite-element thermal model for WS328.

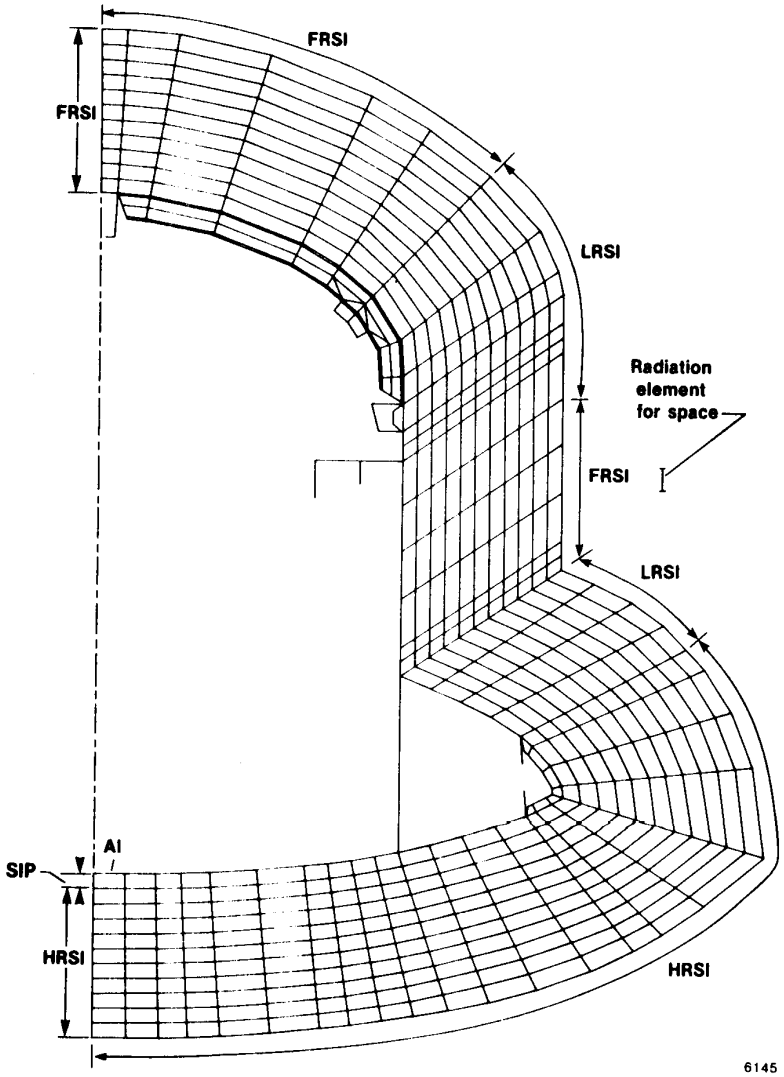

Figure 9. Two-dimensional SPAR finite-element thermal model for FS877.

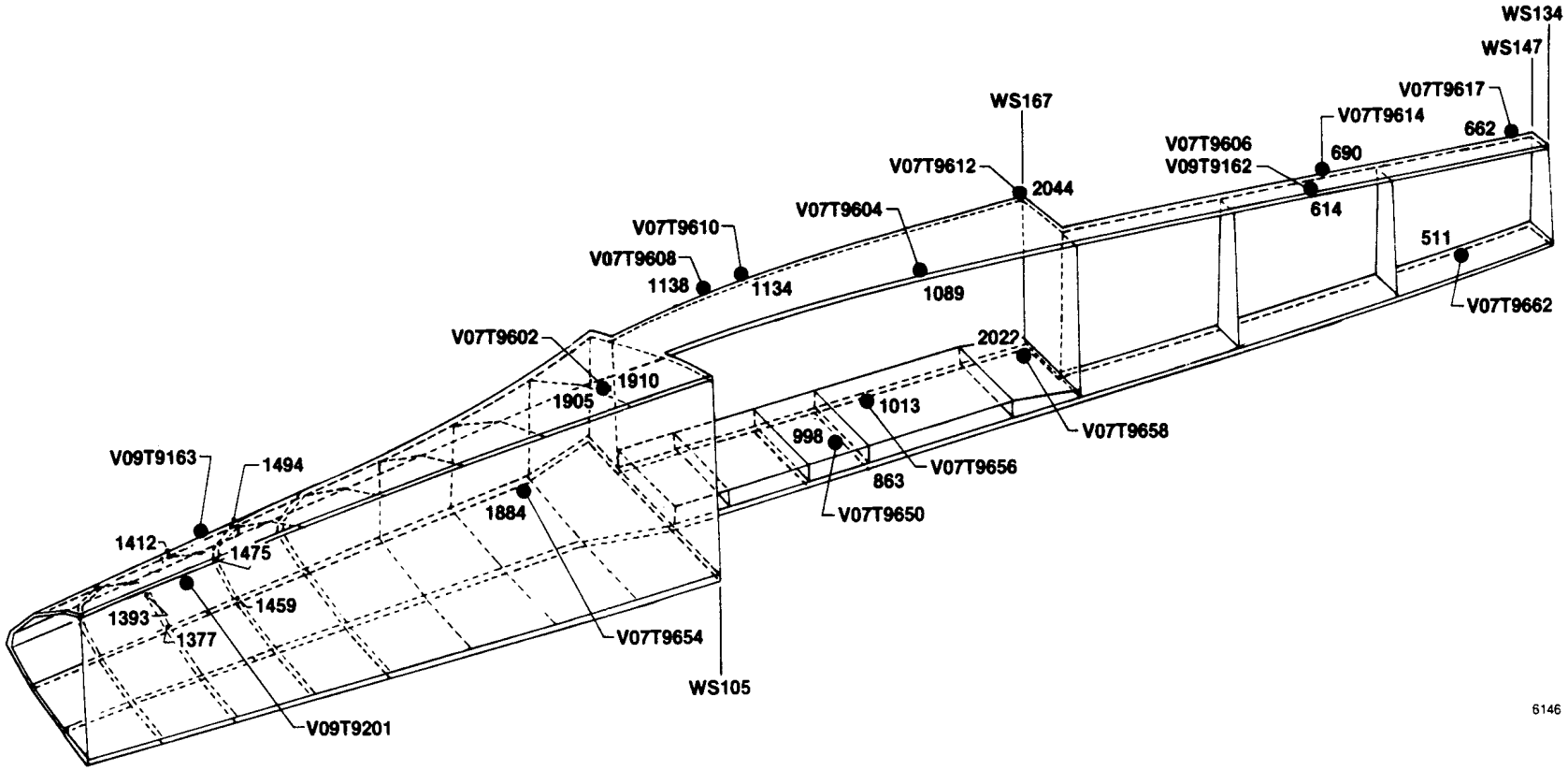

Figure 10. WS134 TPS surface temperature measurement locations and SPAR joint locations.

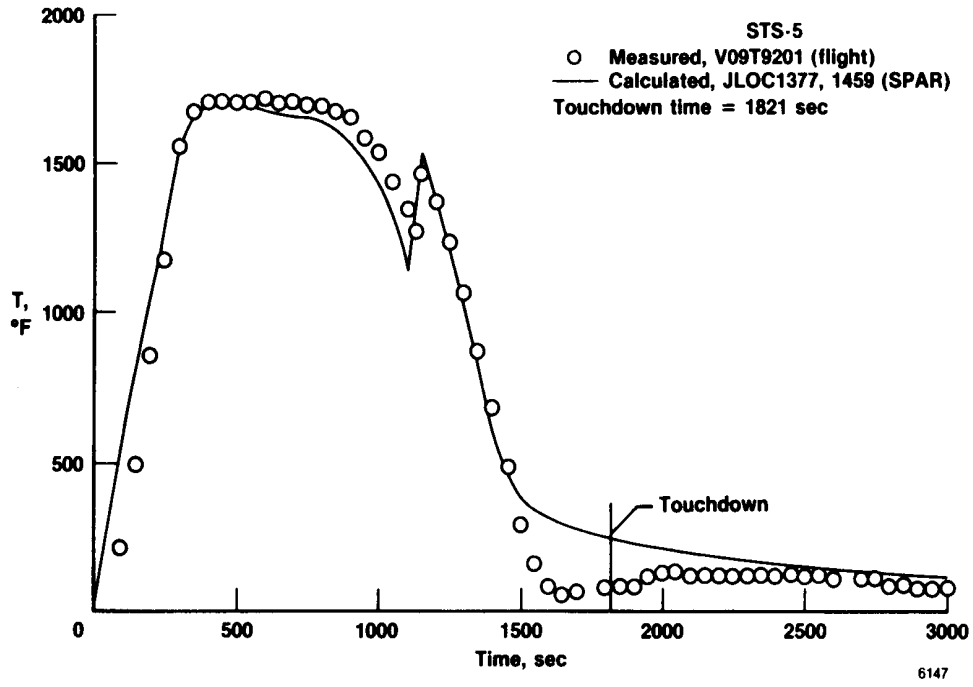

(a) Lower glove, part 1 of 2.

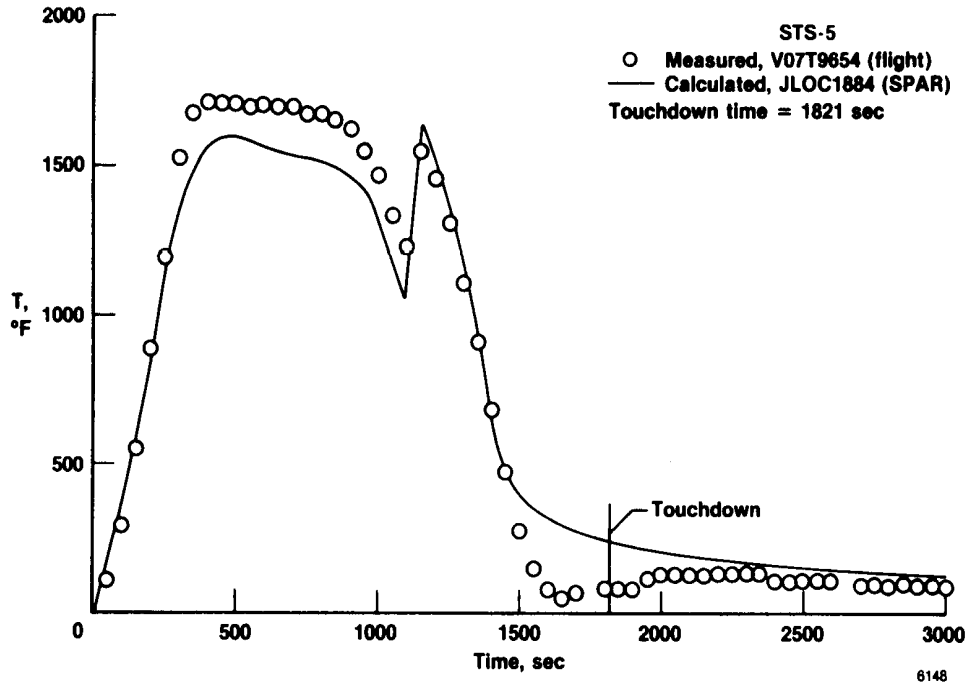

(b) Lower glove, part 2 of 2.

Figure 11. Comparisons of calculated and measured TPS lower surface temperatures, WS134.

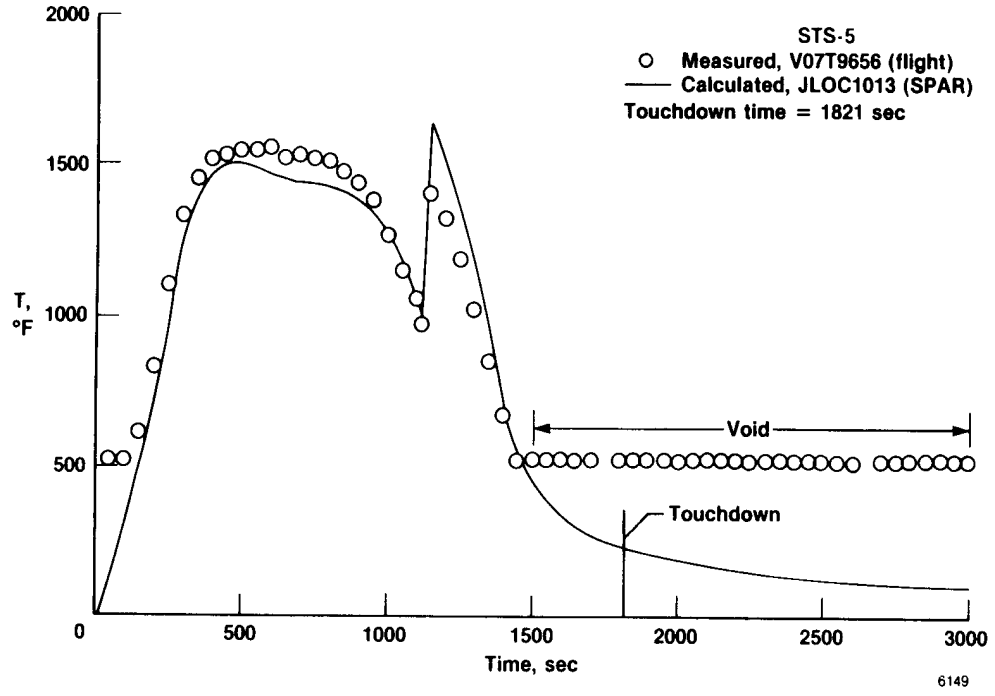

(c) Lower surface wheelwell, part 1 of 3.

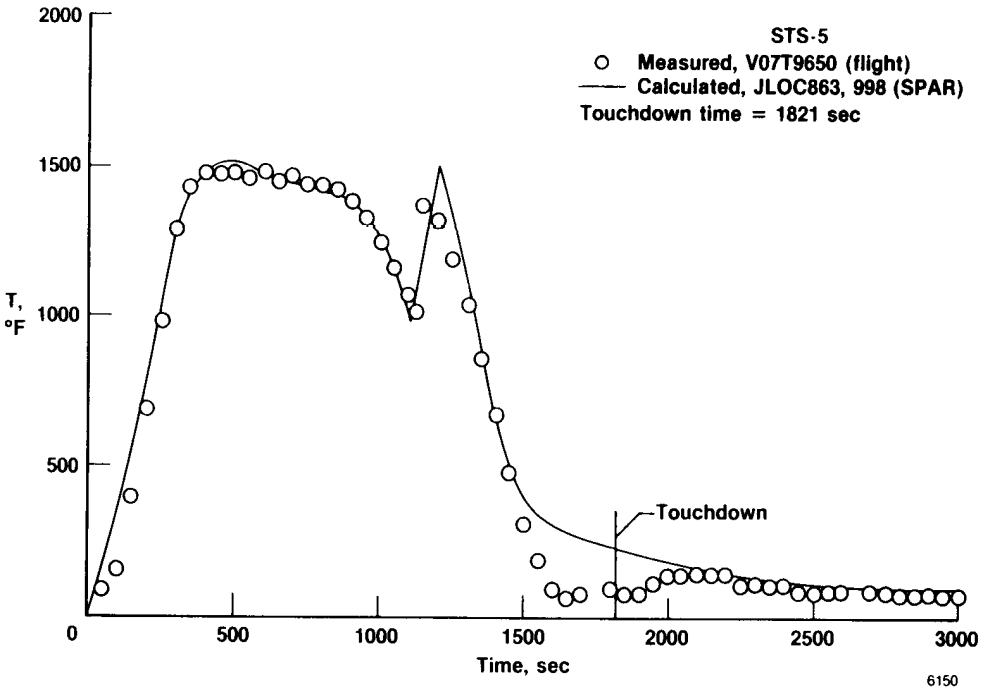

(d) Lower surface wheelwell, part 2 of 3.

Figure 11. Continued.

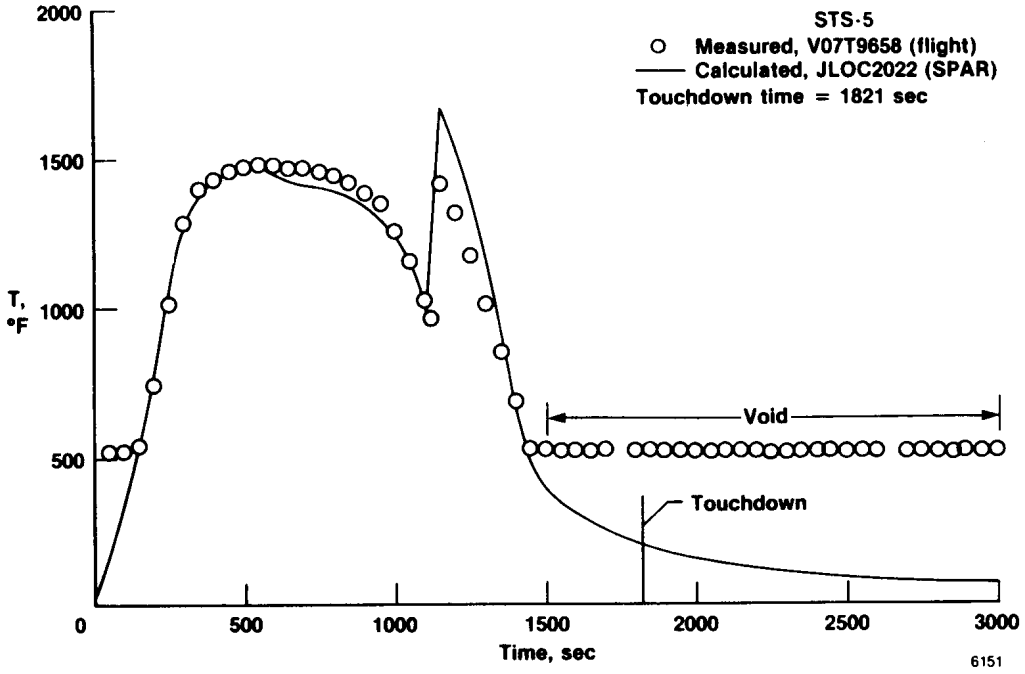

(e) Lower surface wheelwell, part 3 of 3.

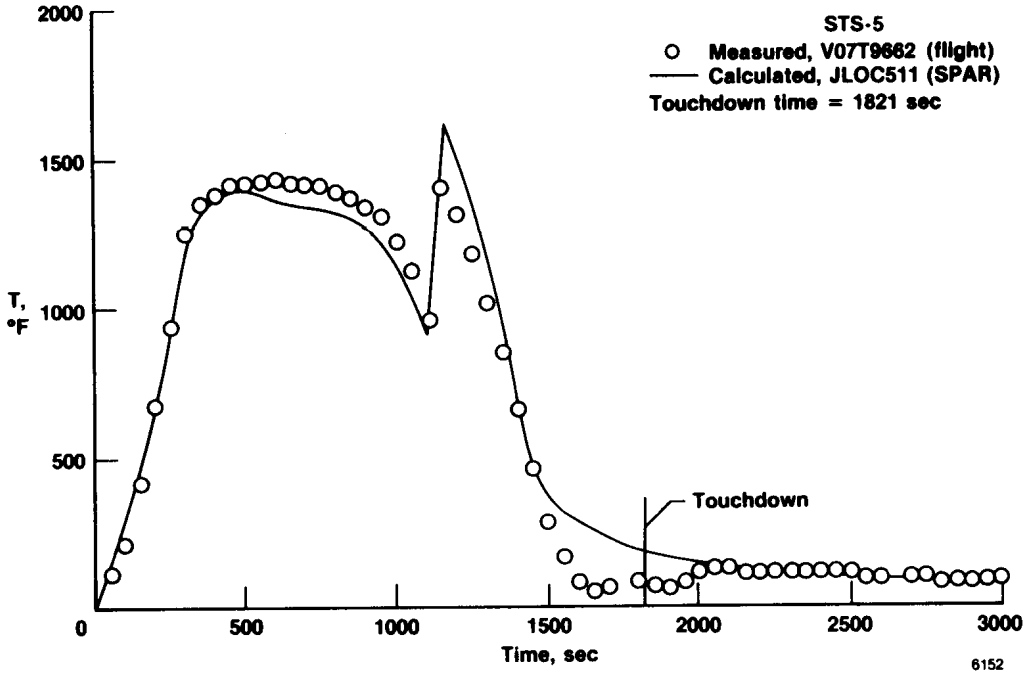

(f) Lower surface aft section, bay 4.

Figure 11. Concluded.

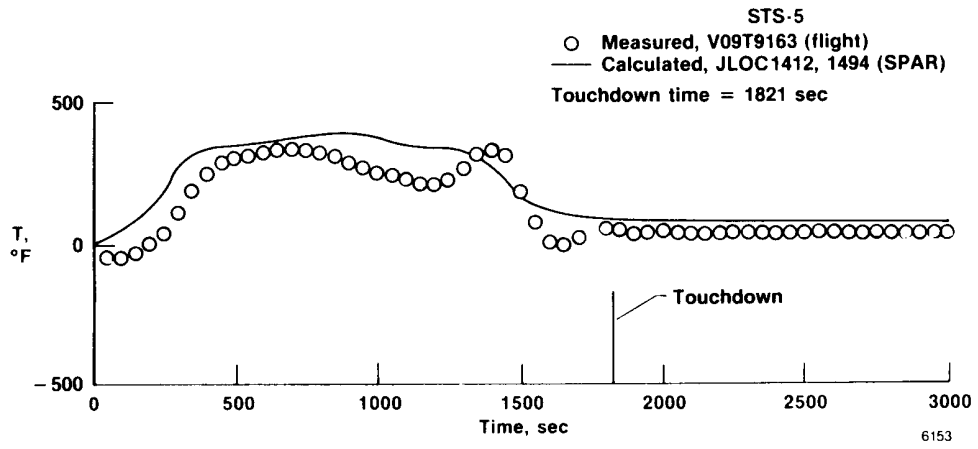

(a) Upper glove, part 1 of 2.

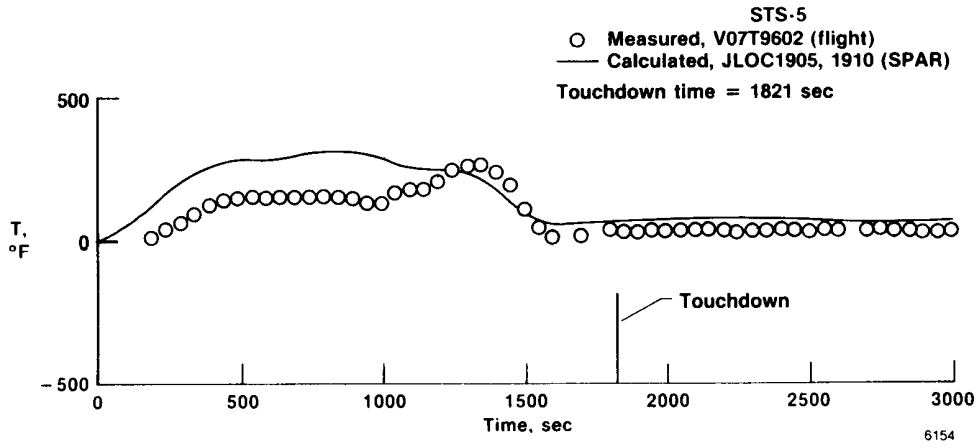

(b) Upper glove, part 2 of 2.

Figure 12. Comparisons of calculated and measured TPS upper surface temperatures, WS134.

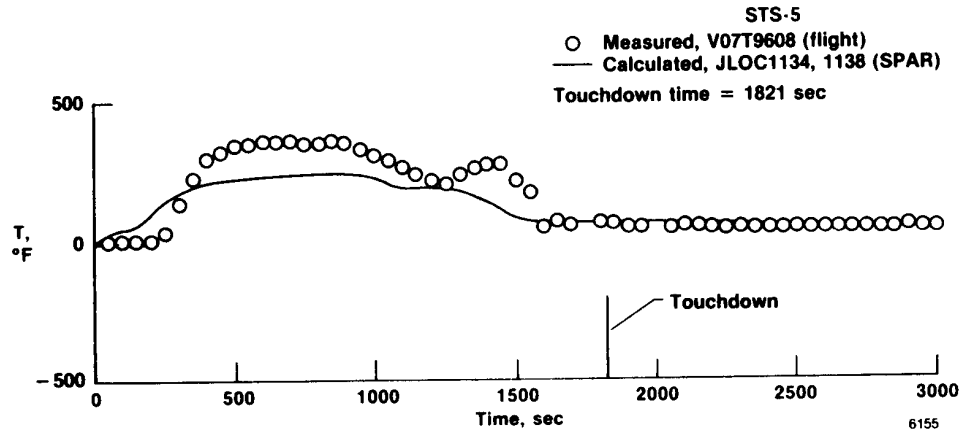

(c) Upper surface wheelwell, part 1 of 4.

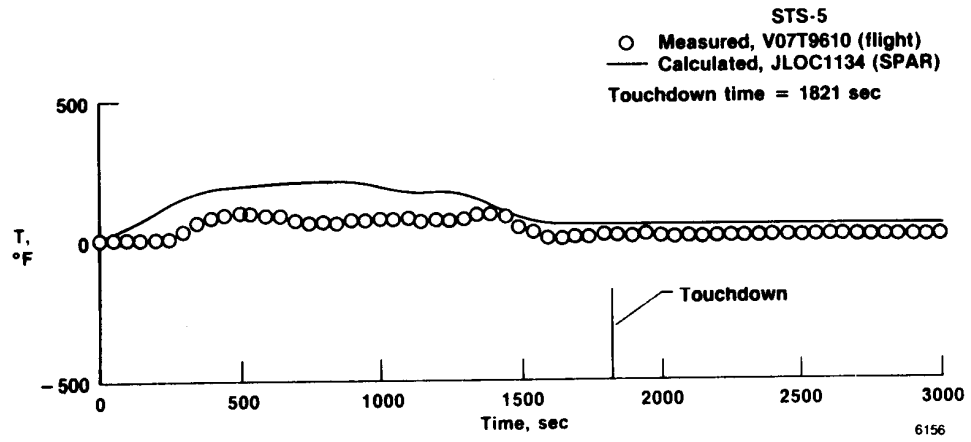

(d) Upper surface wheelwell, part 2 of 4.

Figure 12. Continued.

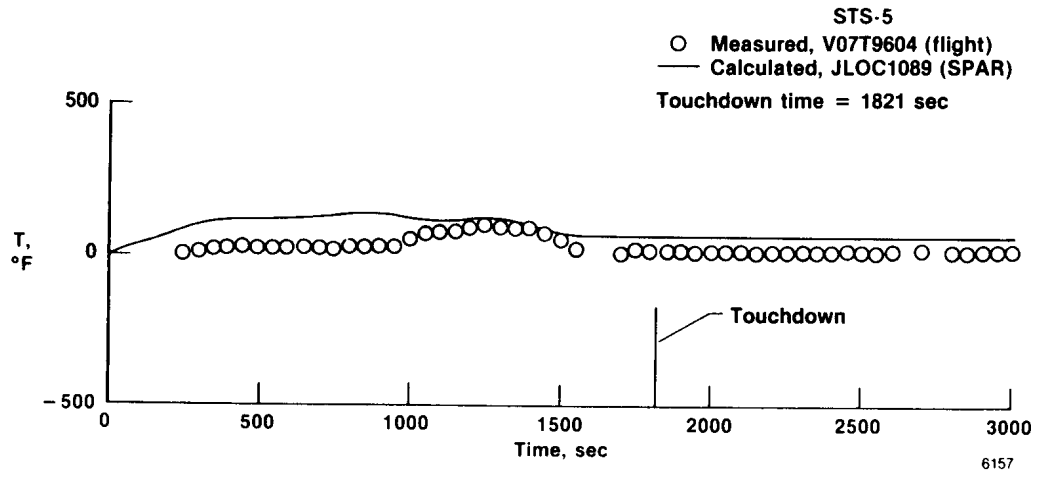

(e) Upper surface wheelwell, part 3 of 4.

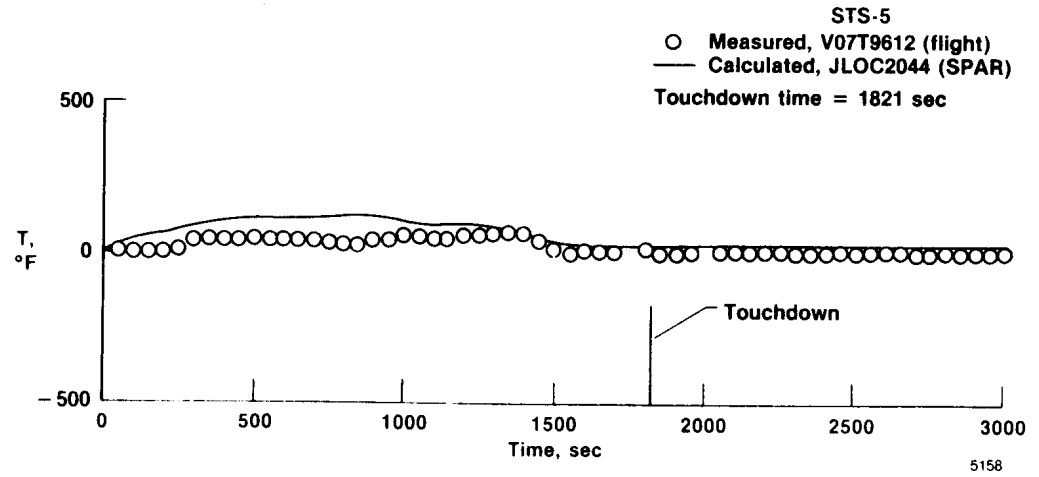

(f) Upper surface wheelwell, part 4 of 4.

Figure 12. Continued.

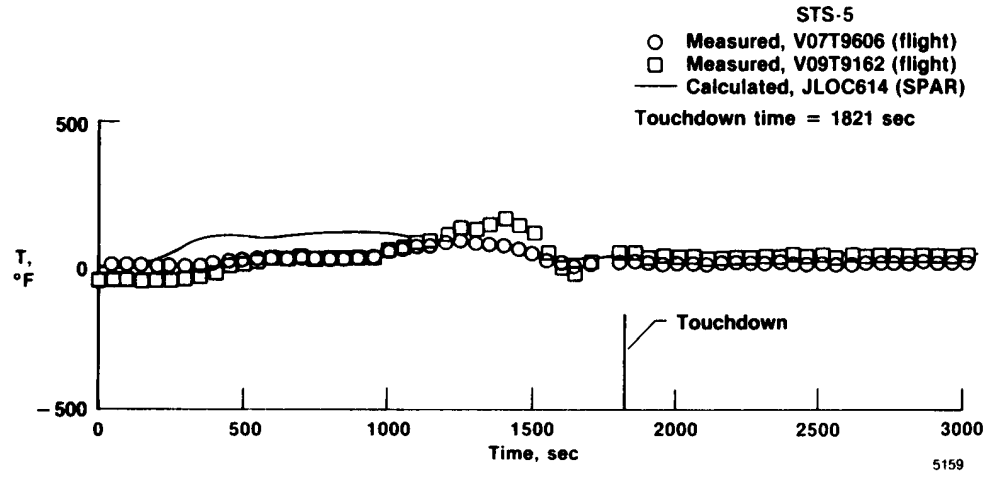

(g) Upper surface, bay 3.

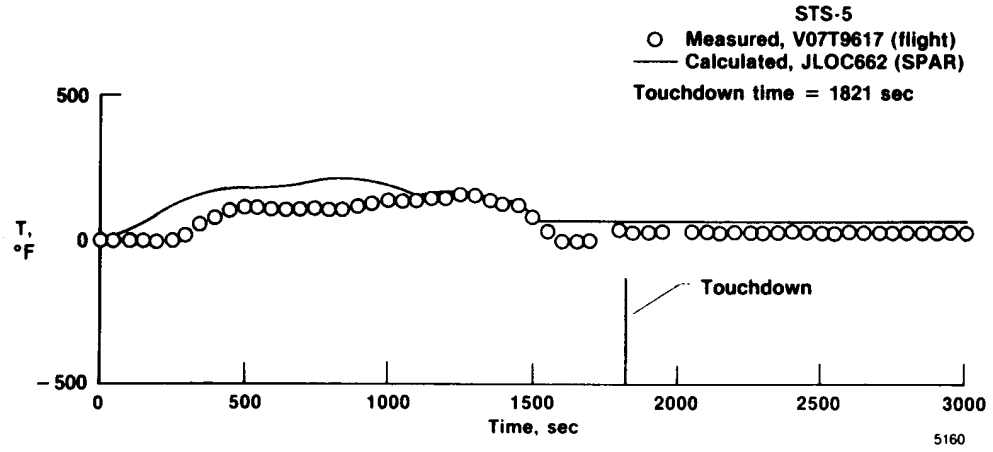

(h) Upper surface, bay 4.

Figure 12. Concluded.

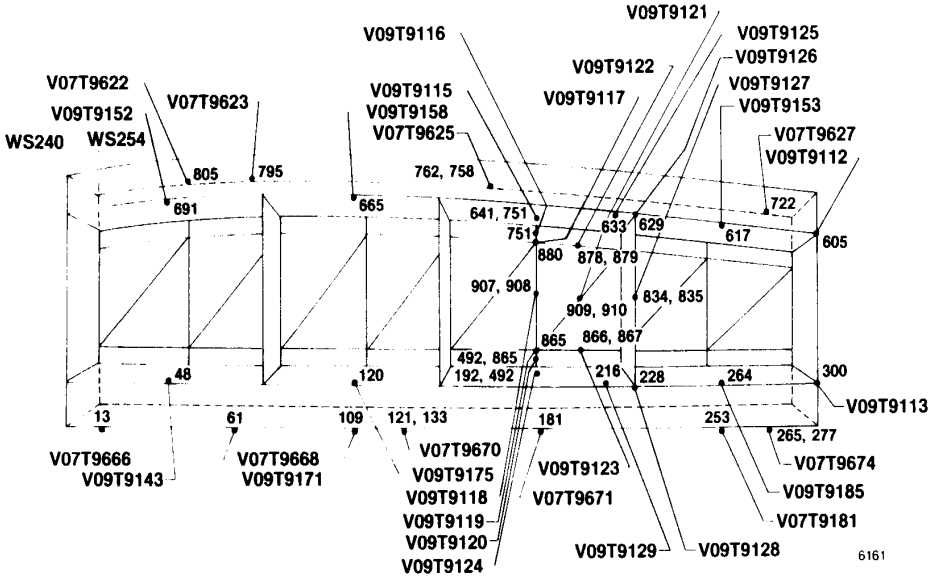

Figure 13. WS240 TPS surface and aluminum structural temperature measurement locations and SPAR joint locations.

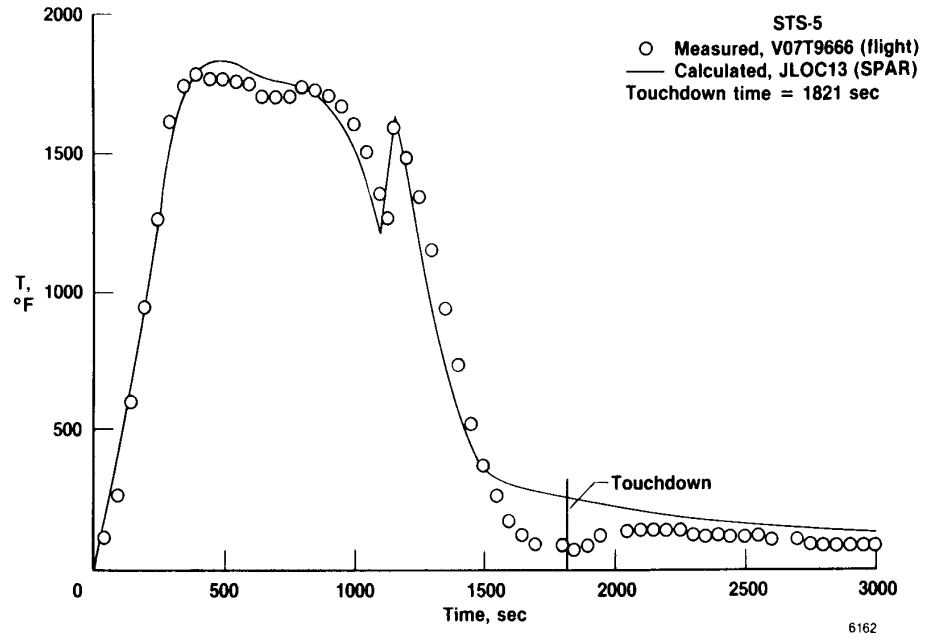

(a) Lower surface, bay 1, part 1 of 2.

Figure 14. Comparisons of calculated and measured TPS lower surface temperatures, WS240.

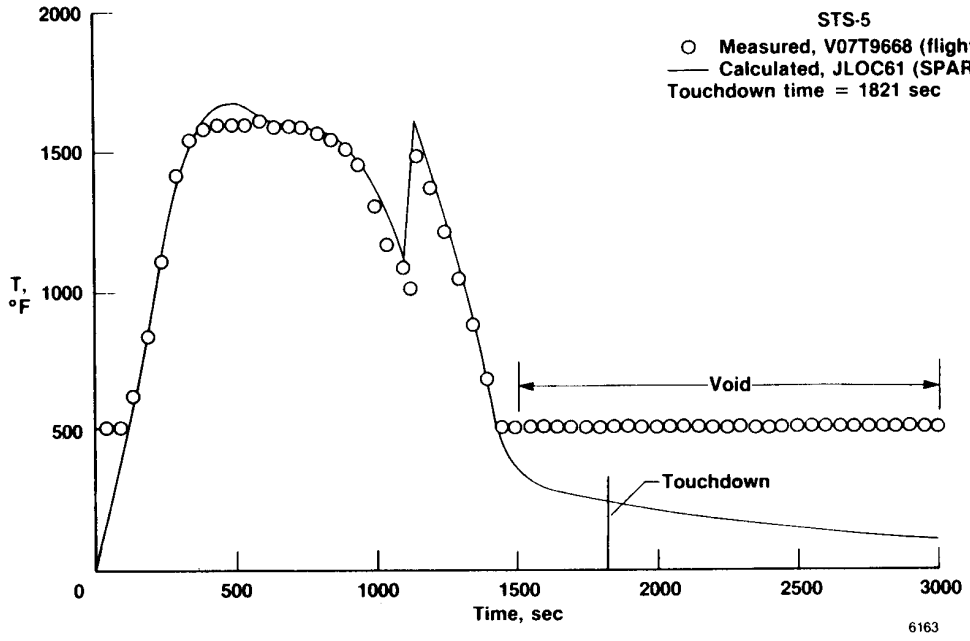

(b) Lower surface, bay 1, part 2 of 2.

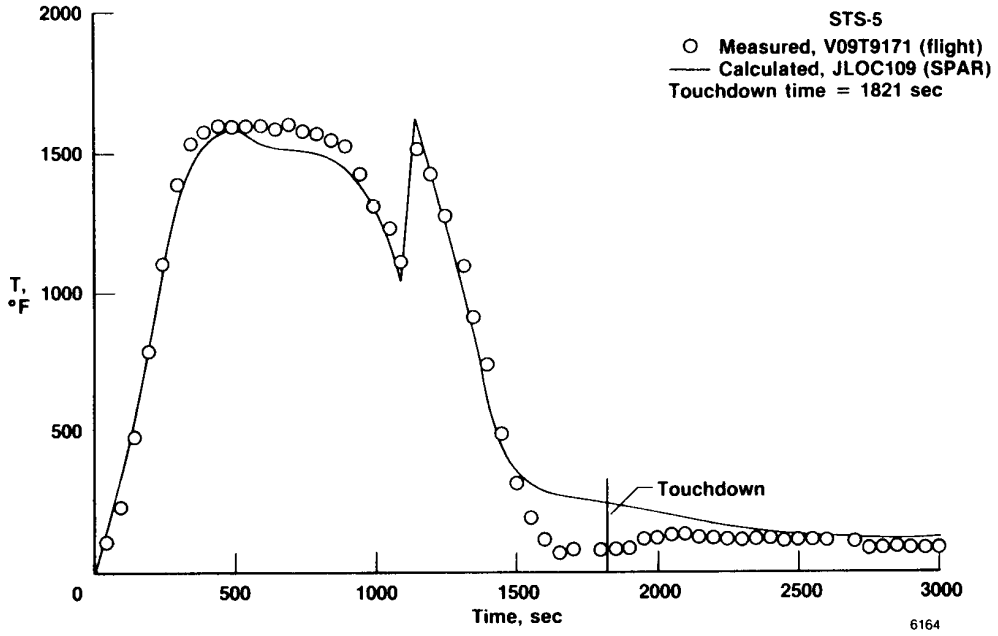

(c) Lower surface, bay 2, part 1 of 2.

Figure 14. Continued.

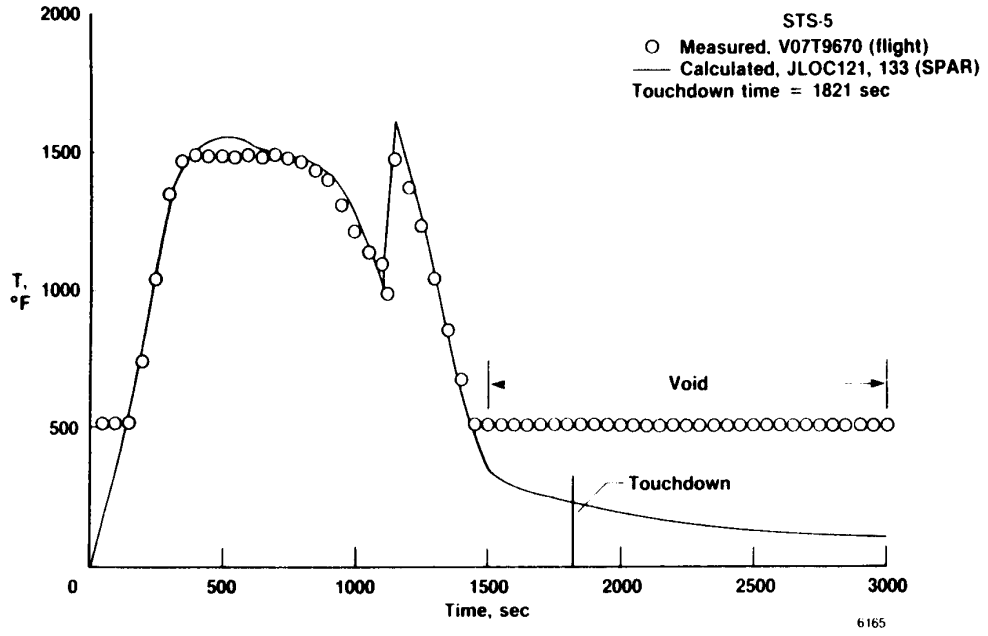

(d) Lower surface, bay 2, part 2 of 2.

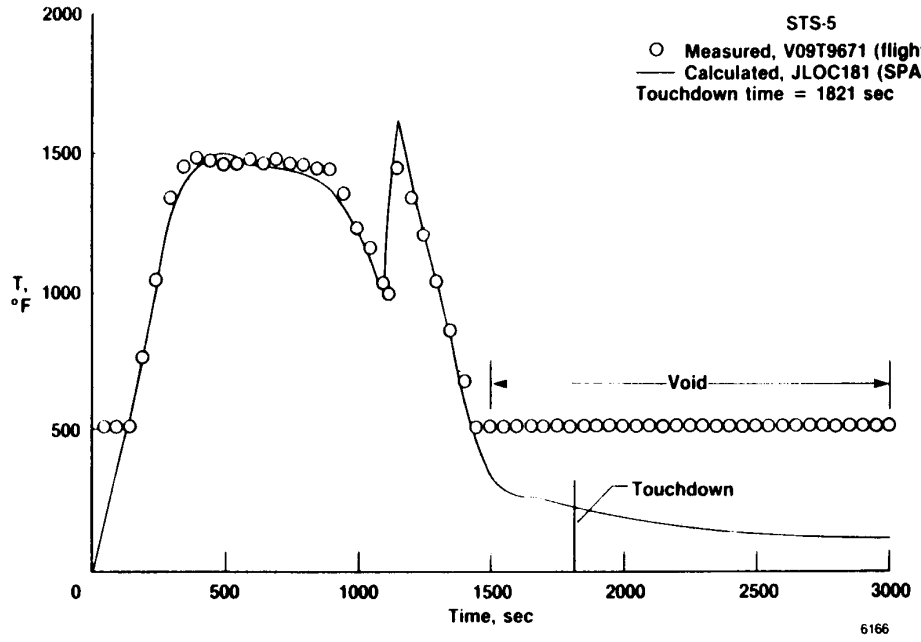

(e) Lower surface, bay 3.

Figure 14. Continued.

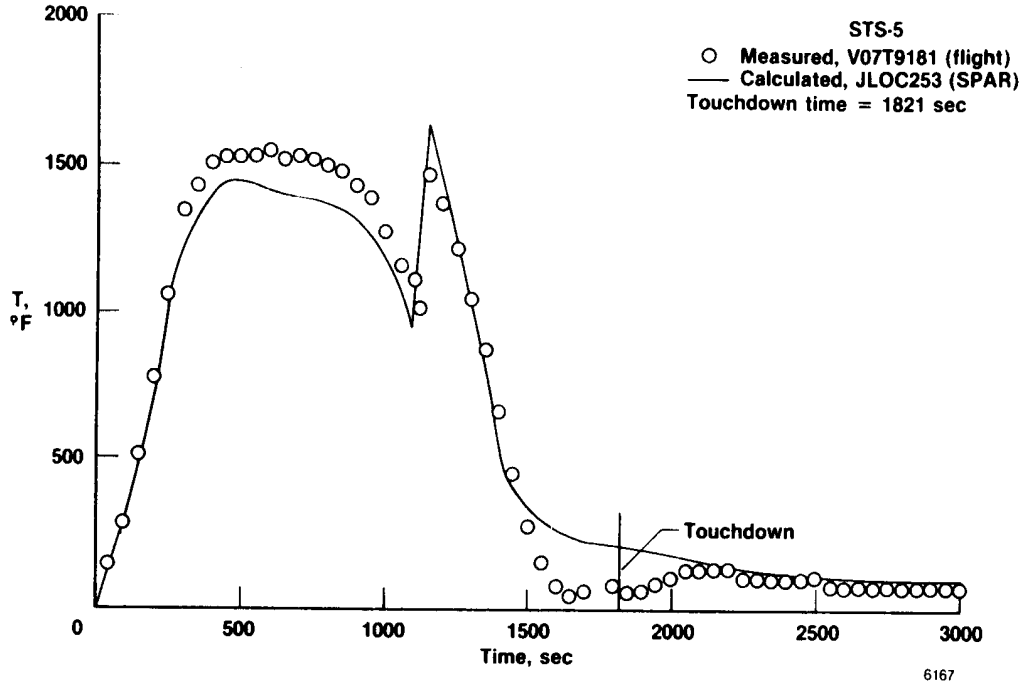

(f) Lower surface, bay 4, part 1 of 2.

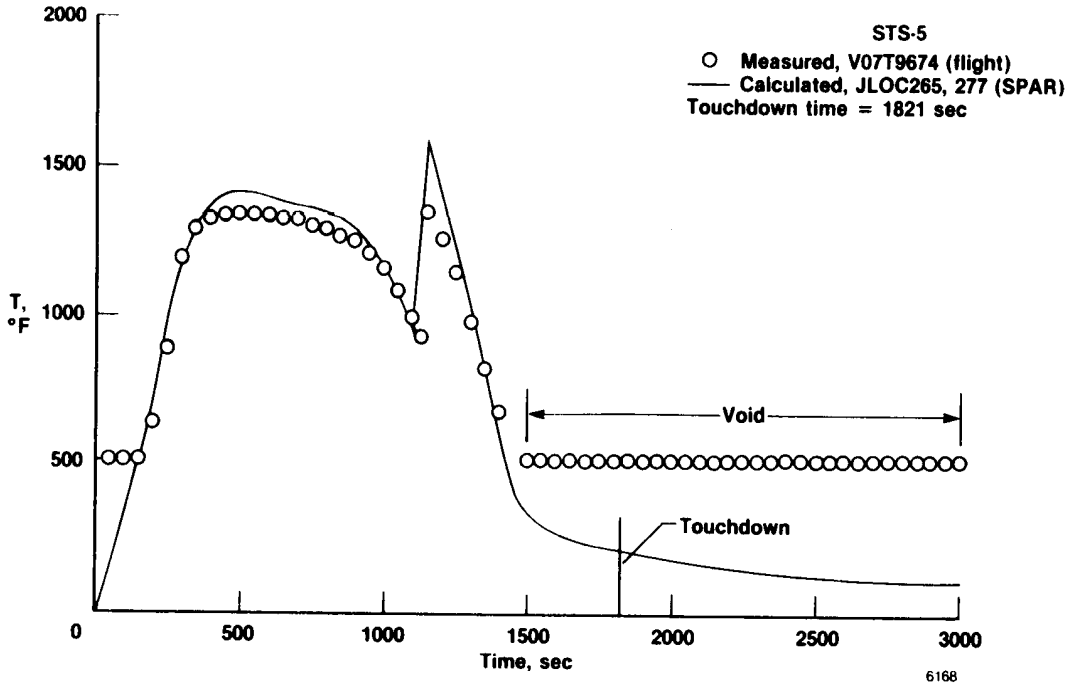

(g) Lower surface, bay 4, part 2 of 2.

Figure 14. Concluded.

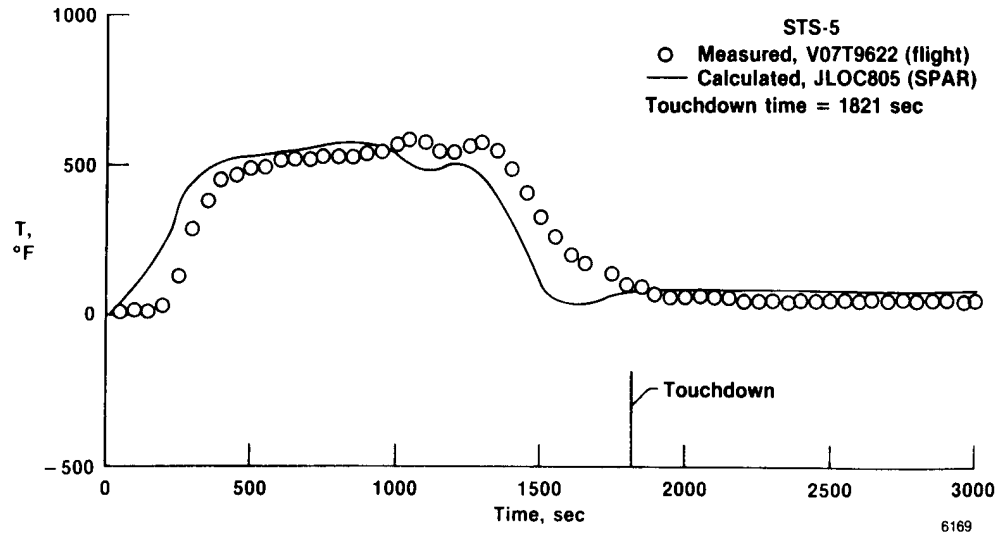

(a) Upper surface, bay 1, part 1 of 2.

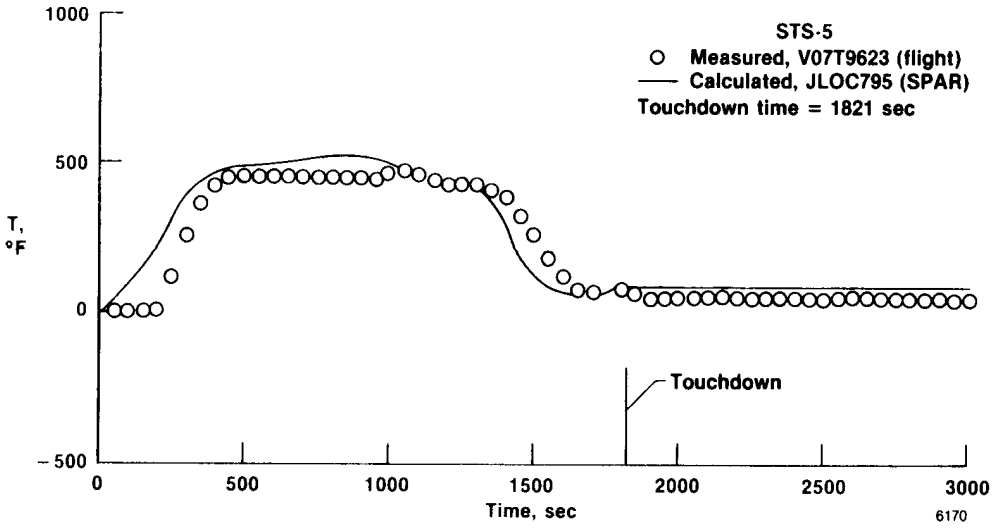

(b) Upper surface, bay 1, part 2 of 2.

Figure 15. Comparisons of calculated and measured TPS upper surface temperatures, WS240.

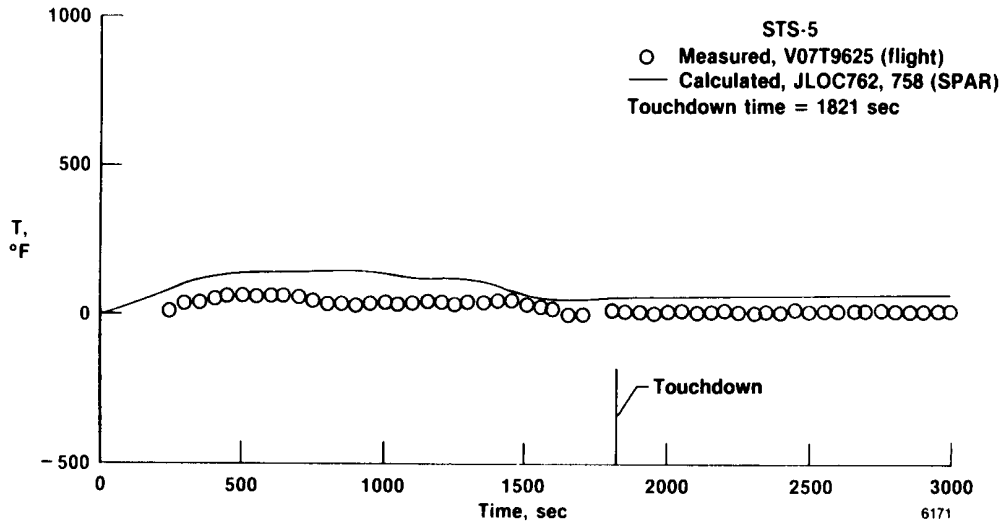

(c) Upper surface, bay 3.

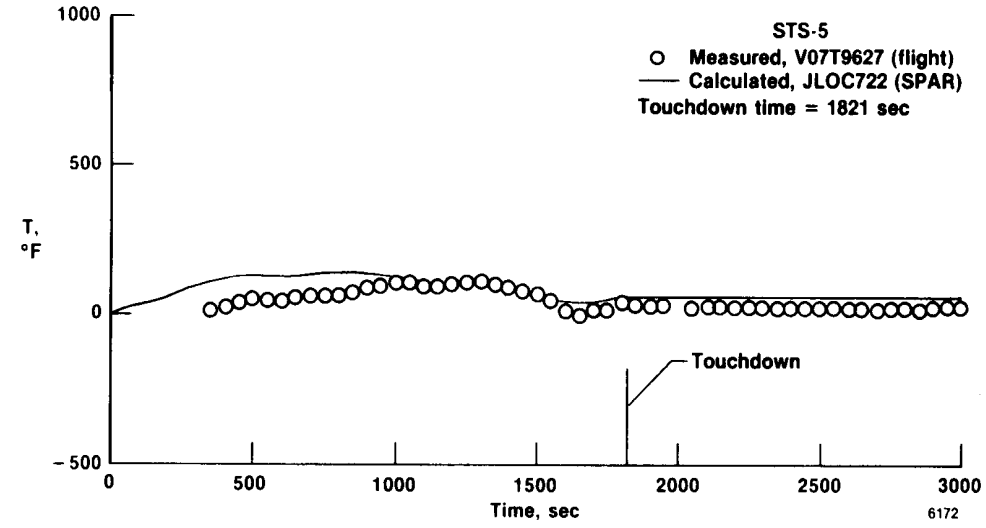

(d) Upper surface, bay 4.

Figure 15. Concluded.

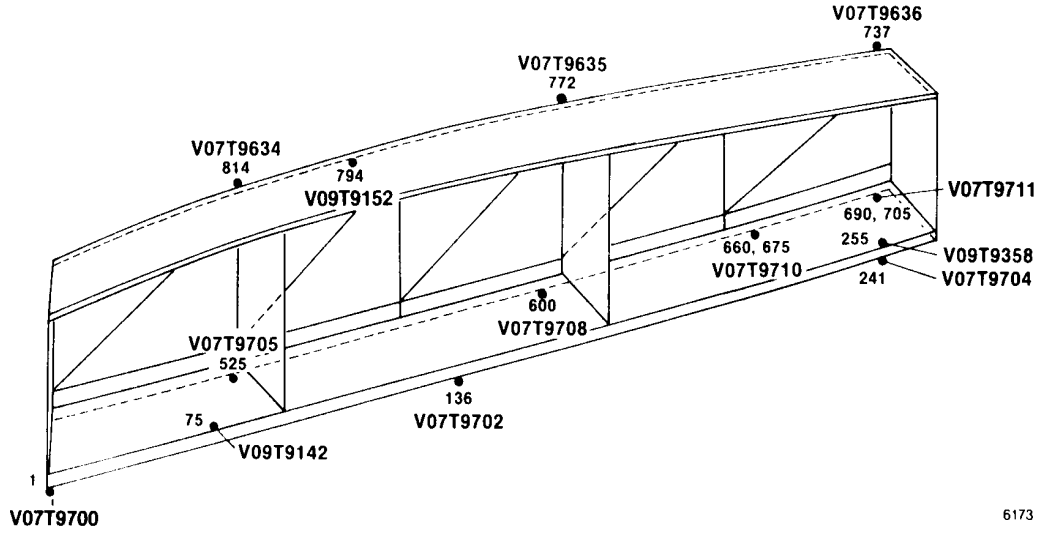

Figure 16. WS328 TPS surface temperature measurement locations and SPAR joint locations.

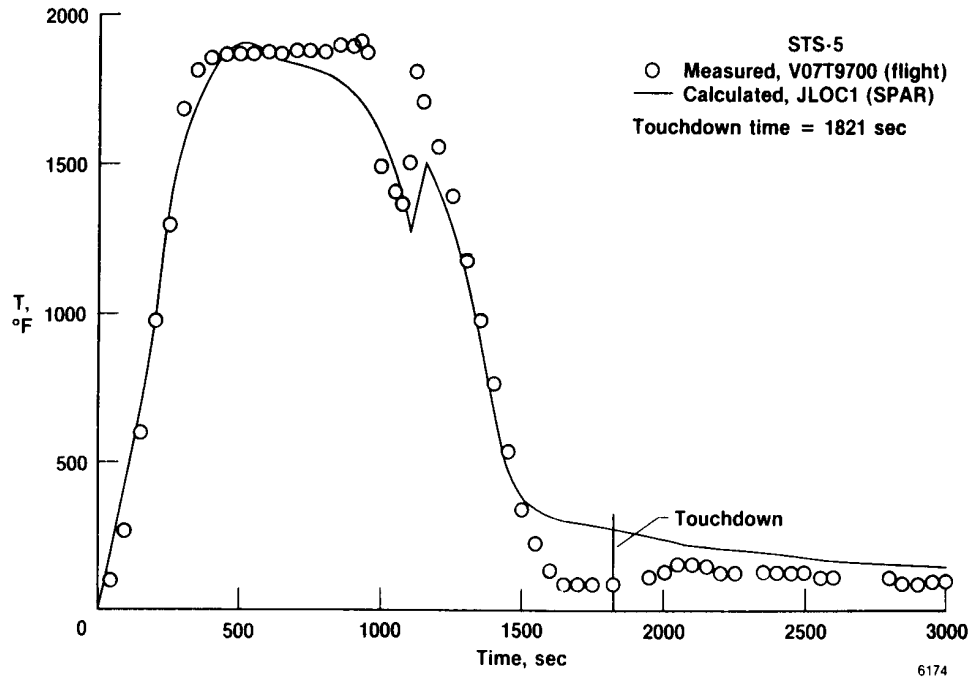

(a) Lower surface, bay 1, part 1 of 2.

Figure 17. Comparisons of calculated and measured TPS lower surface temperatures, WS328.

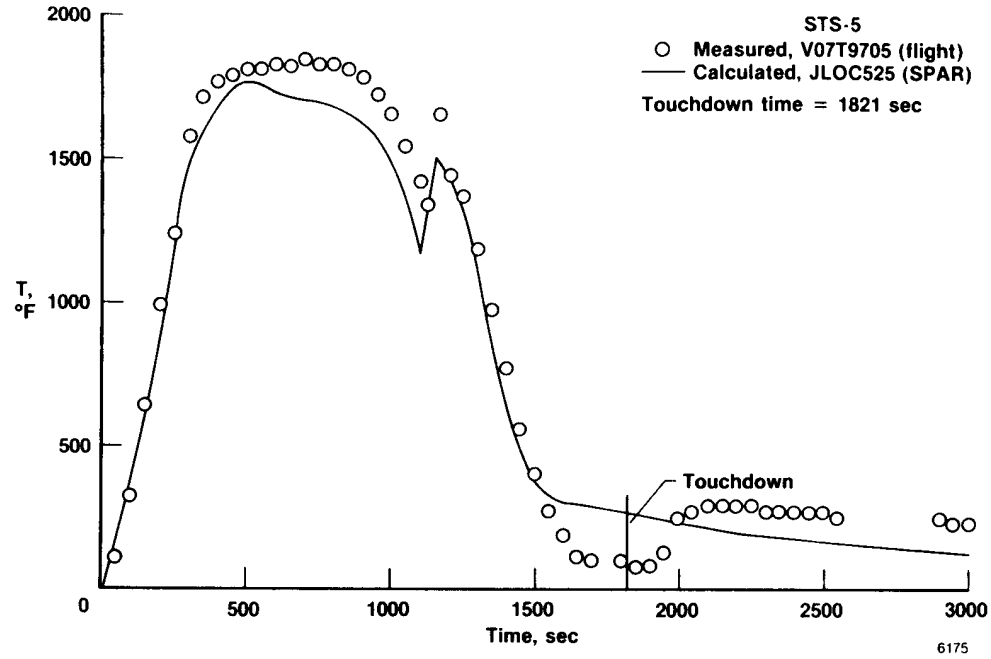

(b) Lower surface, bay 1, part 2 of 2.

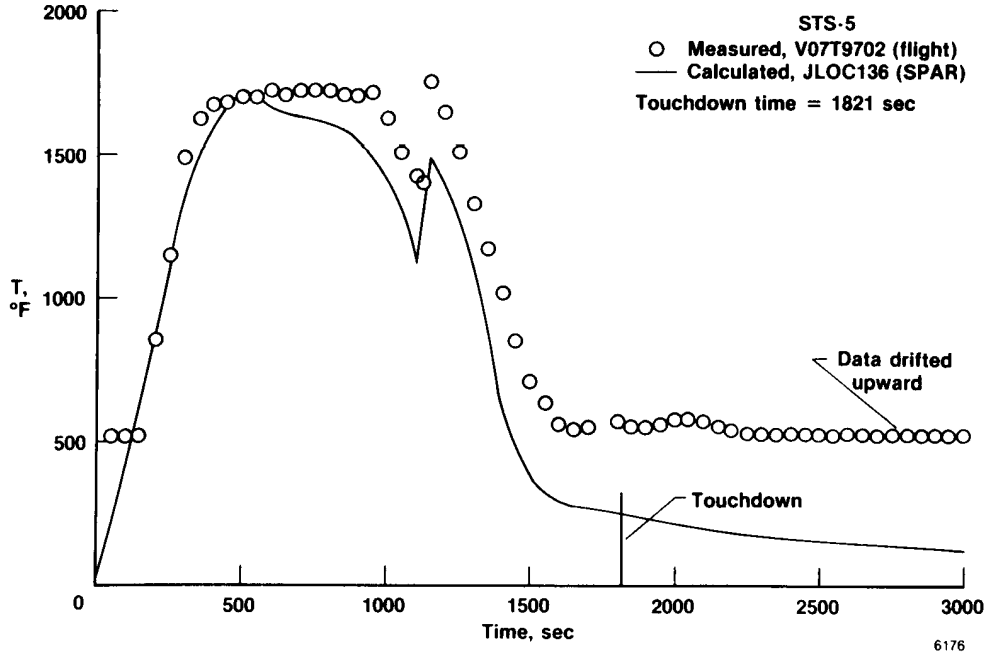

(c) Lower surface, bay 2, part 1 of 2.

Figure 17. Continued.

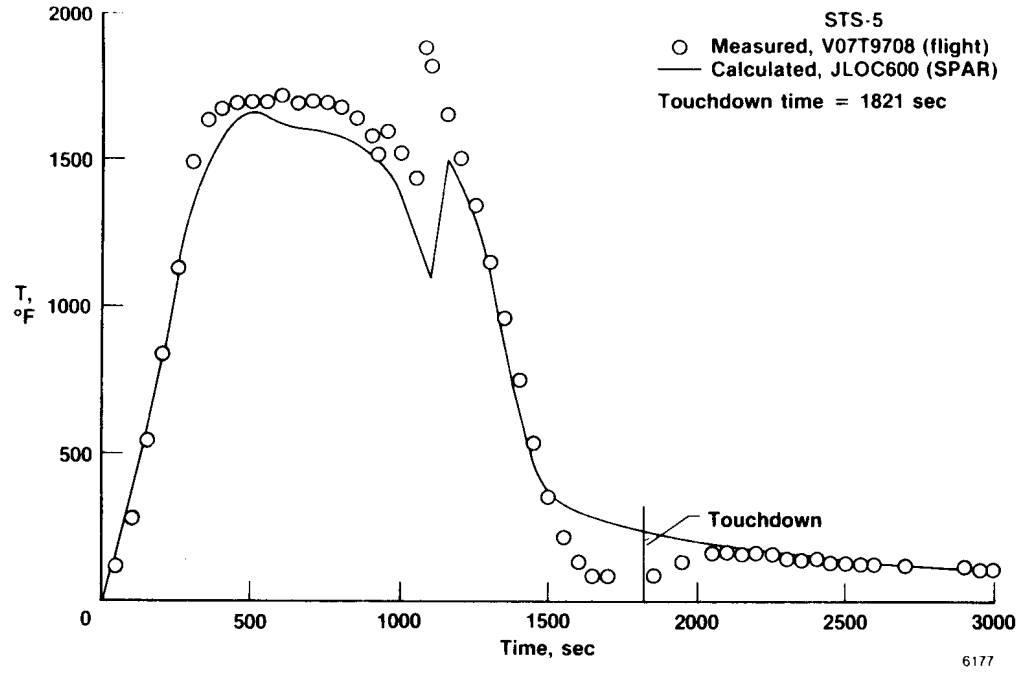

(d) Lower surface, bay 2, part 2 of 2.

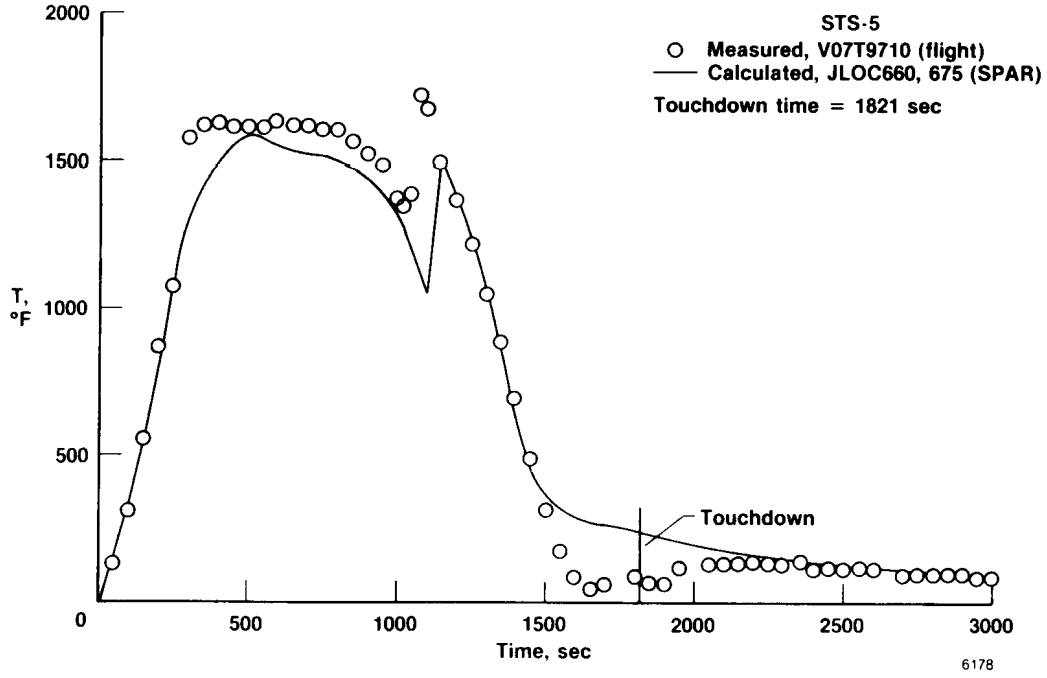

(e) Lower surface, bay 3, part 1 of 3.

Figure 17. Continued.

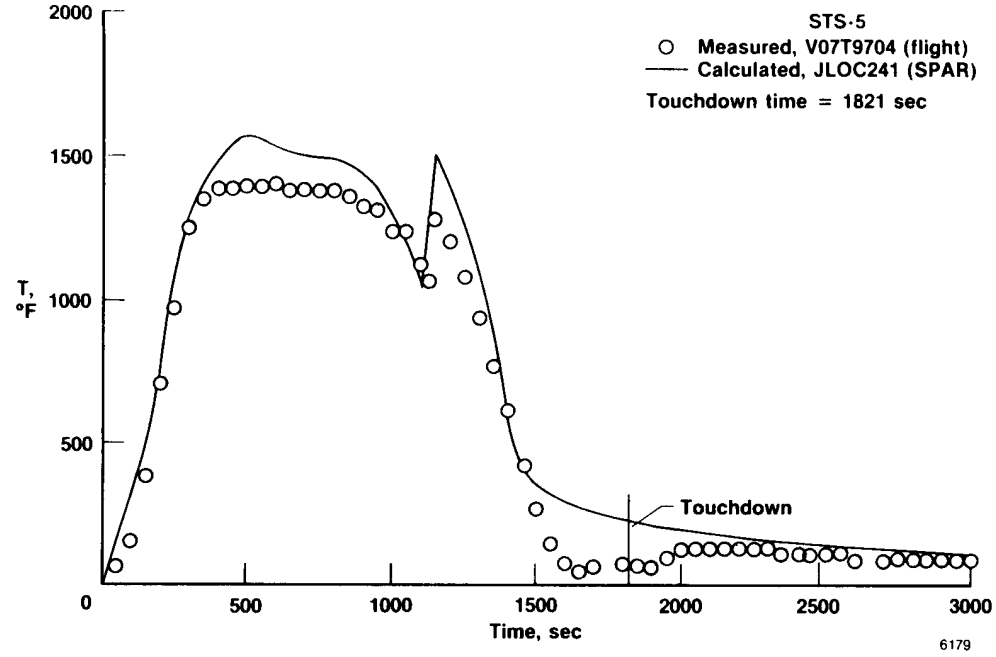

(f) Lower surface, bay 3, part 2 of 3.

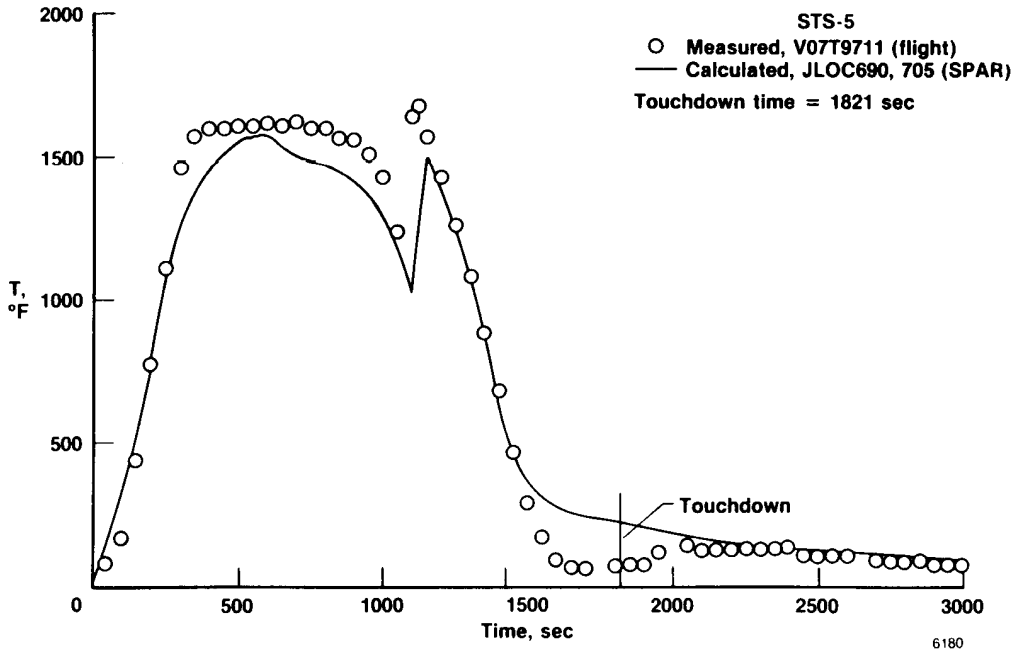

(g) Lower surface, bay 3, part 3 of 3.

Figure 17. Concluded.

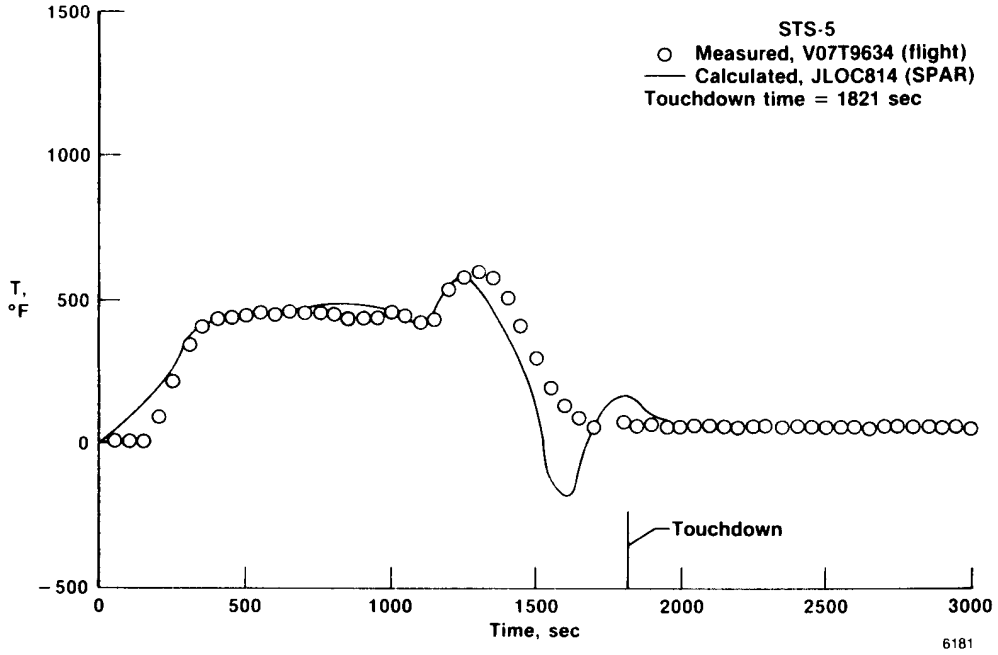

(a) Upper surface, bay 1.

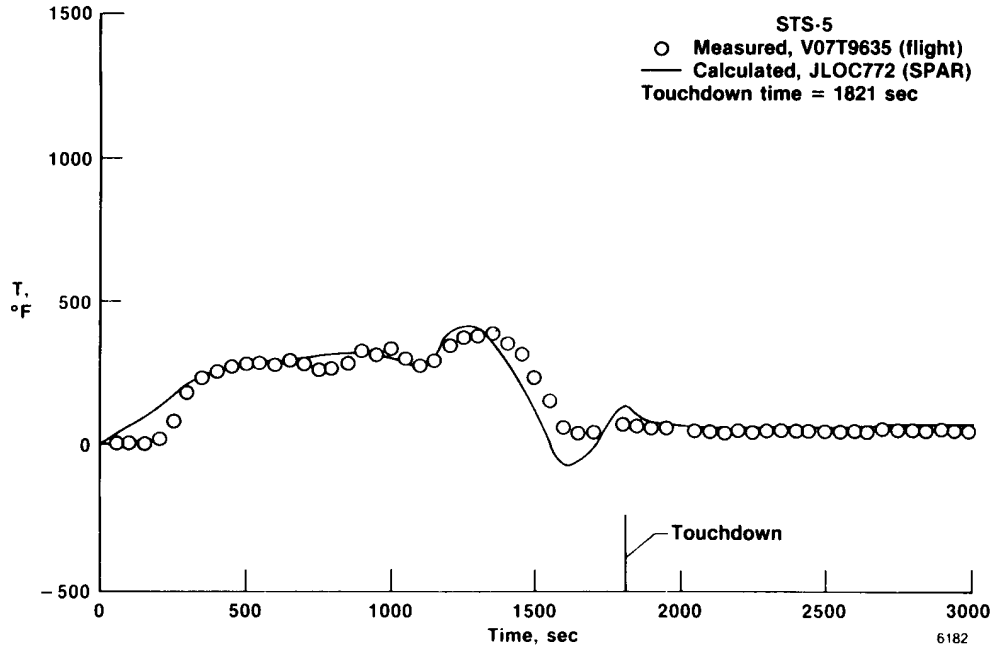

(b) Upper surface, bay 2.

Figure 18. Comparisons of calculated and measured TPS upper surface temperatures, WS328.

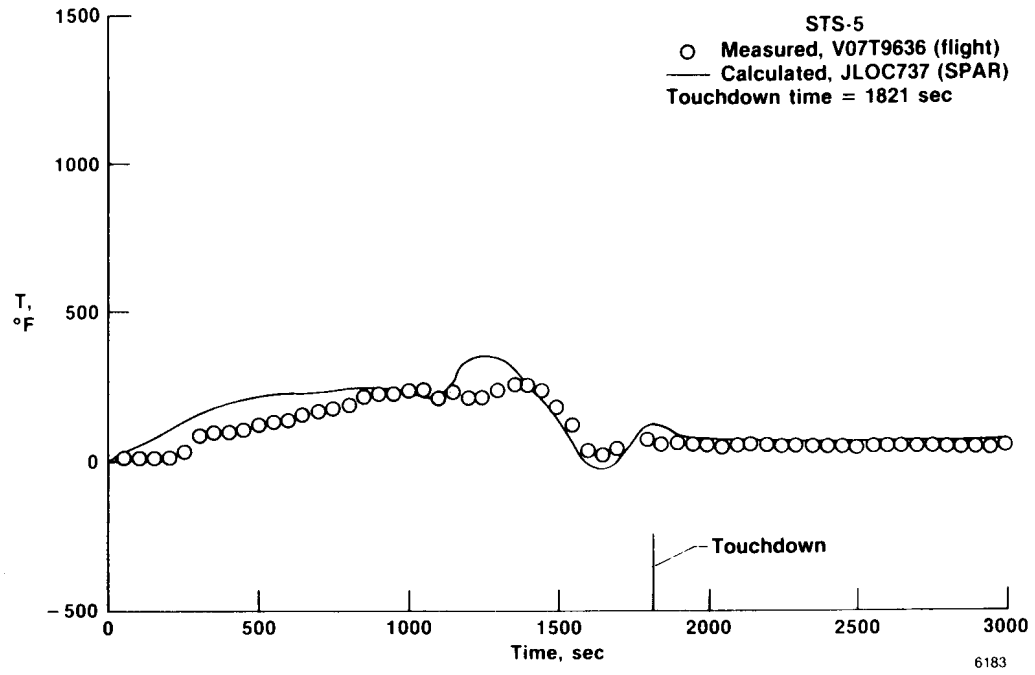

(c) Upper surface, bay 3.

Figure 18. Concluded.

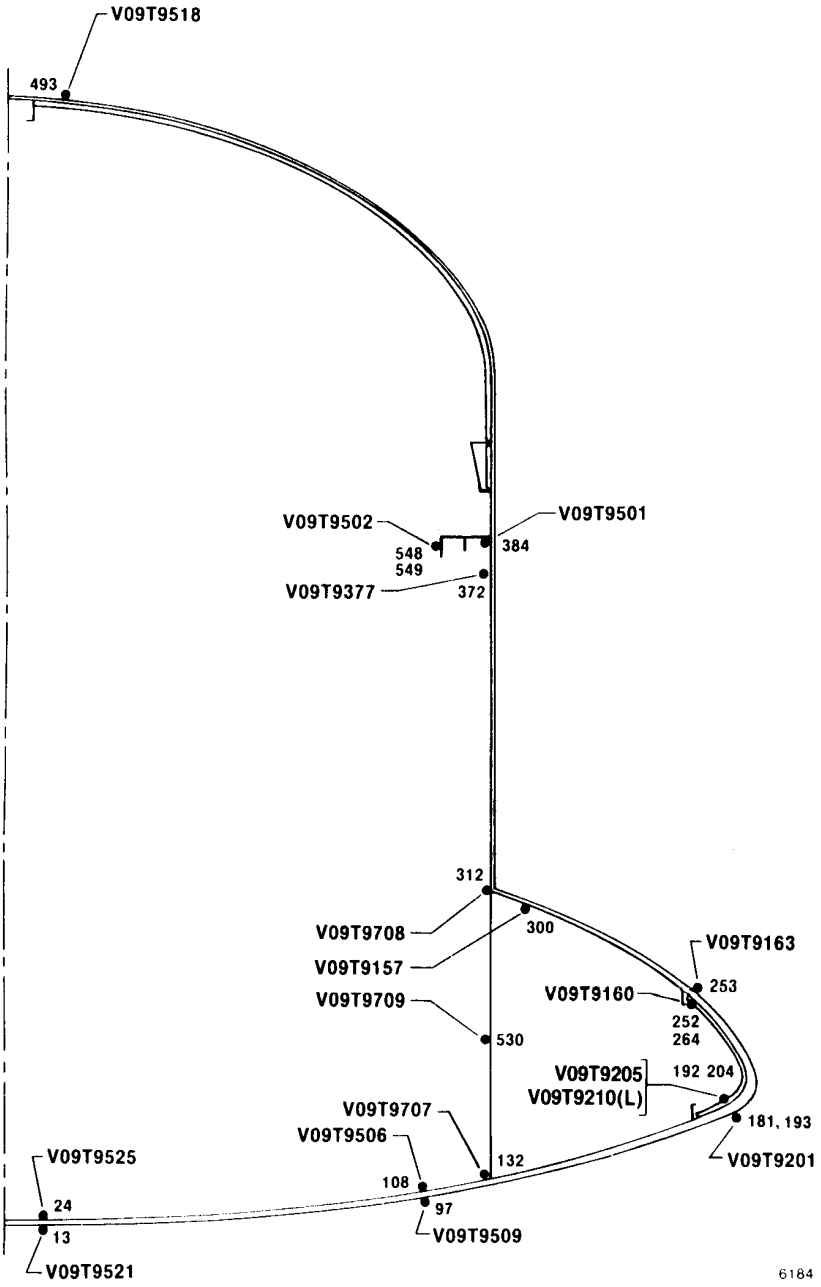

Figure 19. FS877 TPS surface and aluminum structural temperature measurement locations and SPAR joint locations.

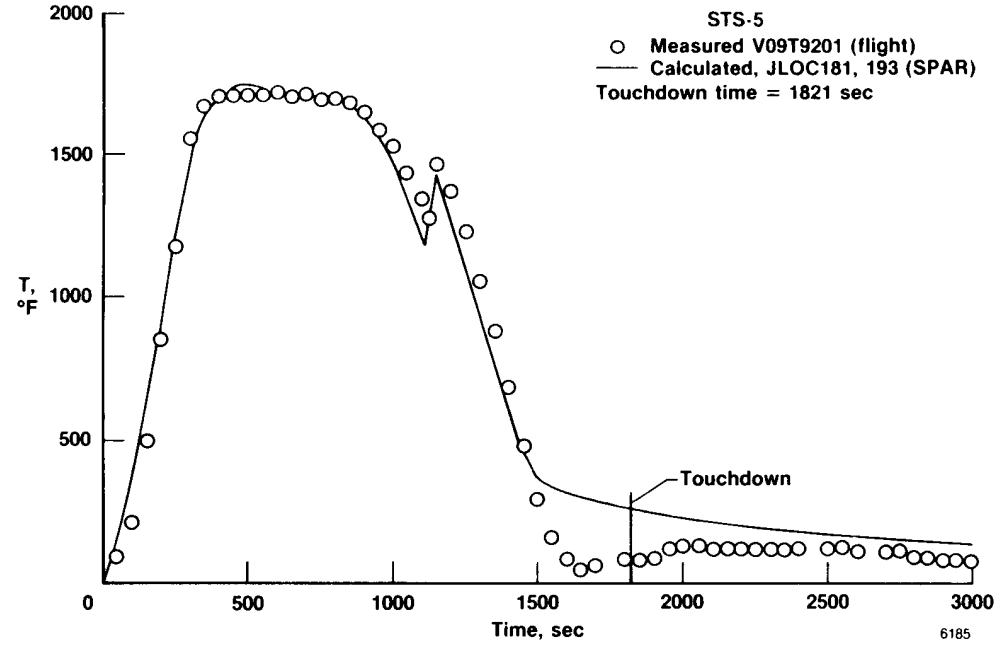

(a) Lower glove.

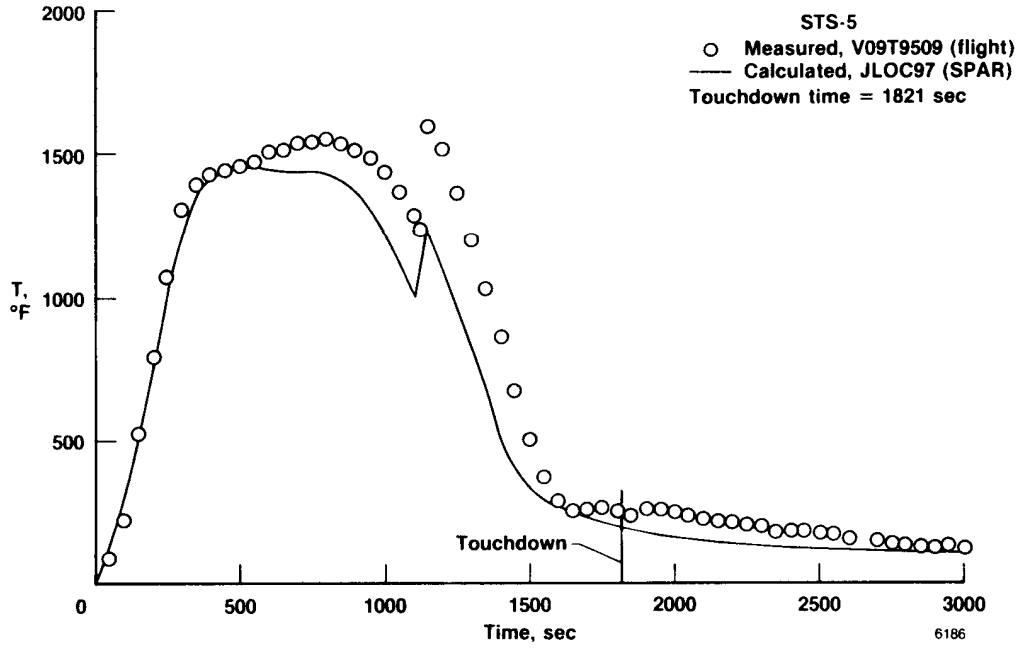

(b) Bottom surface, part 1 of 2.

Figure 20. Comparisons of calculated and measured TPS surface temperatures, FS877.

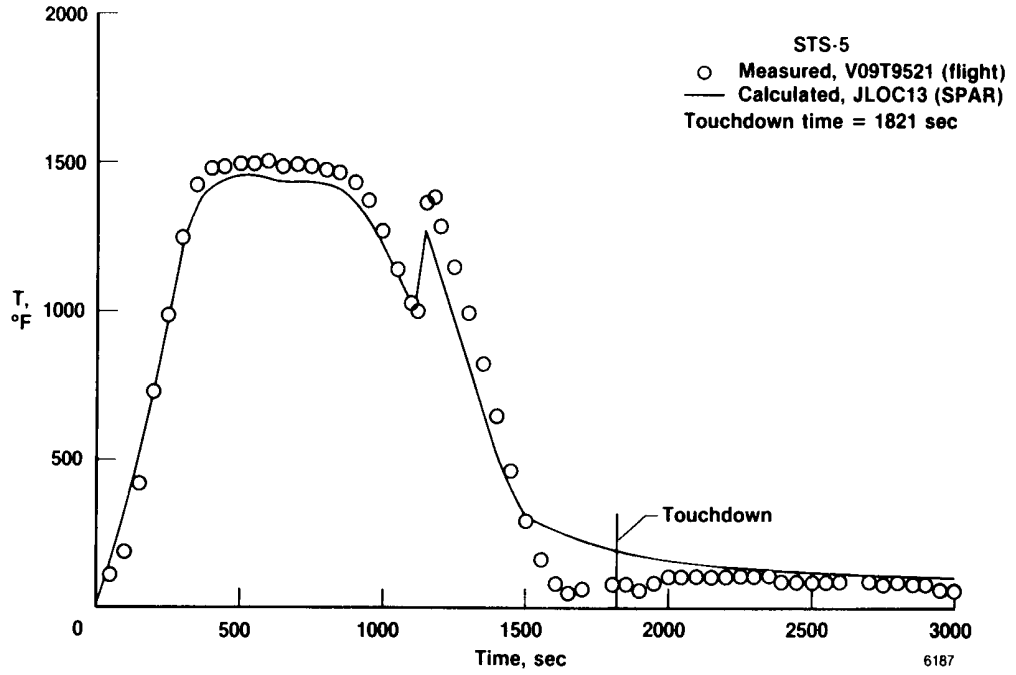

(c) Bottom surface, part 2 of 2.

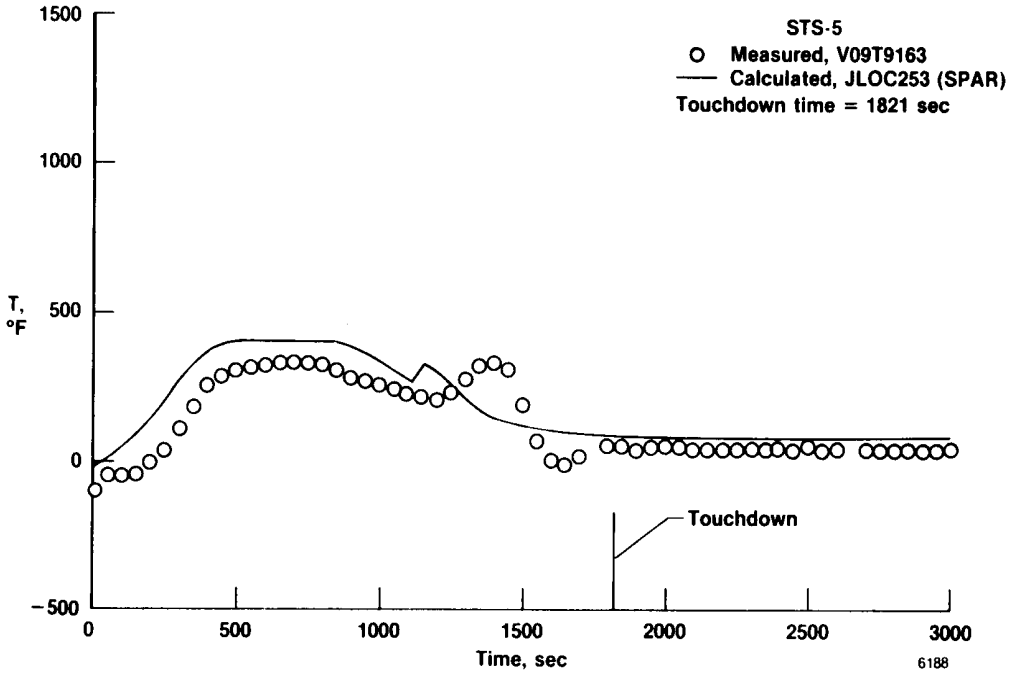

(d) Upper glove.

Figure 20. Continued.

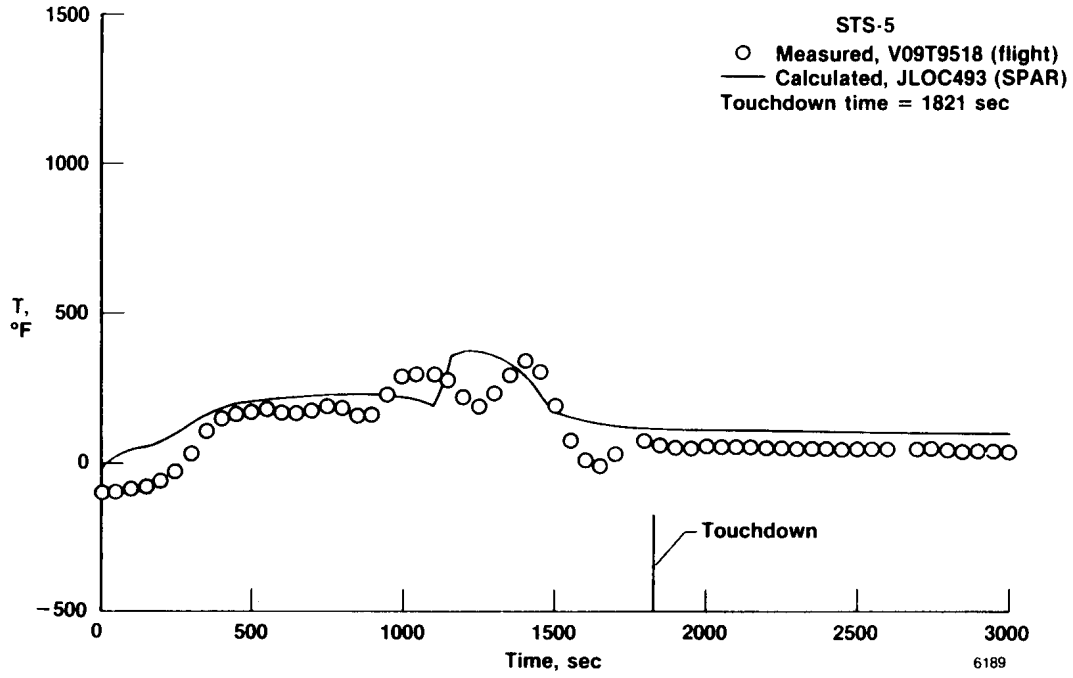

(e) Bay door.

Figure 20. Concluded.

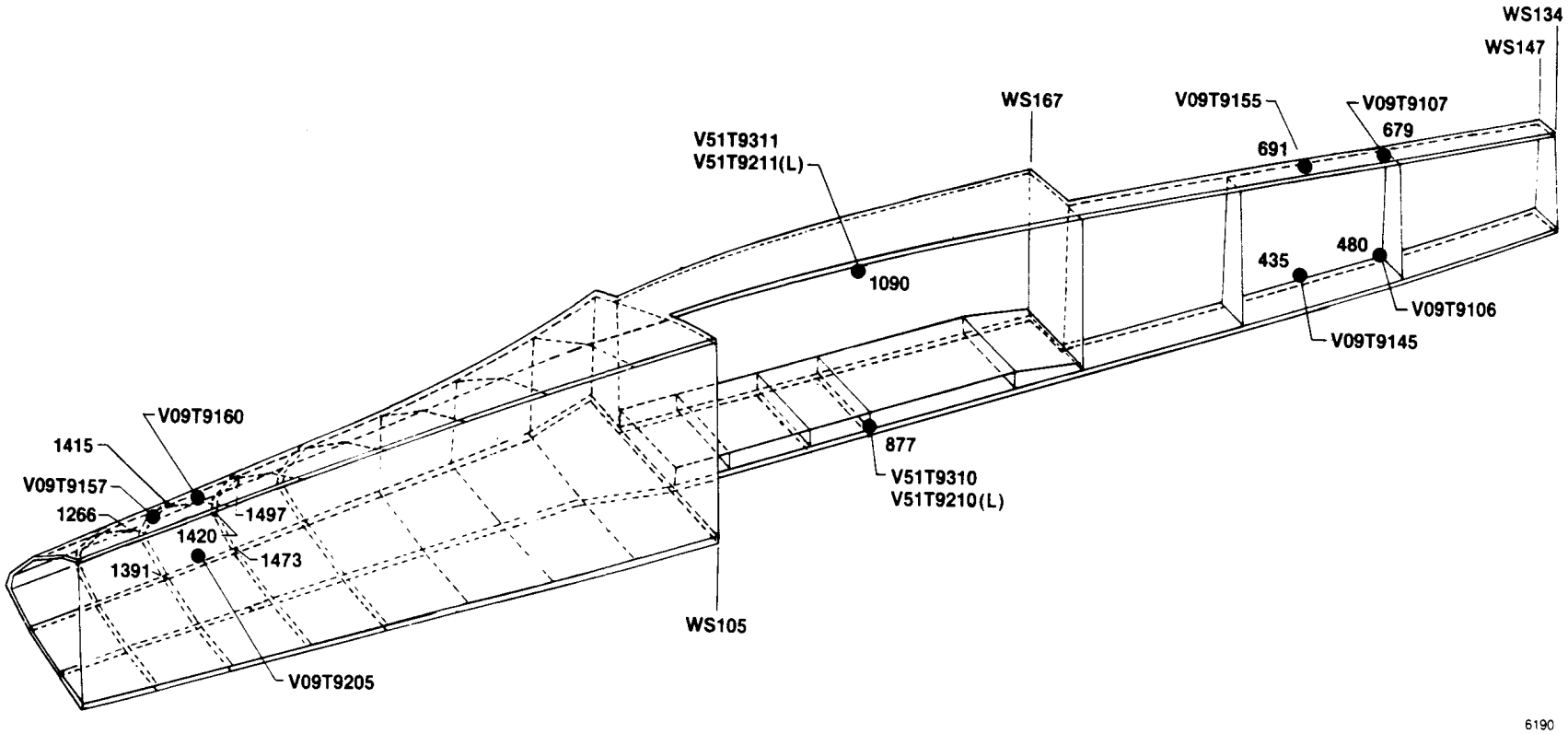

Figure 21. WS134 aluminum structural temperature measurement locations and SPAR joint locations.

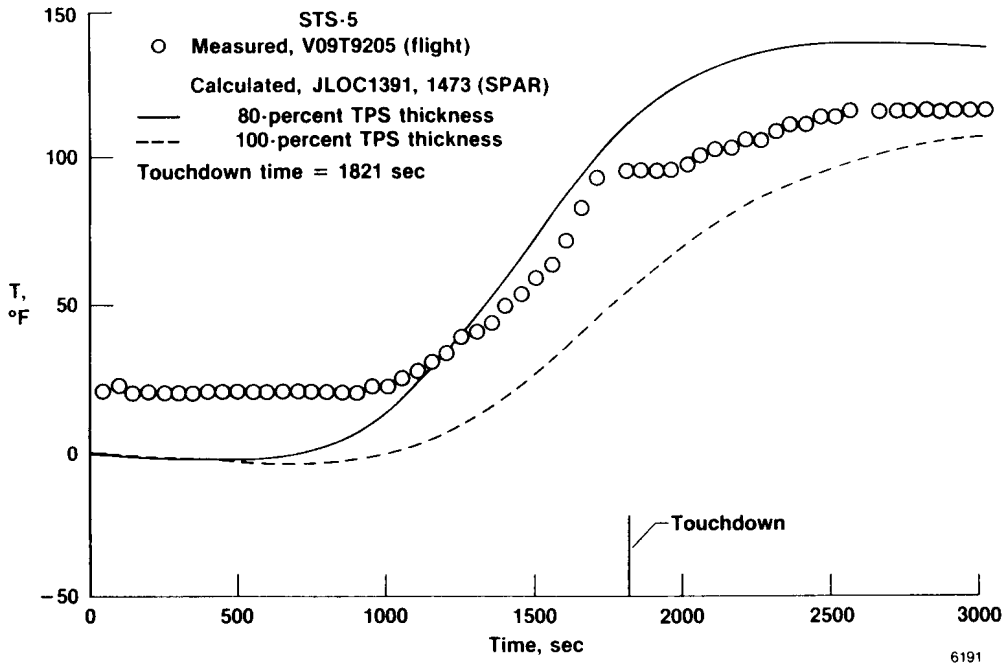

(a) Lower glove.

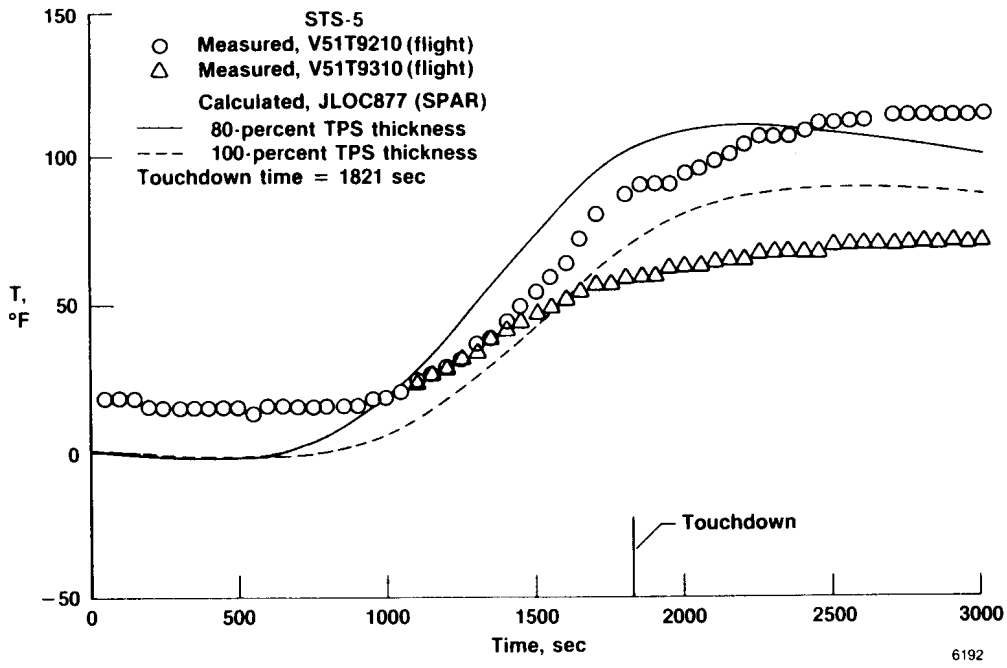

(b) Lower skin, wheelwell.

Figure 22. Comparisons of calculated and measured aluminum structural temperatures, WS134.

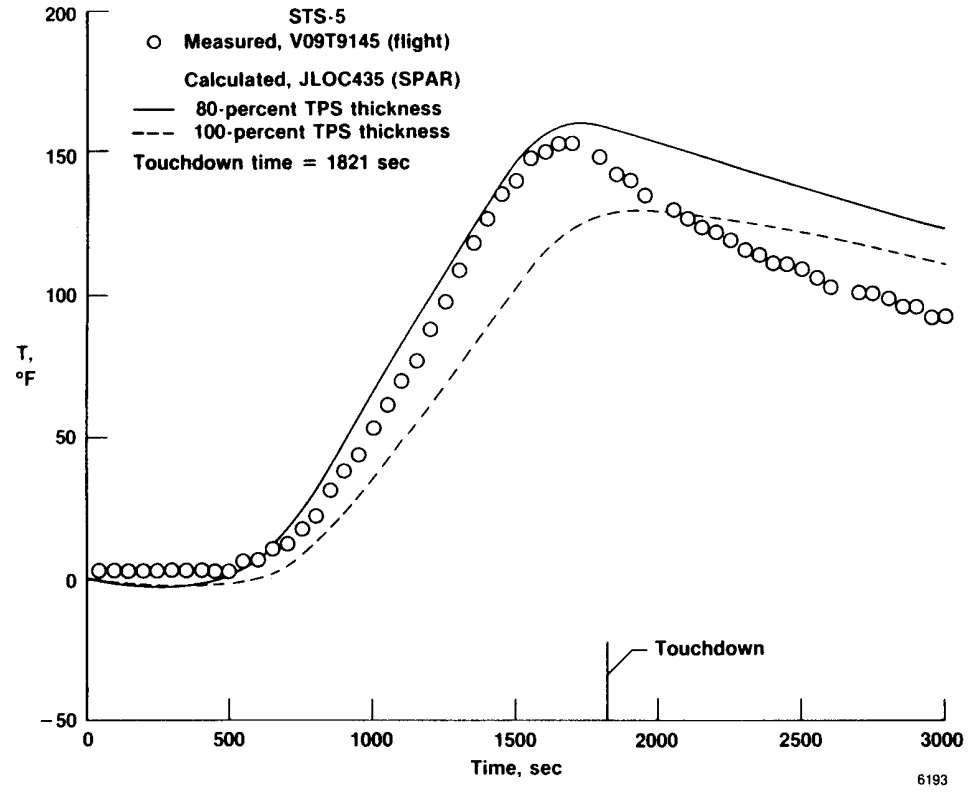

(c) Lower skin, bay 3.

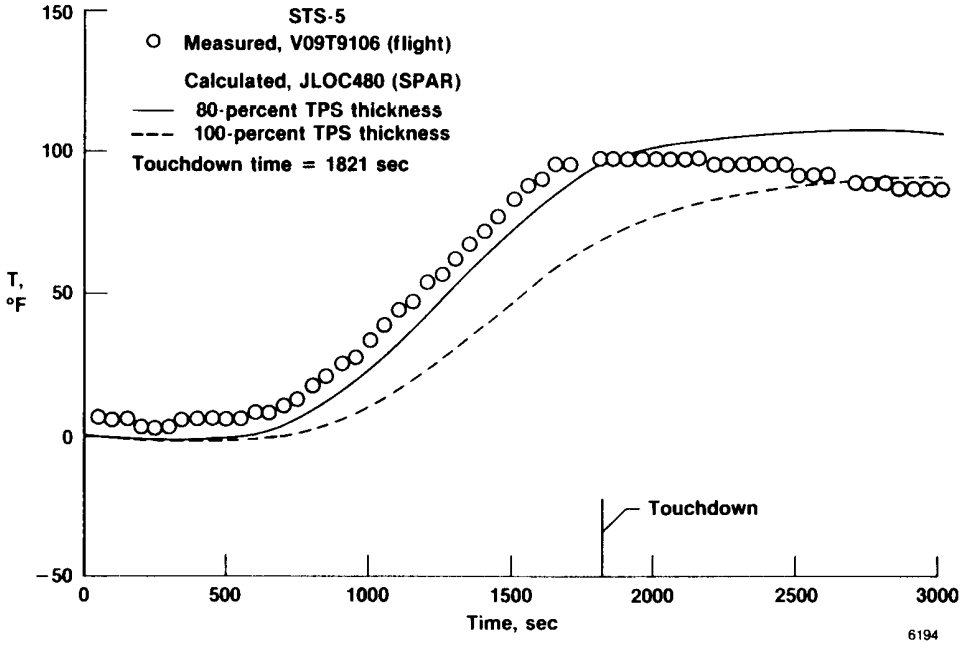

(d) Lower spar cap, bay 3/4.

Figure 22. Continued.

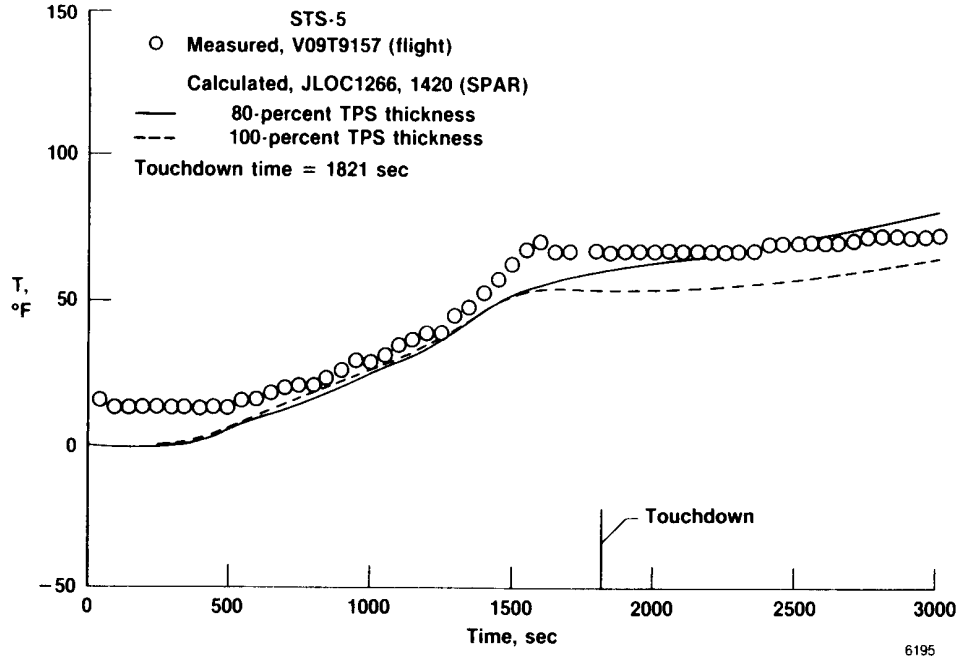

(e) Upper glove skin, part 1 of 2.

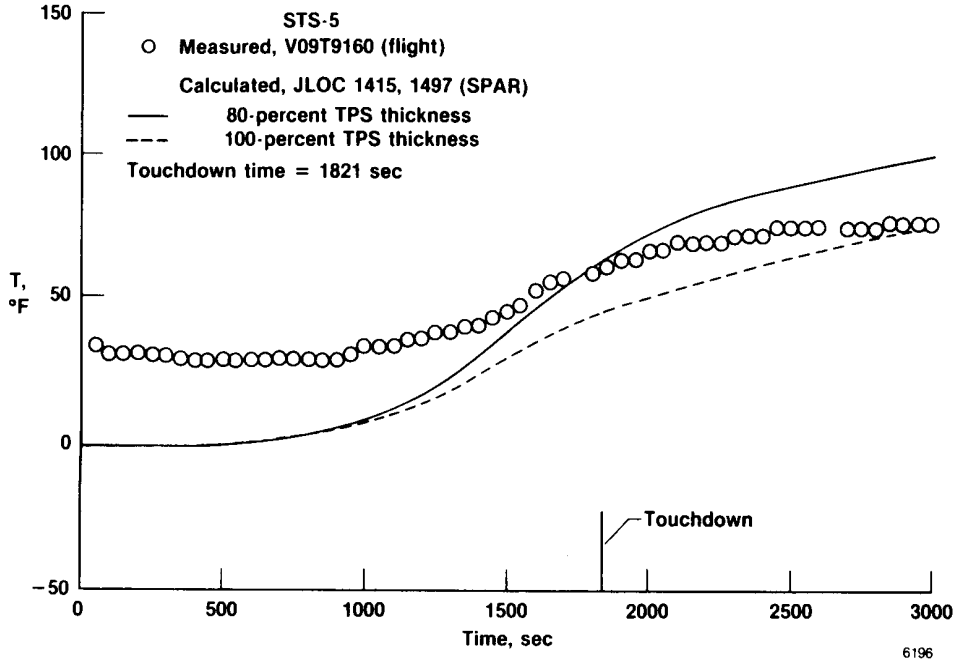

(f) Upper glove skin, part 2 of 2.

Figure 22. Continued.

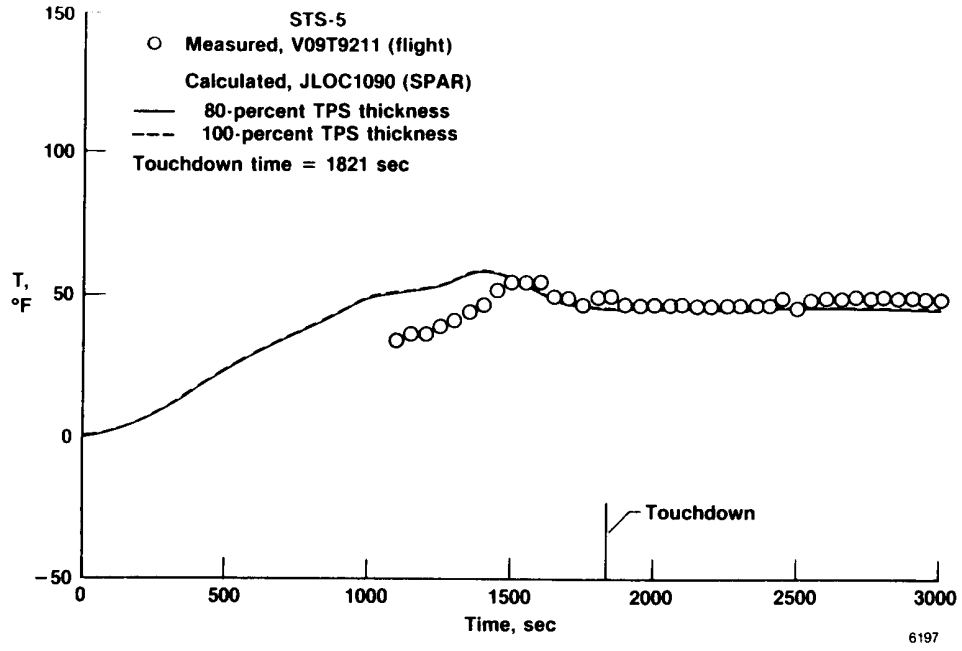

(g) Upper wheelwell, part 1 of 2.

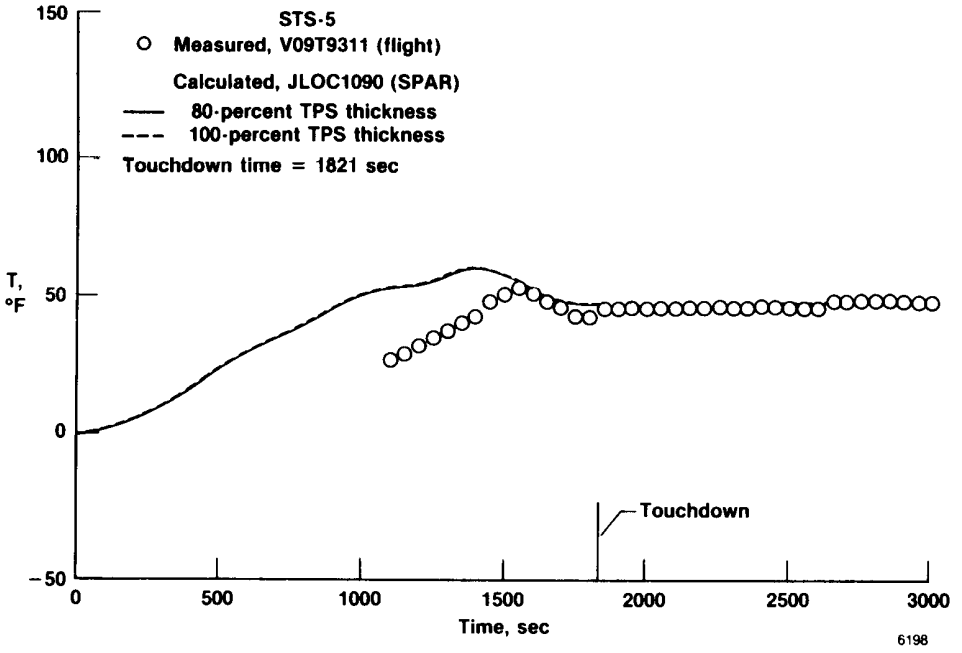

(h) Upper wheelwell, part 2 of 2.

Figure 22. Continued.

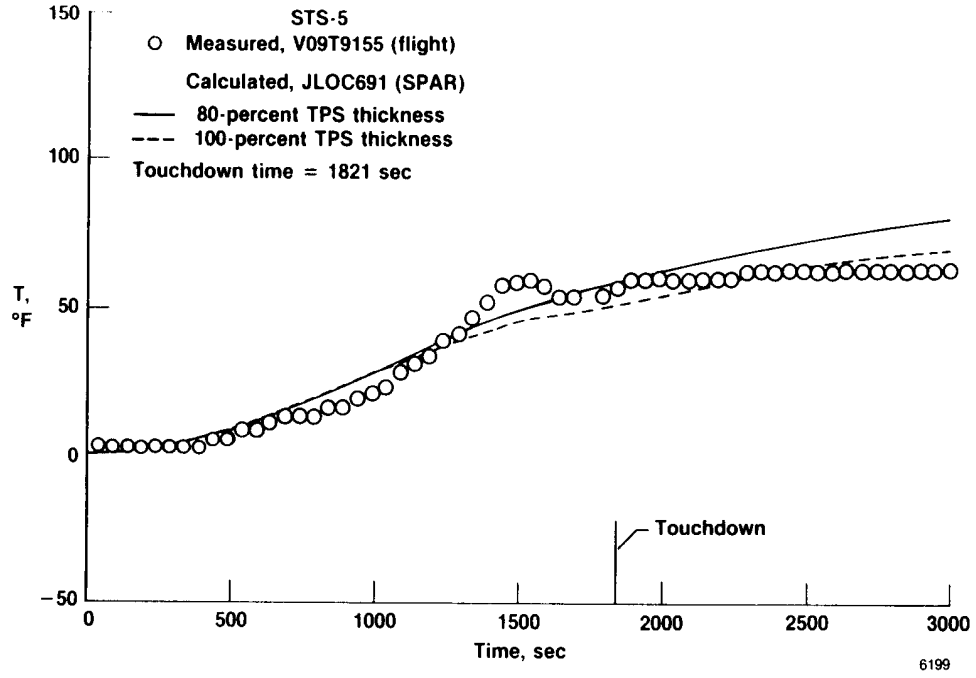

(i) Upper skin, bay 3.

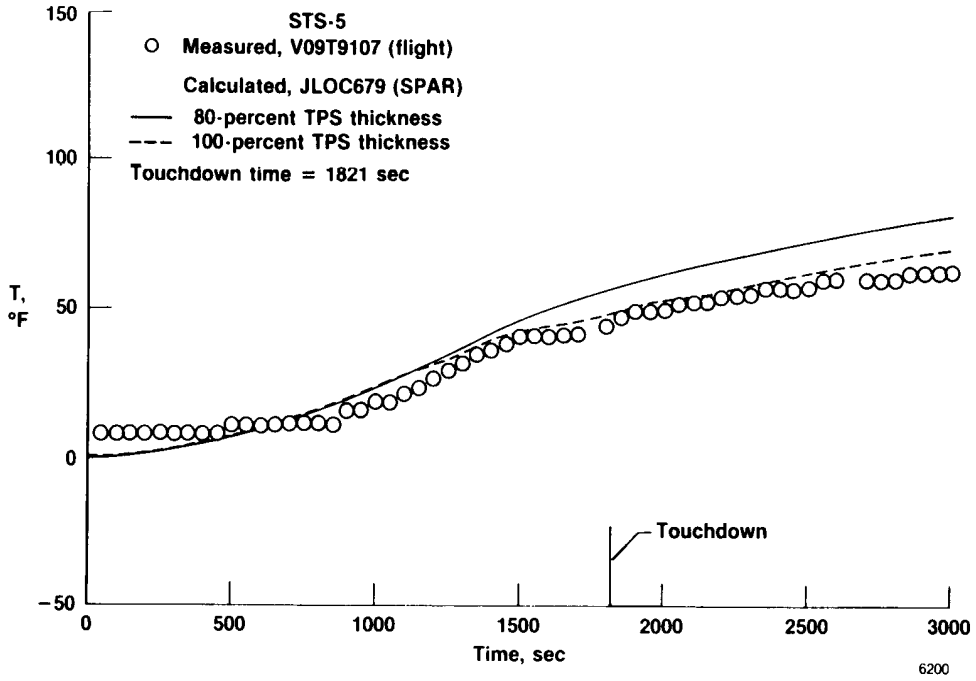

(j) Upper spar cap, bay 3/4.

Figure 22. Concluded.

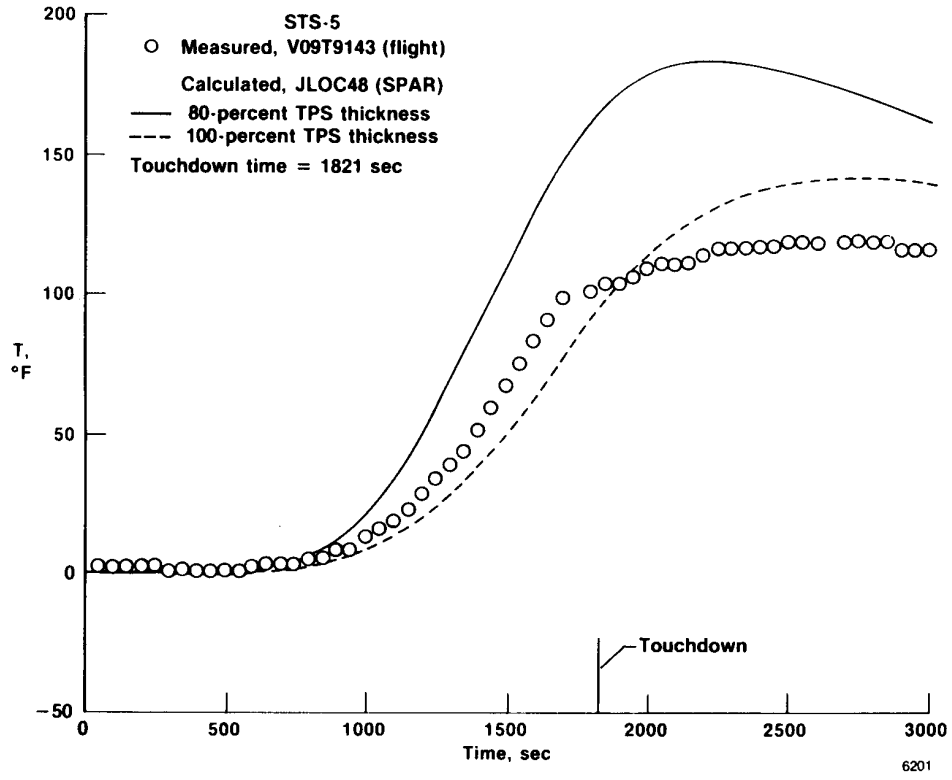

(a) Lower skin, bay 1.

Figure 23. Comparison of calculated and measured aluminum structural temperatures, WS240.

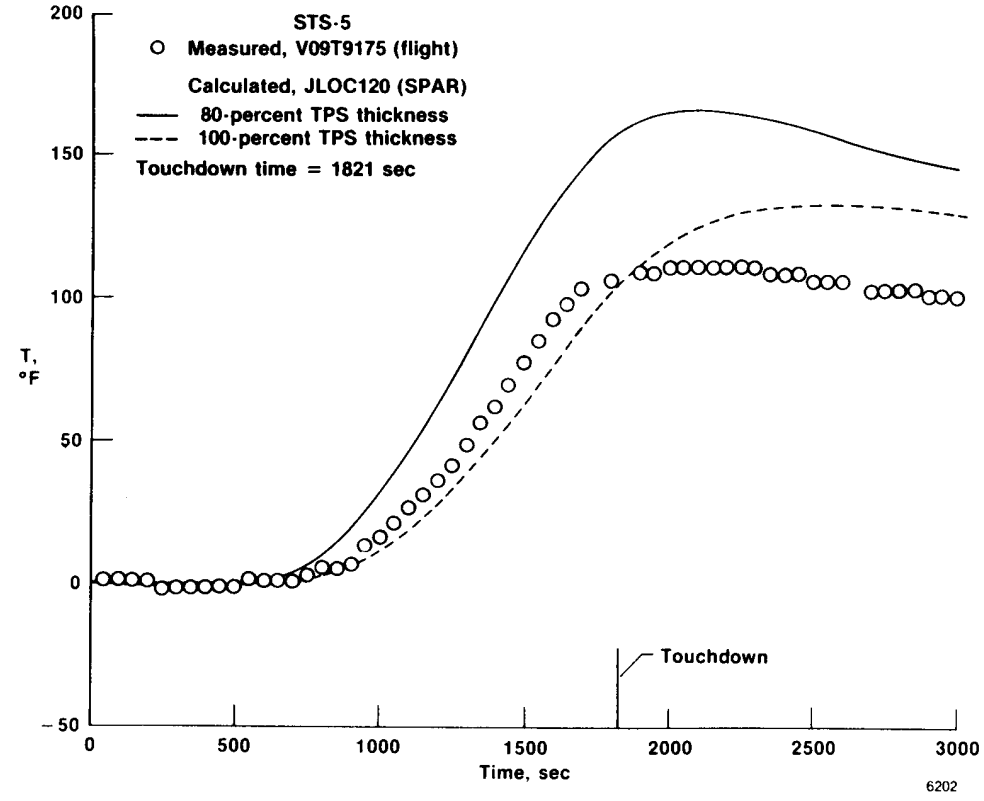

(b) Lower skin, bay 2.

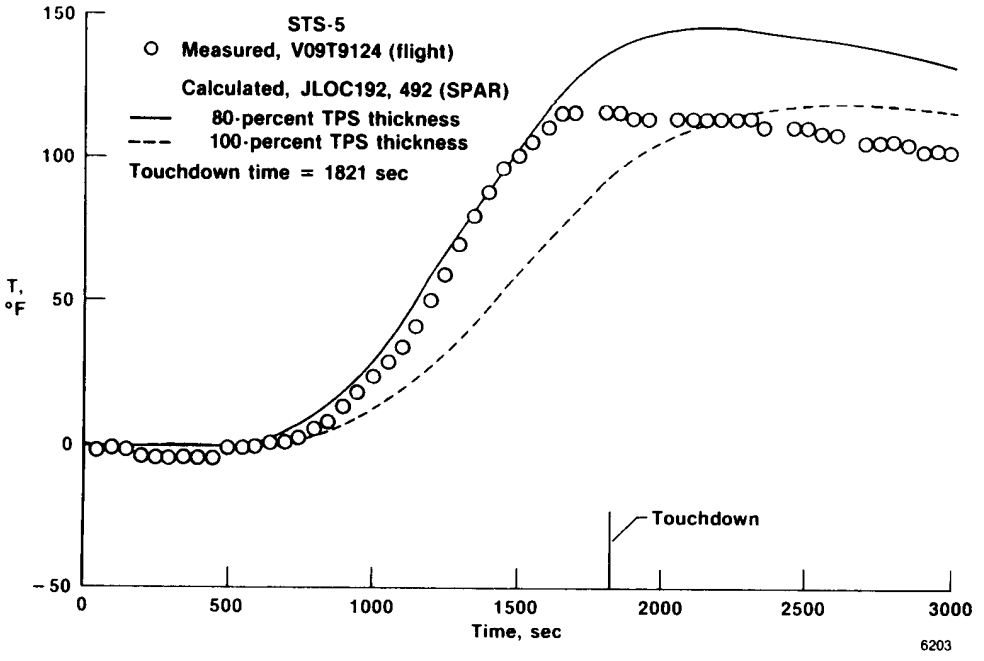

(c) Lower skin, bay 3, part 1 of 2.

Figure 23. Continued.

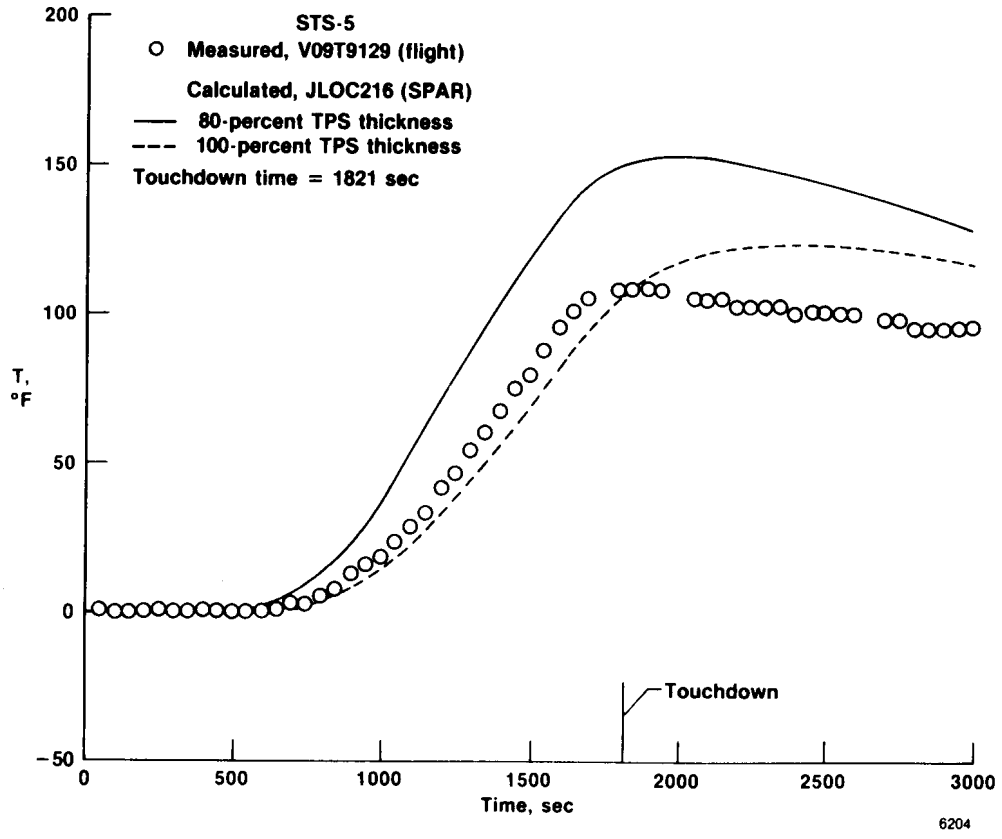

(d) Lower skin, bay 3, part 2 of 2.

Figure 23. Continued.

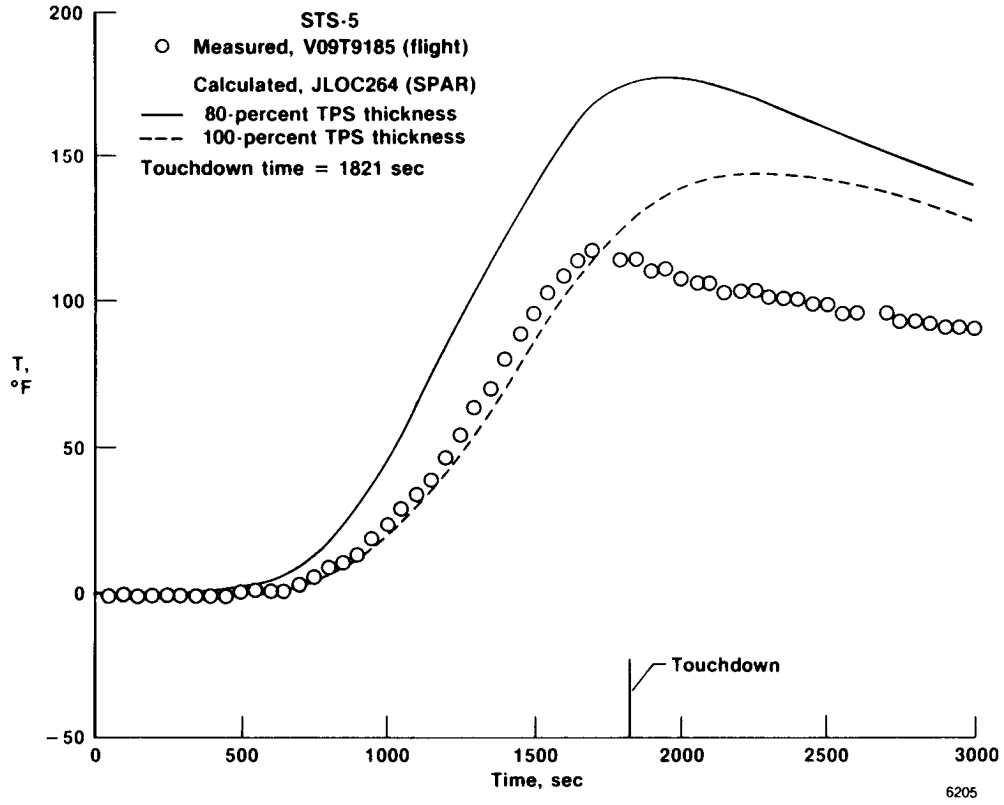

(e) Lower skin, bay 4.

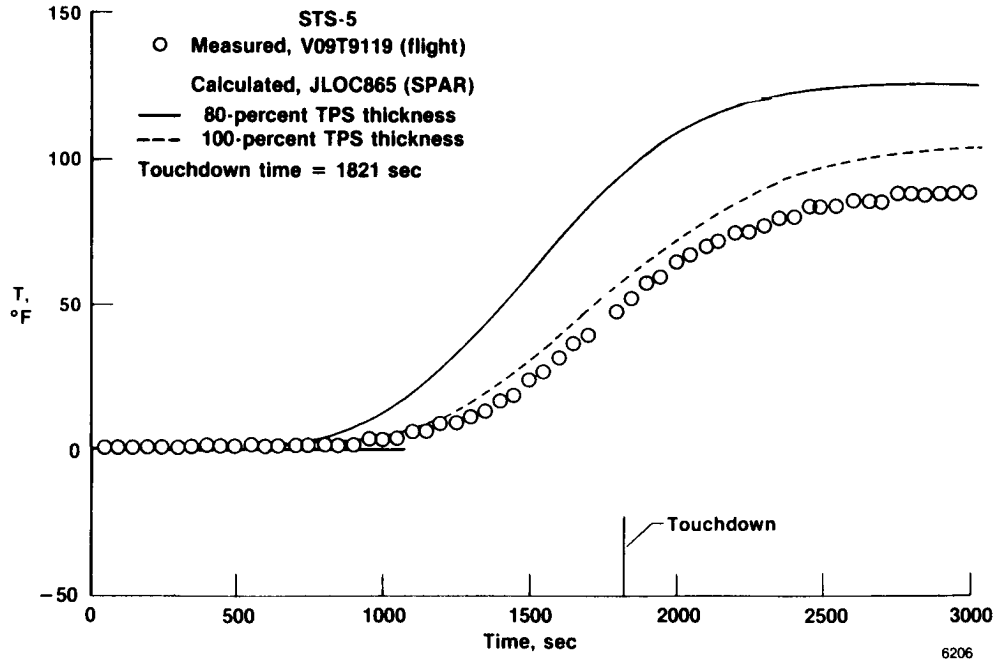

(f) Lower rib cap, bay 3, part 1 of 2.

Figure 23. Continued.

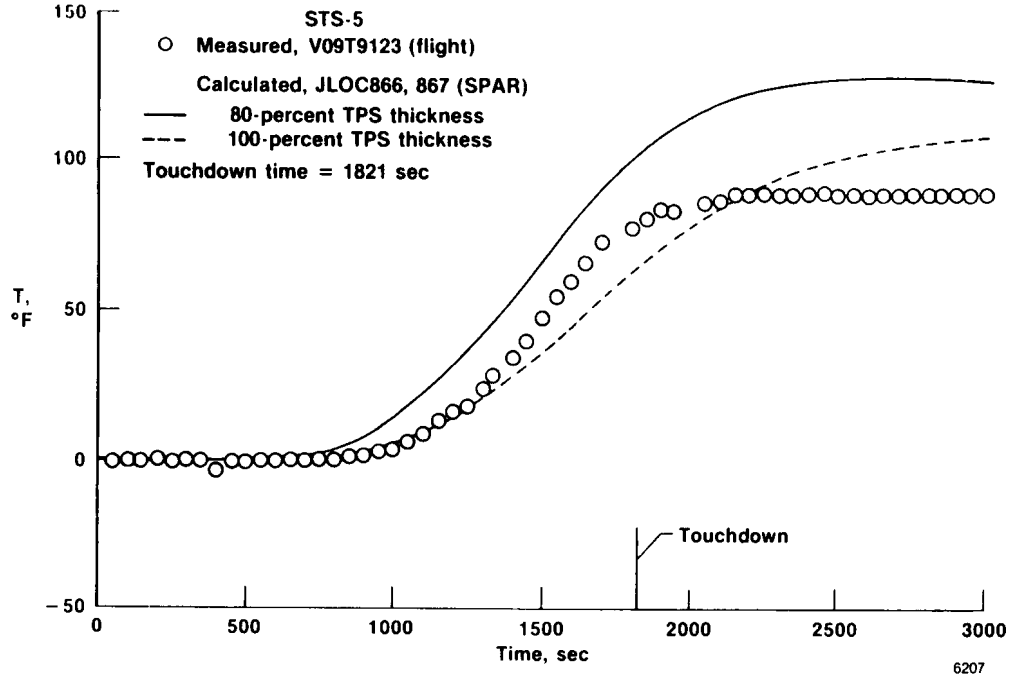

(g) Lower rib cap, bay 3, part 2 of 2.

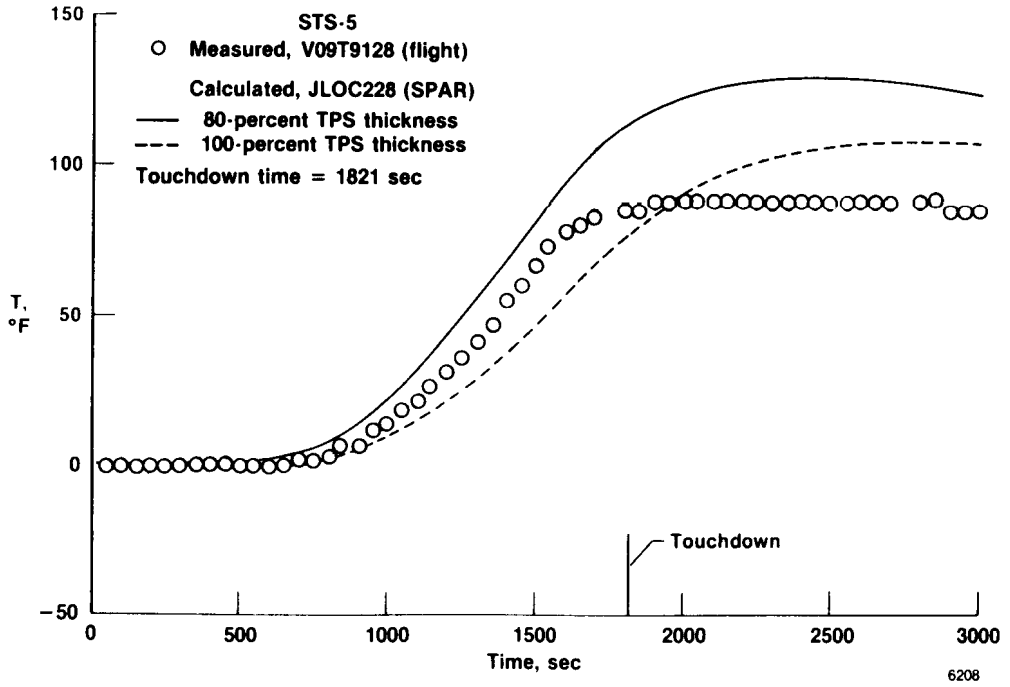

(h) Lower spar cap, bay 3/4.

Figure 23. Continued.

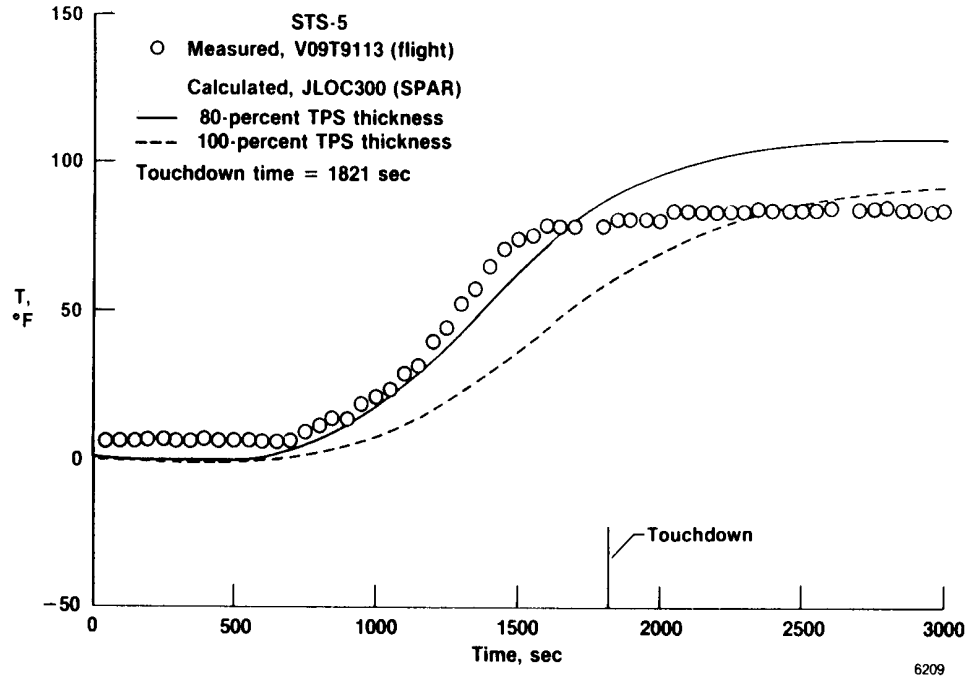

(i) Lower spar cap, aft bay 4.

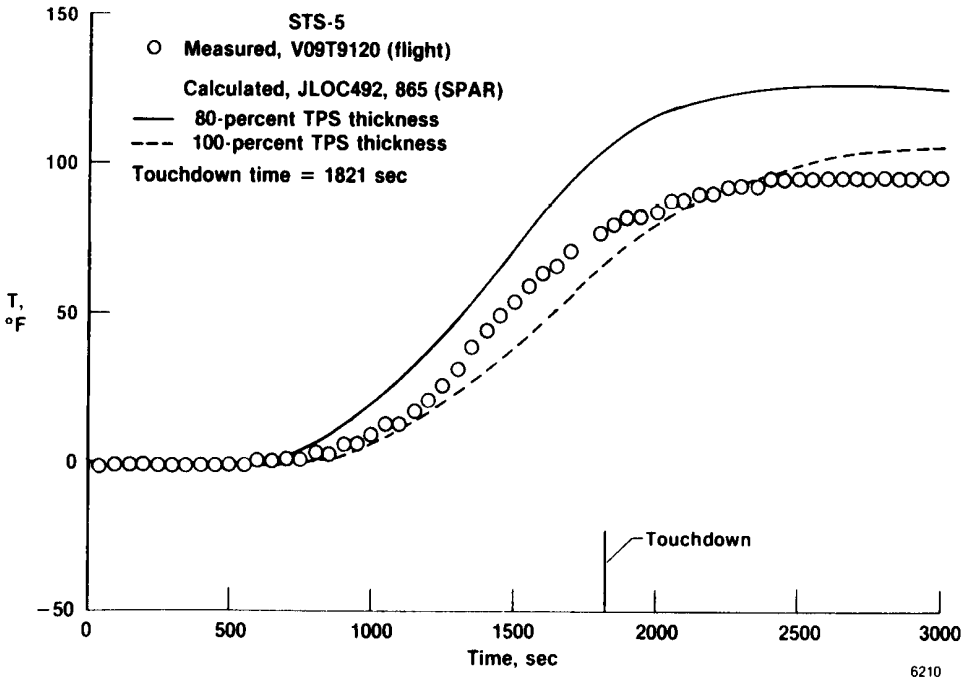

(j) Lower truss (vertical), bay 3.

Figure 23. Continued.

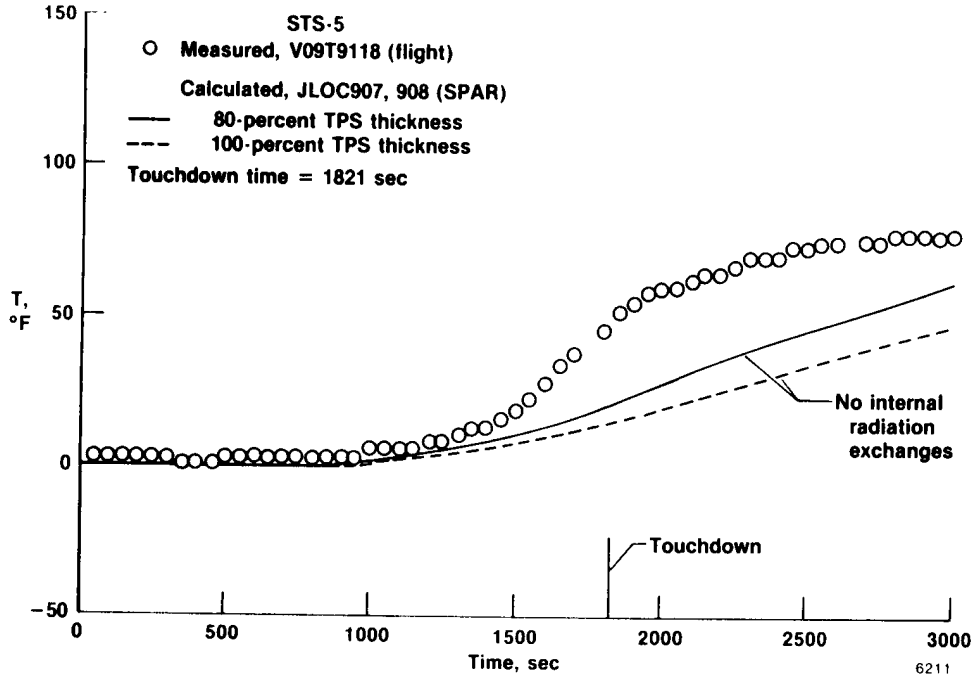

(k) Midtruss (vertical), bay 3.

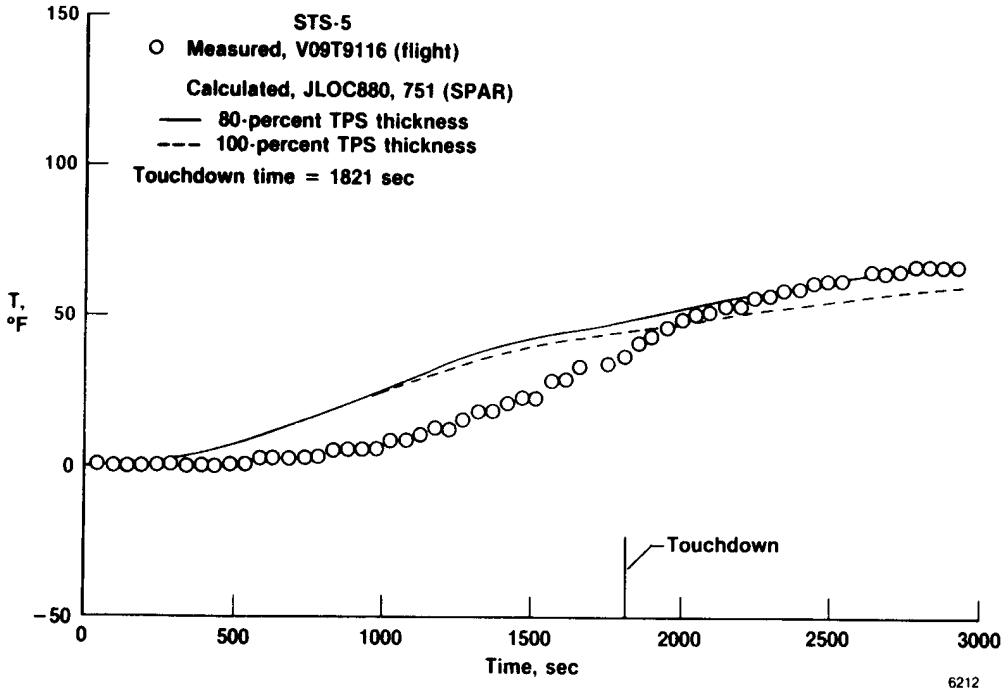

(l) Upper truss (vertical), bay 3.

Figure 23. Continued.

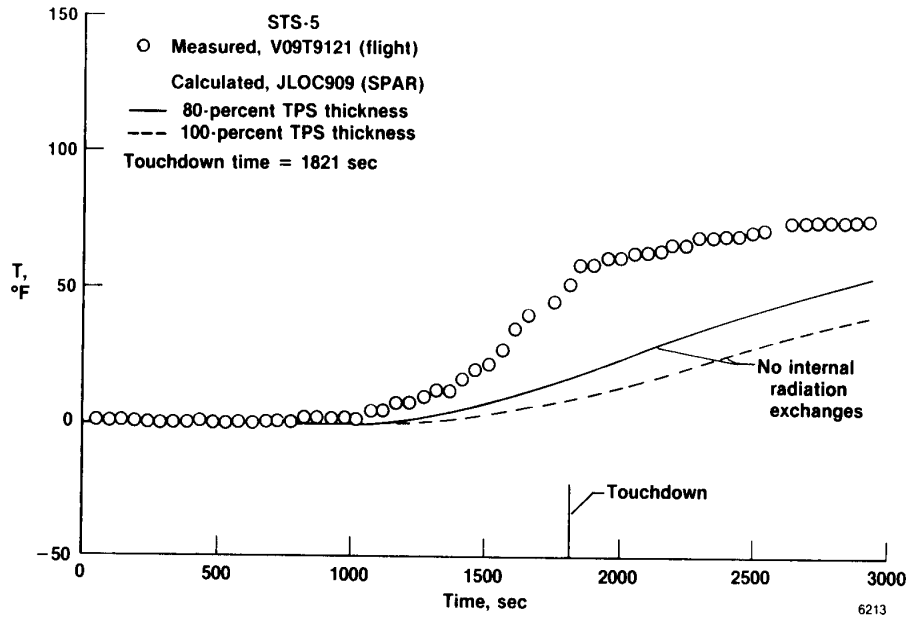

(m) Diagonal truss, bay 3.

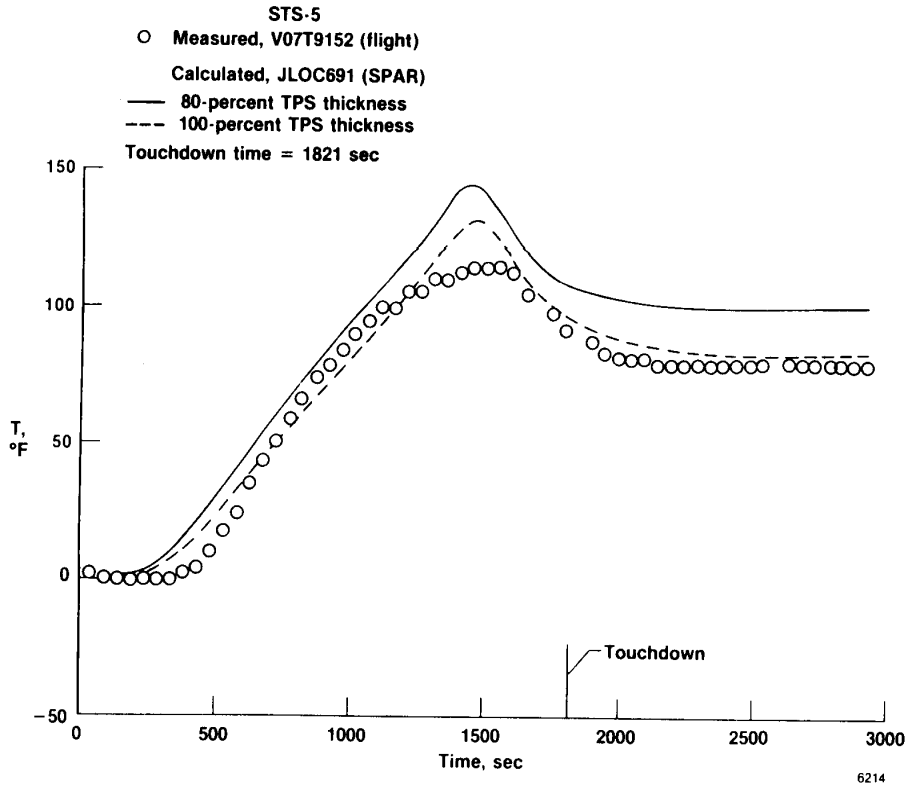

(n) Upper skin, bay 1.

Figure 23. Continued.

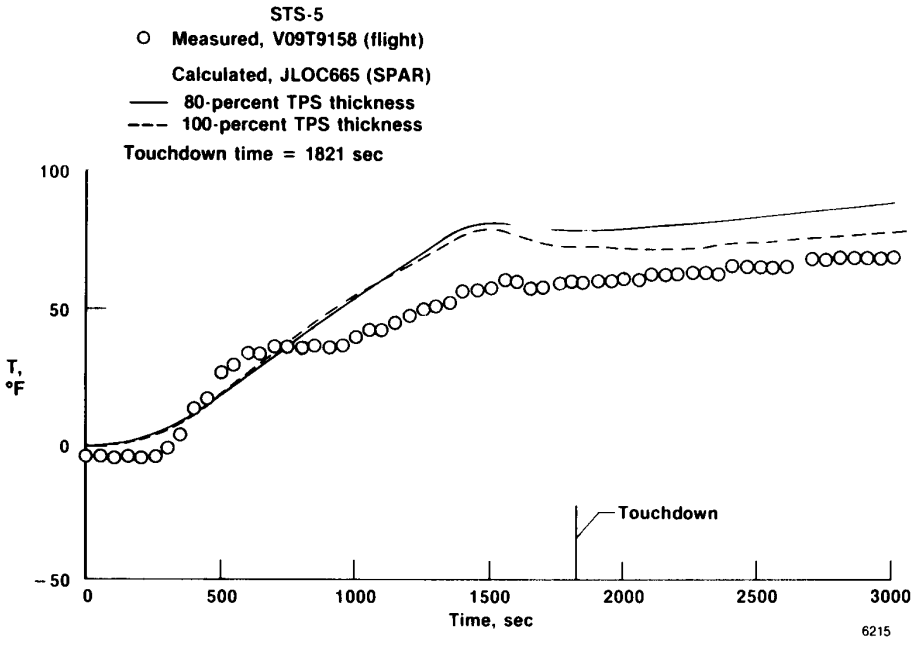

(o) Upper skin, bay 2.

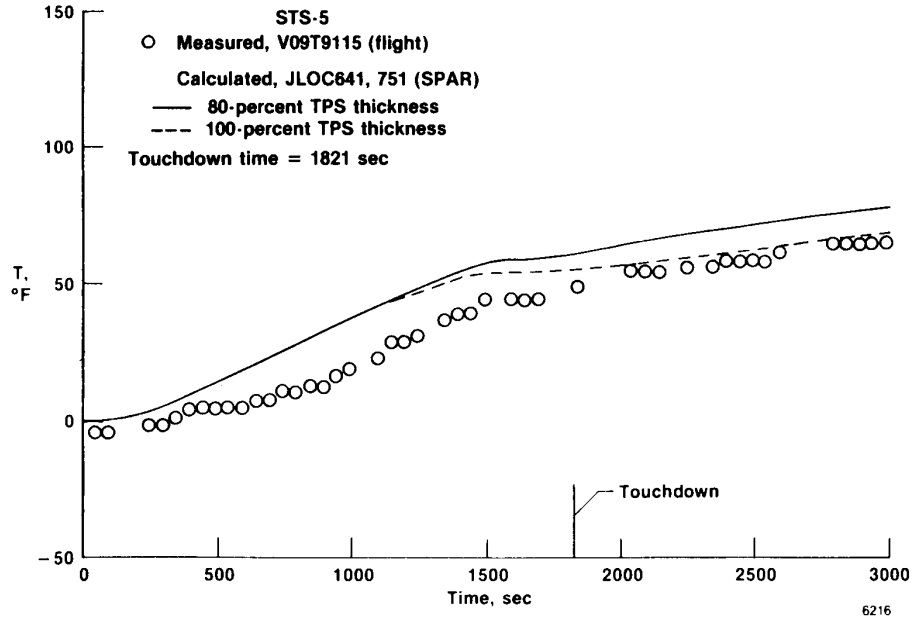

(p) Upper skin, bay 3, part 1 of 2.

Figure 23. Continued.

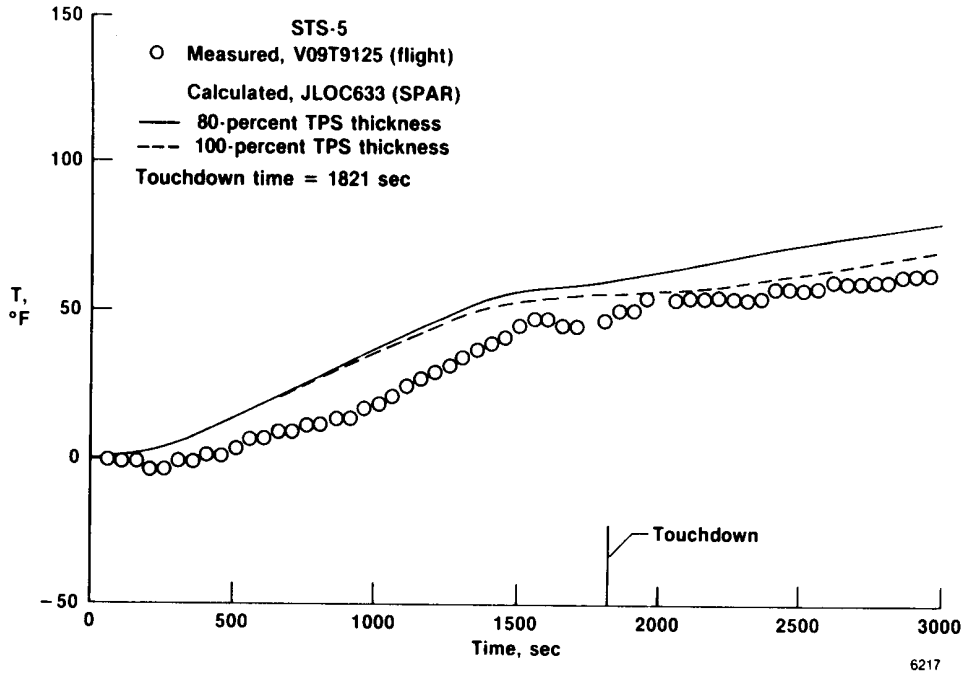

(q) Upper skin, bay 3, part 2 of 2.

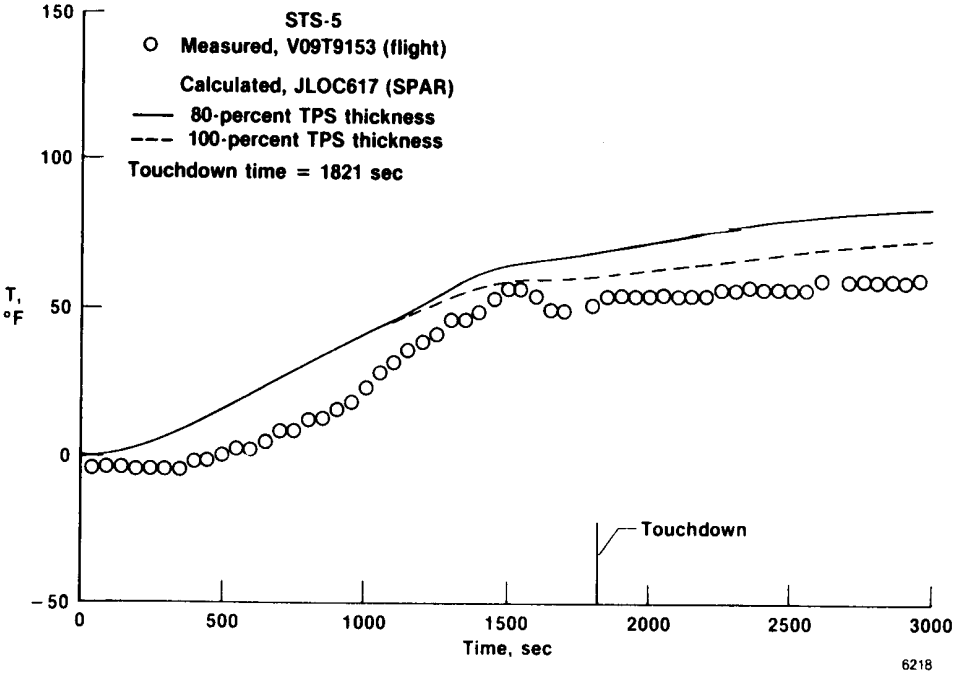

(r) Upper skin, bay 4.

Figure 23. Continued.

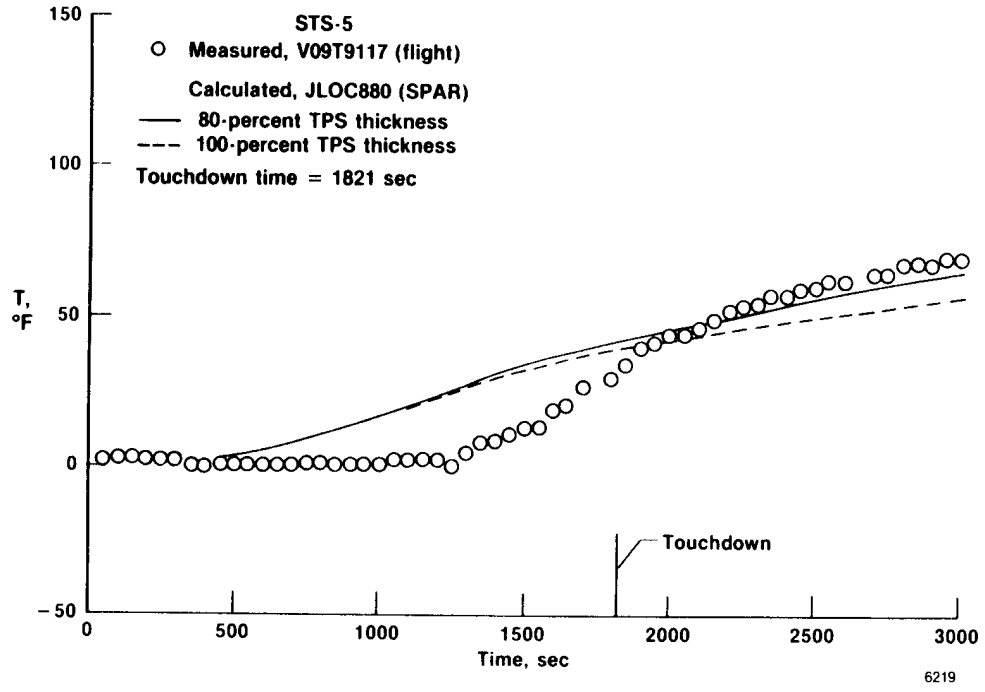

(s) Upper rib cap, bay 3, part 1 of 2.

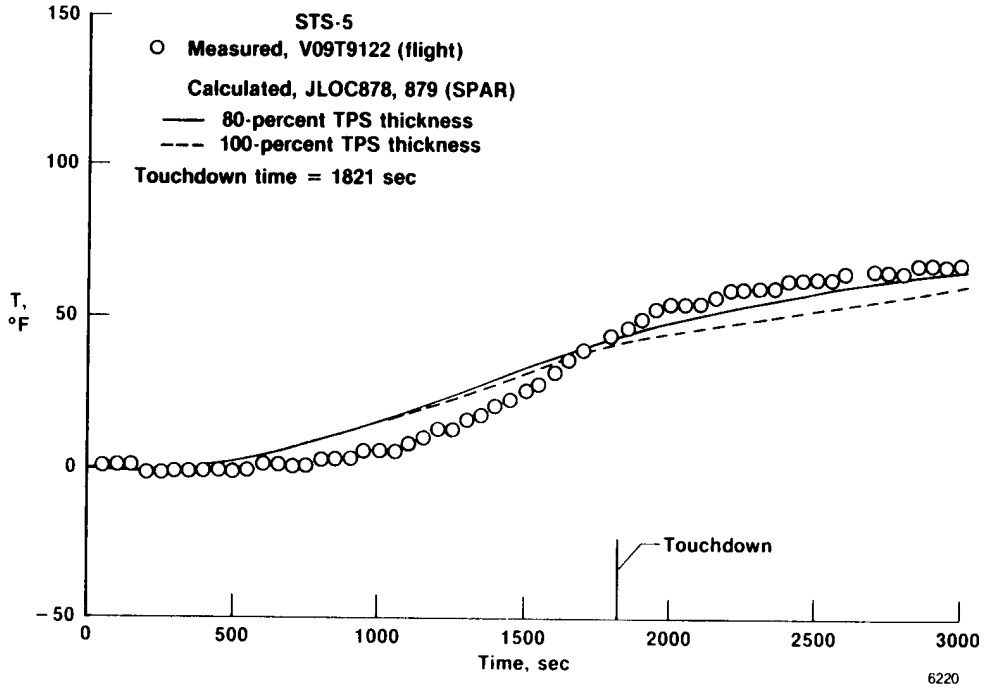

(t) Upper rib cap, bay 3, part 2 of 2.

Figure 23. Continued.

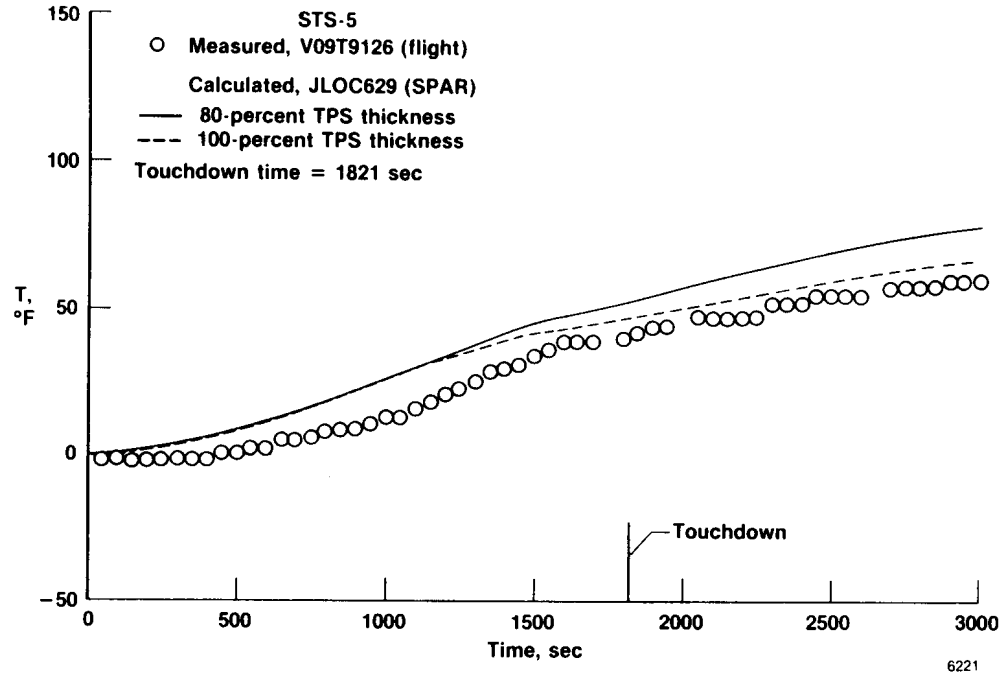

(u) Upper spar cap, bay 3/4.

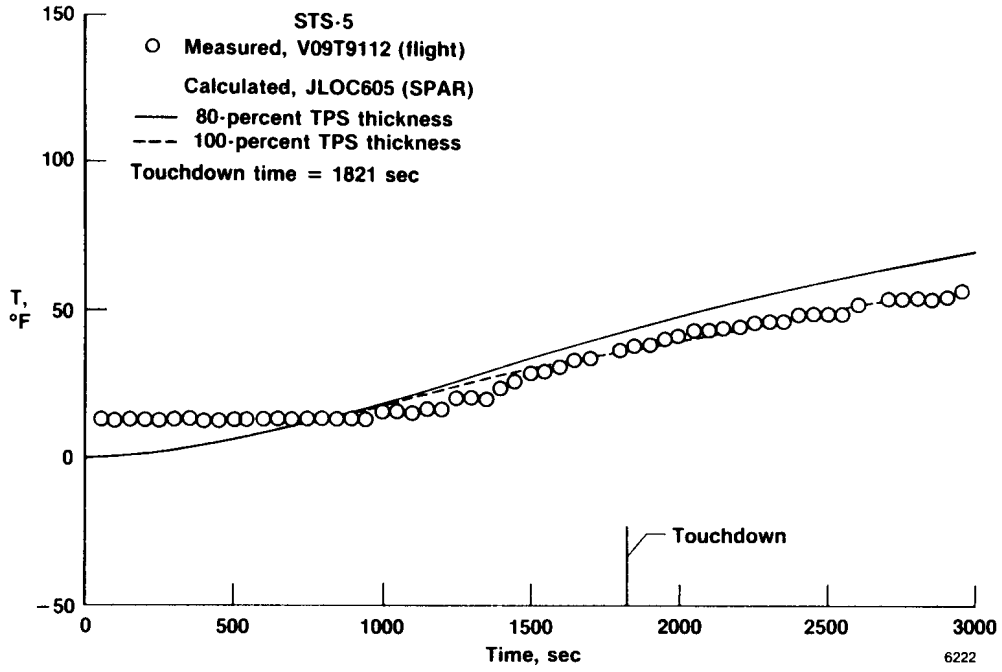

(v) Upper spar cap, aft bay 4.

Figure 23. Continued.

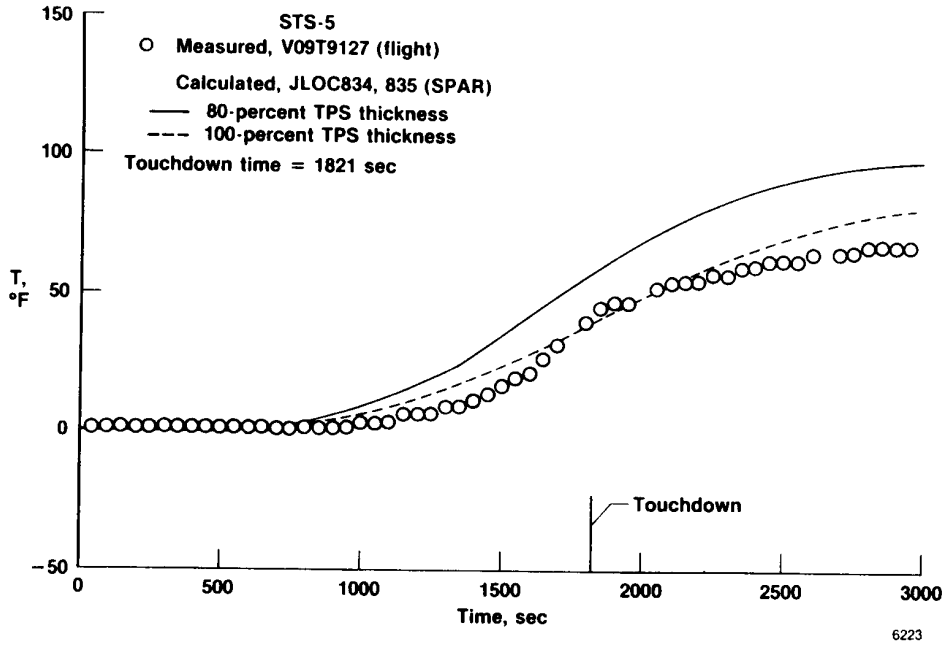

(w) Web, bay 3/4.

Figure 23. Concluded.

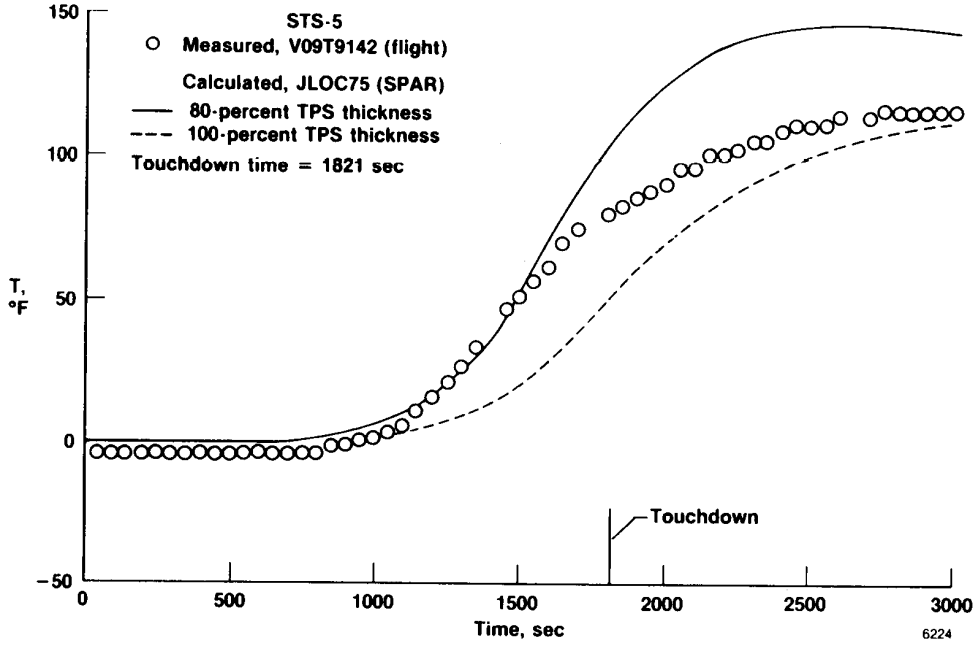

(a) Lower skin, bay 1.

Figure 24. Comparisons of calculated and measured aluminum structural temperatures, WS328.

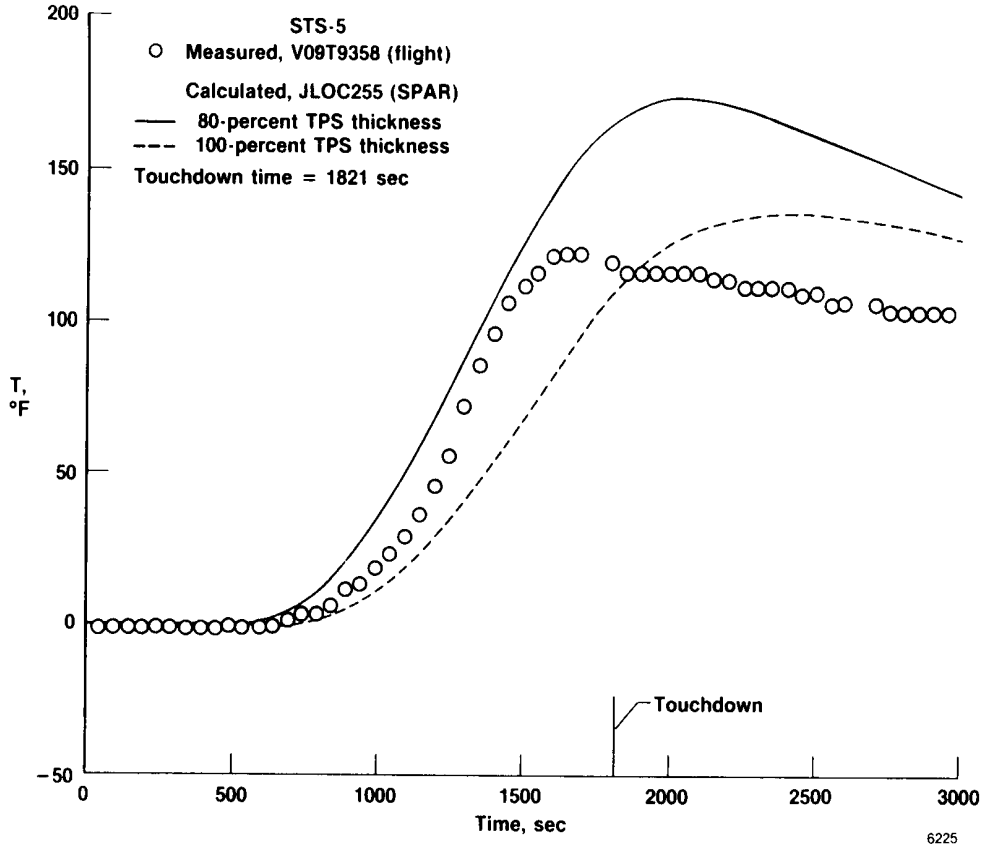

(b) Lower skin, bay 3.

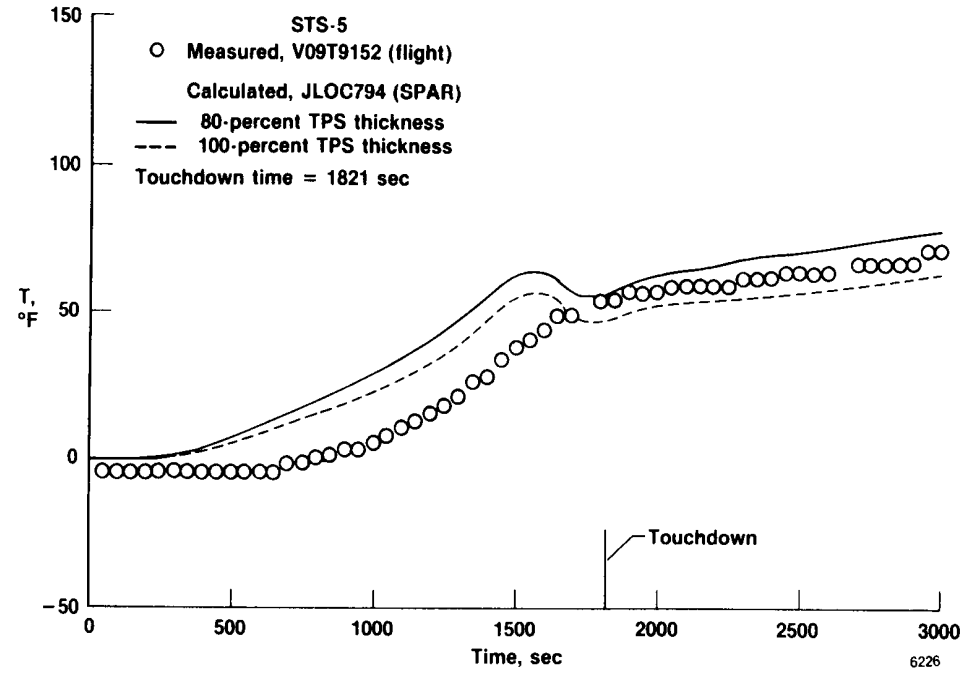

(c) Upper skin, bay 2.

Figure 24. Concluded.

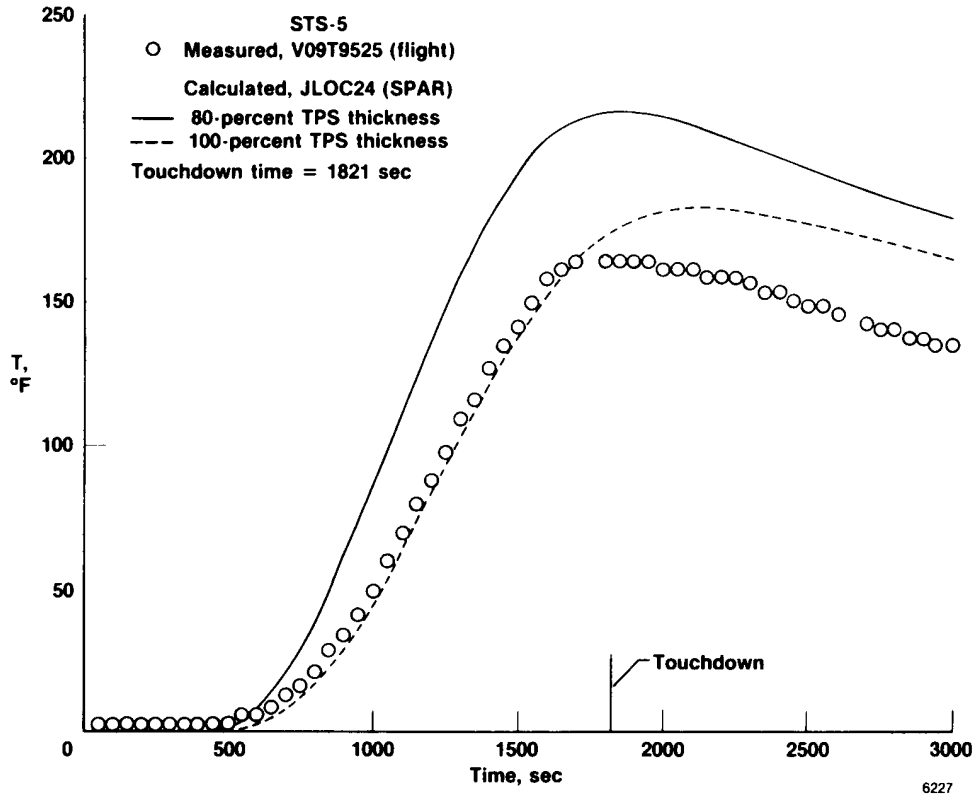

(a) Bottom skin, part 1 of 3.

Figure 25. Comparisons of calculated and measured aluminum structural temperatures, FS877.

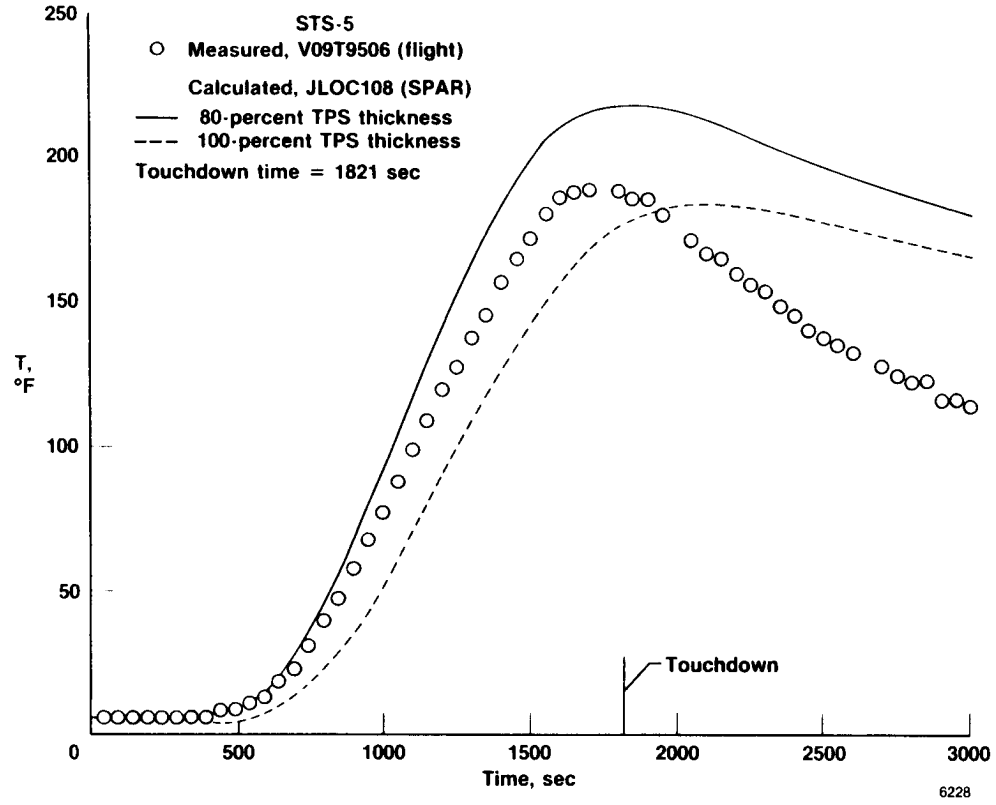

(b) Bottom skin, part 2 of 3.

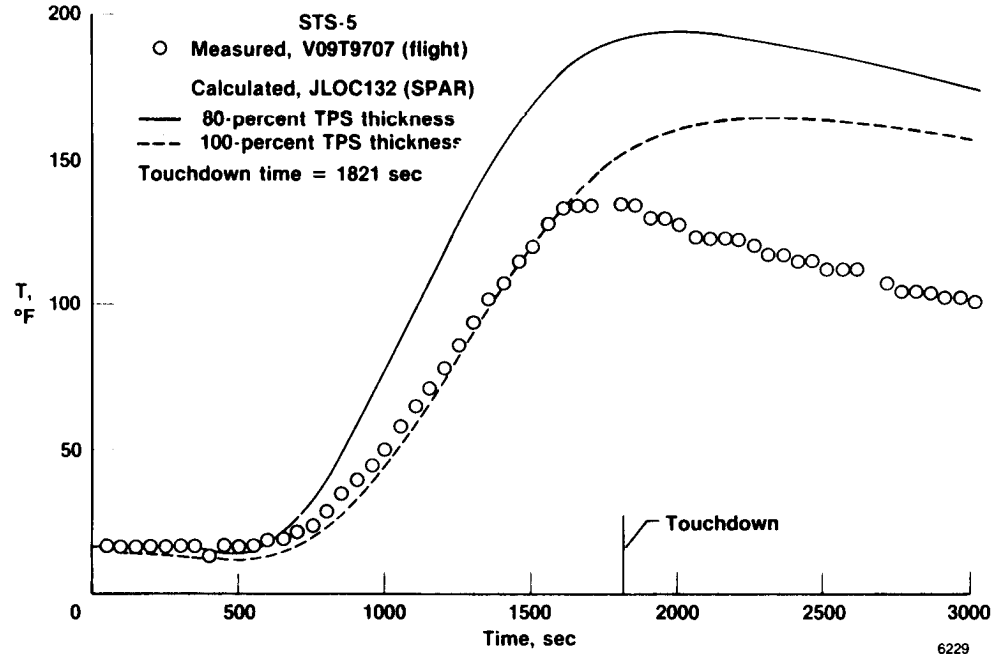

(c) Bottom skin, part 3 of 3.

Figure 25. Continued.

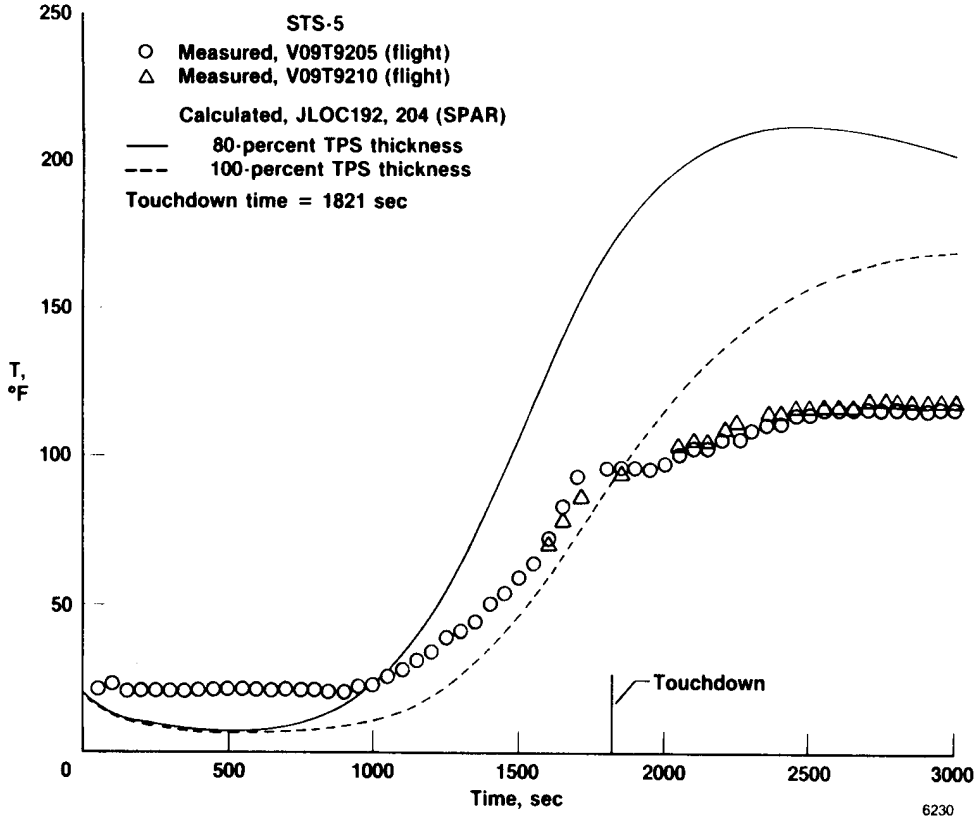

(d) Lower glove.

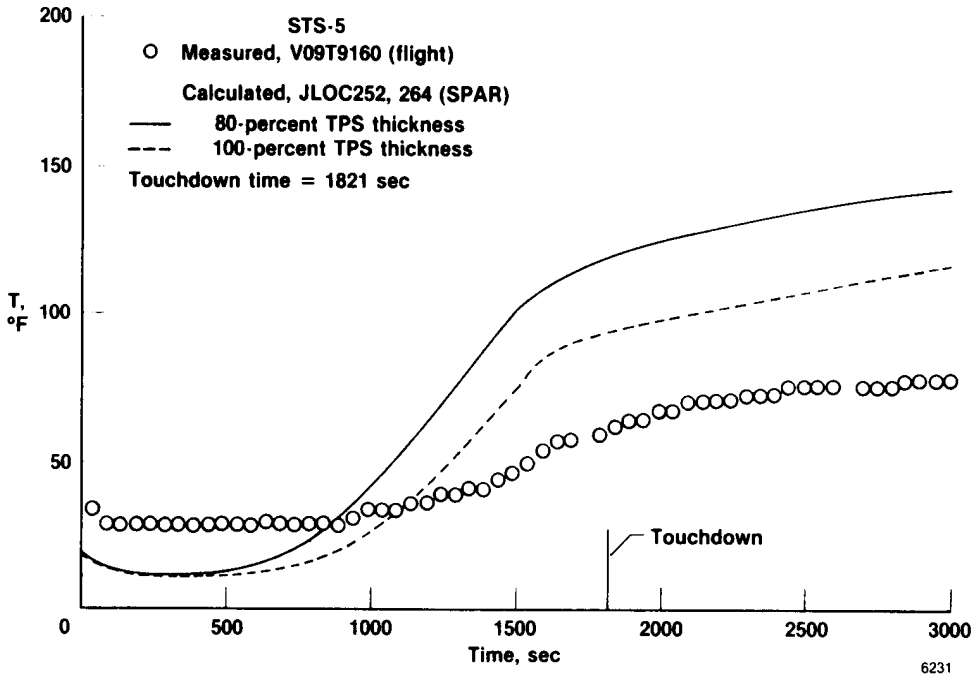

(e) Upper glove, part 1 of 2.

Figure 25. Continued.

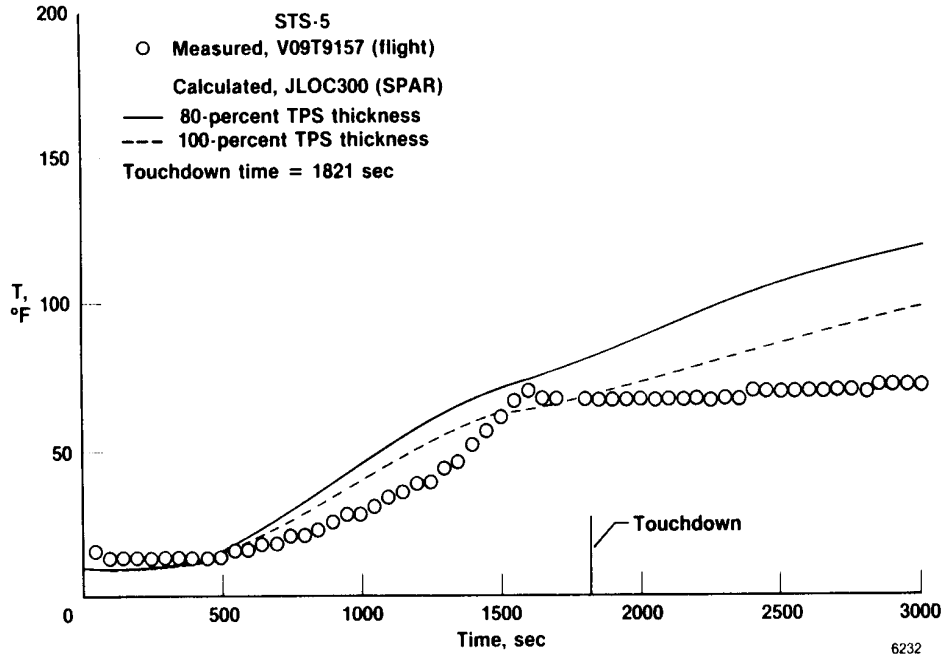

(f) Upper glove, part 2 of 2.

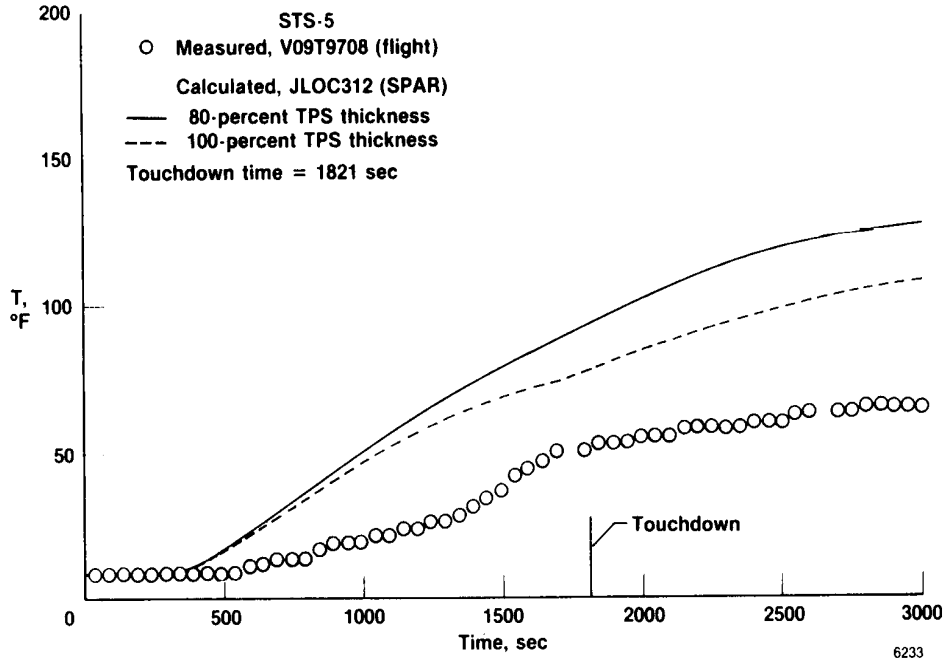

(g) Sidewall/upper glove.

Figure 25. Continued.

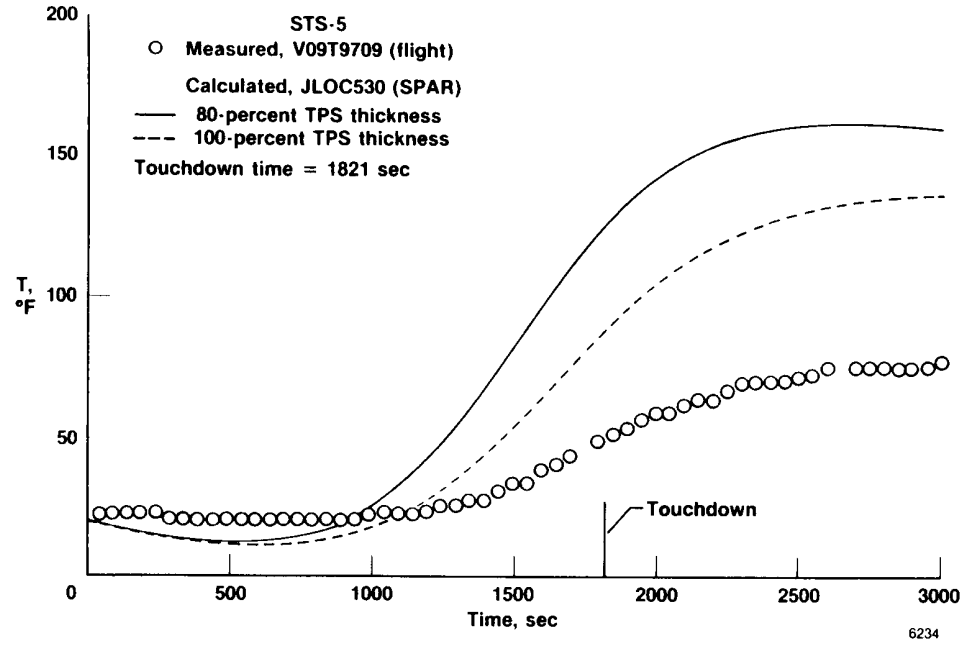

(h) Sidewall, part 1 of 4.

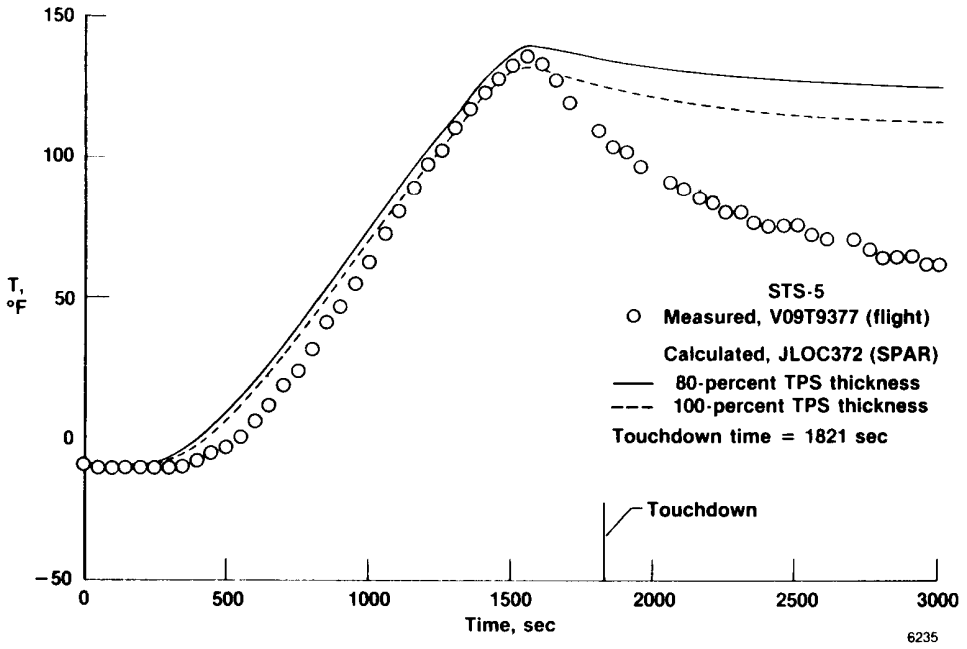

(i) Sidewall, part 2 of 4.

Figure 25. Continued.

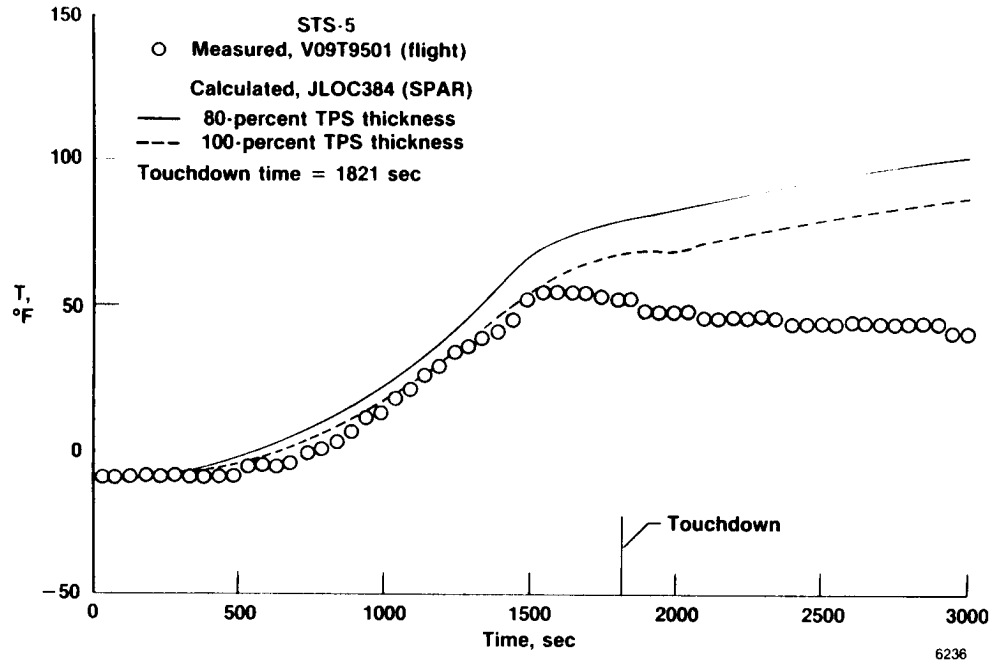

(j) Sidewall, part 3 of 4.

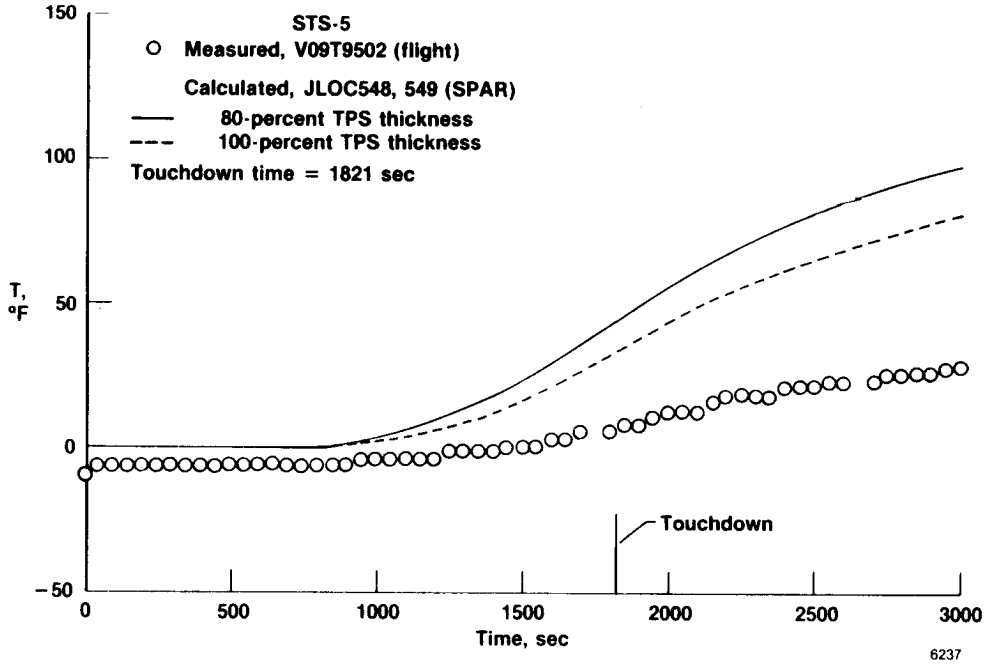

(k) Longeron, part 4 of 4.

Figure 25. Concluded.

1. Report No.	2. Government Accession No.	3. Recipient's Catalog No.
NASA TM-88278		

4. Title and Subtitle	5. Report Date
Comparison of Flight-Measured and Calculated Temperatures on the Space Shuttle Orbiter	November 1987
	6. Performing Organization Code

7. Author(s)	8. Performing Organization Report No.
Leslie Gong, William L. Ko, Robert D. Quinn, and W. Lance Richards	H-1384
	10. Work Unit No. RTOP 506-43-71

9. Performing Organization Name and Address	11. Contract or Grant No.
NASA Ames Research Center Dryden Flight Research Facility P.O. Box 273 Edwards, CA 93523-5000	
	13. Type of Report and Period Covered Technical Memorandum

12. Sponsoring Agency Name and Address	14. Sponsoring Agency Code
National Aeronautics and Space Administration Washington, DC 20546	

15. Supplementary Notes

16. Abstract

Structural temperatures and thermal protection system surface temperatures were measured on the space shuttle during the flight of the space transportation system 5. The measured data are compared with values calculated at wing stations 134, 240, and 328 and at fuselage station 877. The theoretical temperatures were calculated using the structural performance and resizing finite-element thermal analysis program. The comparisons show that the calculated temperatures are, generally, in good agreement with the measured data.

17. Key Words (Suggested by Author(s))	18. Distribution Statement
Heat-transfer analysis Reentry heating Space shuttle orbiter Space transportation system data	Unclassified — Unlimited Subject category 34

19. Security Classif. (of this report)	20. Security Classif. (of this page)	21. No. of Pages	22. Price*
Unclassified	Unclassified	72	A04

For sale by the National Technical Information Service, Springfield, Virginia 22161.